

Copyright

by

Nikola Vujic

2002

Power Regeneration in Actively Controlled Structures

by

Nikola Vujic

Thesis submitted to the Faculty of the
Virginia Polytechnic Institute and State University
in partial fulfillment of the requirements for the degree of

Master of Science

in

Mechanical Engineering

Donald J. Leo, Chair
Daniel J. Inman
Douglas K. Lindner

May 2002

Blacksburg, Virginia

Power Regeneration in Actively Controlled Structures

Approved by
Advising Committee:

To my father,
Milan Vujic,
and my mother,
Marie-Agnès Vujic

Power Regeneration in Actively Controlled Structures

Nikola Vujic, M.S.

Virginia Polytechnic Institute and State University, 2002

Advisor: Donald J. Leo

ABSTRACT

The power requirements imposed on an active vibration isolation system are quite important to the overall system design. In order to improve the efficiency of an active isolation system we analyze different feedback control strategies which will provide electrical energy regeneration. The active isolation system is modeled in a state-space form for two different types of actuators: a piezoelectric stack actuator and a linear electromagnetic (EM) actuator. During regenerative operation, the power is flowing from the mechanical disturbance through the electromechanical actuator and its switching drive into the electrical storage device (batteries or capacitors). We demonstrate that regeneration occurs when controlling one or both of the flow states (velocity and/or current). This regenerative control strategy affects the closed loop dynamics of the isolator which sees its damping reduced.

Acknowledgments

First I would like to thank my advisor, Dr. Donald J. Leo, for his help and patience throughout my graduate studies. His guidance and complete support made my working and learning experience, a very special one. Also, I want to extend my thanks to Dr. Douglas K. Lindner and Dr. Daniel J. Inman for their support and enthusiasm as members of my advisory committee.

In addition, I want to thank my colleagues in the Center for Intelligent Material Systems and Structures (CIMSS). The good humor of everybody made it an enjoyable experience. Also my great thanks to Dr. S. Griffin for starting this topic and choosing us for collaborators. I gratefully acknowledge the support of Air Force Research Laboratory Space-Vehicles Directorate (AFRL/VS), that made possible this research. The POC for this effort is Dr. Steven A. Lane. Additional support was provided by Concepts Inc.

Finally, I would like to thank my parents and family for their love and support during my years at Virginia Tech.

NIKOLA VUJIC

Virginia Polytechnic Institute and State University

May 2002

Contents

Abstract	v
Acknowledgments	vi
List of Tables	x
List of Figures	xi
Chapter 1 Introduction	1
1.1 Literature Review	2
1.1.1 Energy Regeneration and the concept of Energy Harvesting	2
1.1.2 Power flow Analysis	6
1.1.3 Electrical driver, a key element in regenerative systems	7
1.1.4 Actively controlled Vibration Isolation Systems	7
1.2 Energy regeneration for active vibration suppression	10
1.2.1 Regenerative Actuation Concept	12
1.3 Overview of thesis	14
1.3.1 Research Objectives	14
1.3.2 Contributions	14
1.3.3 Approach	15
Chapter 2 Electromechanical regenerative systems for vibration suppression	17
2.1 Introduction	17
2.2 Model of a Piezoelectric stack actuator	17
2.2.1 About the piezoelectricity	17

2.2.2	PZT Stack Actuators (Translators)	19
2.3	Linear Electromagnetic actuators	25
2.4	Electrical Power Supplies	27
2.4.1	Power Operational Amplifiers	27
2.4.2	Switching amplifiers	29
2.4.3	Conclusion on Electrical Power Supplies	33
2.5	Power absorption in a single input system	33
2.5.1	Generalized definition of Power and system classification	33
2.5.2	System classification	35
2.6	Summary	36

Chapter 3 Two examples of active vibration isolator and their power flow analysis in closed loop 37

3.1	Introduction	37
3.2	Example of an active vibration isolation system realized with an Electromagnetic (EM) actuator	38
3.2.1	Modeling of the electromagnetic system	38
3.2.2	Normalization of the differential equations in the case of a linear electromagnetic actuator	39
3.3	Example of an active vibration isolation system realized with a Piezoelectric (PZT) actuator	41
3.3.1	Modeling of the piezo-based vibration isolation system	42
3.3.2	Normalization of the differential equations in the case of a PZT actuator	43
3.3.3	Comparison of the two active control vibration isolation systems . .	45
3.3.4	Analytical expression for electrical power in closed loop	46
3.4	Summary on the regenerative control topologies and their influence on the vibration of the payload	53
3.4.1	Influence of regenerative control on the isolator dynamics	53

Chapter 4 Measurements and simulation 57

4.1	Introduction	57
4.2	Experimental Setup	59
4.3	Open loop Results	60

4.3.1	Mechanical parameters	60
4.3.2	Electrical Parameters	62
4.4	Resistive Control	63
4.4.1	Implementation of the Resistive Control	64
4.4.2	Results and their comparison with estimated results	65
4.5	Velocity Control	69
4.5.1	Implementation of the Velocity feedback Control	69
4.5.2	Results and their comparison with estimated results	71
4.6	Flow Control	75
4.6.1	Results and their comparison with estimated results	75
4.7	Summary on the experimental verification	80
Chapter 5 Conclusions		83
5.1	Recommendations and Future Work	85
Bibliography		87
Appendix A Experimental and Simulated powers and efficiency plots in flow control topology with $g_1 = 4$		92
Appendix B Elctrical Power Expresion in closed loop		96
Vita		98

List of Tables

2.1	Effort and flow quantities for various dynamic systems.	34
3.1	State-space matrix coefficients comparison for two active vibration system using two different actuators	45
4.1	System comparison	58
4.2	Experimentally obtained and simulated optimum regenerative flow gains comparison	81

List of Figures

1.1	Conceptual diagram of the “smart” structure [Culshaw (1996)]	2
1.2	Energy harvesting eel concept (Ocean Power Technologies, Inc.)	4
1.3	Experimental setup developed by Nakano et al. (2000)	9
1.4	Regenerative control concept applied to rocket payload vibration protection	12
1.5	Regenerative Control Concept	13
2.1	Typical PZT crystal: A) before poling B) after poling [Physik Instrumente (2002)]	19
2.2	Electrical dipole in Weiss domains:(A) unpoled ferroelectric ceramic, (B) during and (C) after polling [Physik Instrumente (2002)]	20
2.3	Stack design and wafers wiring [Physik Instrumente (2002)]	21
2.4	Force-stroke characteristic curves	24
2.5	Charge-voltage characteristic curves	24
2.6	Voice Coil Motor Cross-section (Honeywell)	25
2.7	Power Operational Amplifier	28
2.8	Push-pull circuit	29
2.9	Typical pulse-width-modulated switch voltage waveform [Erickson and Maksimovic (1999)]	30
2.10	Bi-Directional Single Phase Inverter	31
2.11	Operational Principle of a Bi-Directional current inverter	32
3.1	Vibration isolation system	38
3.2	Electrical circuit in a case of a EM actuator	38
3.3	Vibration isolation system	41
3.4	Electrical circuit in a case of a PZT actuator	41

3.5	Regenerative electrical power flow vs \tilde{g}_1 and $\tilde{g}_2 = \tilde{g}_3 = 0$ for three different values of Ω	47
3.6	Regenerated Electrical power vs \tilde{g}_1 and \tilde{g}_2 for the case where $\Omega = 1.5$ and $\tilde{g}_3 = 0$	49
3.7	Regenerative area vs \tilde{g}_1 and \tilde{g}_2 for three different values of Ω and $\tilde{g}_3 = 0$. .	50
3.8	Curves of \tilde{P}_{el} vs \tilde{g}_1 for three different values of \tilde{g}_1 at $\Omega = 1.5$ and $\tilde{g}_3 = 0$. .	50
3.9	Regenerated Electrical power vs \tilde{g}_2 and \tilde{g}_3 for the case where $\Omega = 1.5$ and $\tilde{g}_1 = 0$	50
3.10	Regenerative area vs \tilde{g}_2 and \tilde{g}_3 for different values of Ω and $\tilde{g}_1 = 0$	51
3.11	Curves of \tilde{P}_{el} vs \tilde{g}_1 for three different values of Ω ($\tilde{g}_1 = \tilde{g}_2 = 0$)	51
3.12	Regenerated Electrical power vs \tilde{g}_2 and \tilde{g}_3 for the case where $\Omega = 1.5$ and $\tilde{g}_2 = 0$	52
3.13	Regenerative area vs \tilde{g}_2 and \tilde{g}_3 for different values of Ω and $\tilde{g}_1 = 0$	52
3.14	Curves of \tilde{P}_{el} vs \tilde{g}_1 for three different values of \tilde{g}_3 ($\Omega = 1.5$ and $\tilde{g}_2 = 0$) . . .	52
3.15	$ T.R. $ in the case of the resistive control	54
3.16	$ T.R. $ around the mechanical resonance	54
3.17	$ T.R. $ in the case of the velocity control	55
3.18	$ T.R. $ around the mechanical resonance	55
3.19	Open and closed loop poles location for regenerative control	55
4.1	Difference between the analyzed and experimental system	57
4.2	Simplified schematics of the experimental setup	59
4.3	Open loop transfer function between displacement and input force (short circuit boundary condition)	61
4.4	Open loop electrical impedance Z_{el} (mechanically unconstrained shaker) . .	62
4.5	Resistive control schematics	64
4.6	Regenerated simulated and measured powers in resistive control configuration	66
4.7	Input mechanical simulated and measured powers in resistive control configuration	67
4.8	Simulated and experimental efficiencies in resistive control configuration . .	68
4.9	Velocity control schematics	69
4.10	Bode plot of an pseudo integrator and an ideal integrator	70

4.11	Regenerated simulated and measured powers in resistive control configuration	72
4.12	Input mechanical simulated and measured powers in velocity control configuration	73
4.13	Simulated and experimental efficiencies in velocity control configuration . .	74
4.14	Flow control schematics	75
4.15	Regenerated simulated and measured powers in flow control configuration .	77
4.16	Input mechanical simulated and measured powers in flow control configuration	78
4.17	Simulated and experimental efficiencies in flow control configuration	79
5.1	2-DOF regenerative vibration isolation concept	86
A.1	Regenerated simulated and measured powers in flow control configuration .	93
A.2	Input Mechanical simulated and measured powers in flow control configuration	94
A.3	Simulated and experimental efficiencies in flow control configuration	95

Chapter 1

Introduction

In recent years, researchers have been investigating the use of active materials in diverse structural applications such as vibration isolation and structural health monitoring. By the late 1980s, research papers began to appear on any imaginable blend of active materials, host structures materials and control algorithms. Crawley and de Louis (1987) are generally credited with creating a term “intelligent structures” in their paper “Use of Piezoelectric Actuators as Elements of Intelligent Structures”. One of the definitions of smart structures is given by Culshaw (1996): “Smart structure is therefore one that monitors itself and/or its environment in order to respond to changes in its condition”. A conceptual diagram of the “smart” structure is shown on Figure 1.1. The traditional mechanical structure is then augmented with sensors, actuators and a control systems which enables the structure to detect and adapt itself in the presence of time-varying environmental and operational conditions. Intelligent structures require support electronics such as power electronics for their powering and digital electronics (computer processor) for control and network communication. Examples of these mechatronic structures include buildings, bridges and roadways that can sense and control damage, aircraft that can actively monitor structural integrity, and automotive components that use active materials to reduce vibrations and enhance performance.

Current research in this domain is directed towards new active materials for actuating and sensing. The miniaturization of active components, particularly in the case of sensors and actuators has been widely explored with the idea of incorporating large numbers of actuators and sensors into the structure. The most obvious omission in intelligent structures

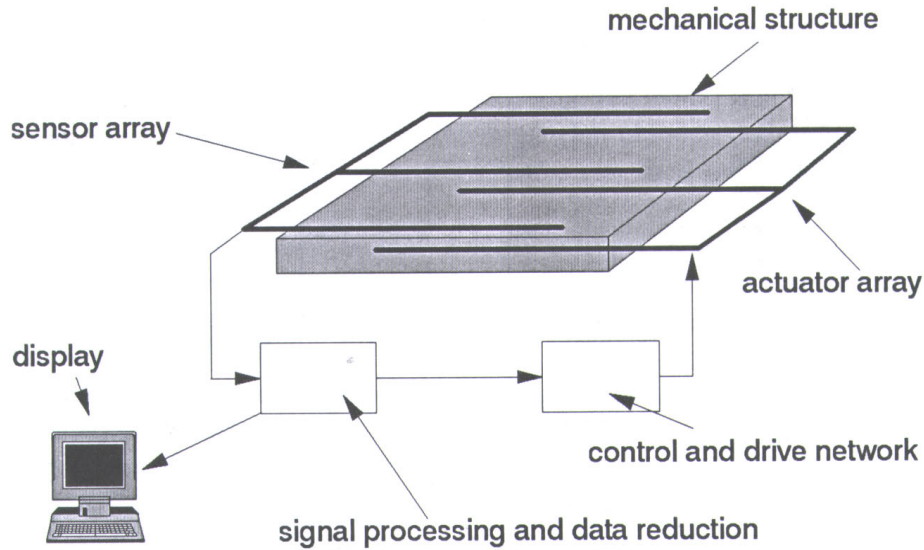


Figure 1.1: Conceptual diagram of the “smart” structure [Culshaw (1996)]

technology, to date, is found in prediction of power requirements and economic feasibility.

Energy requirements are an important design factors in structural control applications. Average power, peak power required and total energy consumed directly influence the size and weight of the overall system. Also, energy dissipated as heat requires the use of heat sinks for thermal management and increasing the supplied energy reduces the effective life-time of the system in battery-operated applications. Hence increasing the overall system efficiency is of tremendous importance especially when size and energy requirements are limited.

This thesis explores the concept of energy regeneration as another alternative to increase the efficiency and life-time of an active or intelligent system. In the following section a literature survey related to the concept of regenerative systems, energy harvesting and power flow analysis is presented.

1.1 Literature Review

1.1.1 Energy Regeneration and the concept of Energy Harvesting

Energy regeneration is a well known concept. A few products based on this principle are commercialized. Commercial applications of energy regeneration are described in this section.

Actual technology in regenerative systems

The self-powered systems or systems that have ability to regenerate part of energy are not only a research trend. Some products using this technology are commercialized today and had a great success. One of them is the Freeplay radio [Freeplay (2002)]. This particular radio device doesn't require any battery or external electrical sources. The required energy is provided by the user who rewinds the radio and stores the energy by compressing set of strip steel springs, which are the primary energy storage device. The steel spring is energized by winding it from one spool to another against a pre-form. As the spring returns to its original position, it applies rotational torque to a transmission, whose output drives a generator. The wind-up radio device achieved its biggest commercial success during the United States military operation in Afghanistan where hundreds of small wind-up radios were dropped along with food ration packs in order to allow the population to be informed with the information broadcasted by the US military [Duffy (2001)].

Another more common self-powered device is the Seiko Kinetic watch. This watch generates electrical energy to power itself, utilizing the movement of the wearer's arm and wrists. The regenerative mechanism is composed of the oscillating weight connected to a rotor which is part of an electromagnetic electrical generator. The generator is connected to a capacitor which stores the electrical energy necessary for operation of the electrical watch circuit [Seiko (2002)].

Piezoelectric-based generators

Following the concept of energy regeneration from different types of parasitic phenomenon, the efficiency of the energy transformers is a key parameter. A few articles and patents on a piezoelectric-based generators are present in literature. Umeda et al. (1997) developed a piezoelectric generator and examined its energy storage characteristics. The generator consists of a steel ball and piezoelectric vibrator. The impact of the ball against the generator produces an electrical energy via piezoelectric effect. A full bridge diode is used to rectify the induced electrical signal from the input and charge the capacitors. The authors achieved a maximum efficiency of 35%. Concerning patents, few examples of PZT generators are found such the one patented by Epstein and Carroll (1996), Hashimoto et al. (1998) and Carroll (2001). All of them convert mechanical strain energy induced in piezoelectric

elements into electrical energy through a rectifying circuit.

Research trends in energy harvesting

Research in regenerative systems is still an important research trend. The Defense Advanced Research Projects Agency (DARPA) lunched an energy harvesting research program in the late 90s. The global objective of this research program was to develop energy storage and conversion components capable of harvesting energy from ambient sources (e.g., solar, wind, thermal, wave-action, electromagnetic radiation, and human activities). One of the examples of research in energy harvesting is the development of a electrical power generating system that extracts energy from the flow of moving water in streams, currents, or pipes. The generating systems are eel-like structures made from piezoelectric polymer films. These “Eels” are scalable in size and have the capacity to generate milliwatts to many watts depending on the system size and the water flow velocity. An illustration of the Eel concept developed by Ocean Power Technologies, Inc is shown in Figure 1.2. Other concepts of en-



Figure 1.2: Energy harvesting eel concept (Ocean Power Technologies, Inc.)

ergy harvesting systems such as compact piezoelectric-based power generator (Continium Control Inc), heel-strike generator using electrostrictive polymers (SRI International and Starner (1998)) and few others are being explored as a part of this program [Nowak (2002)].

Another research trend in regenerative systems is the development of self-powered sensors. Elvin et al. (2001) analyzed and experimentally demonstrated a concept of a self-powered mechanical strain wireless sensor. The novel sensor consists of a piezoelectric material that converts mechanical strain energy into electrical charge. A half-bridge rectifier

is used as a power harvesting circuit which is connected to energy storage devices. The energy stored in the capacitance is then used to power radio frequency (RF) transmitter which transmits the information on strain in the structure sensed by the same PZT element. Elvin et al. (2001) realized a simple beam bending experiment with a polyvinylidene fluoride (PVDF) piezoelectric sensor. The results confirmed the feasibility of a self-powered wireless sensor using mechanical parasitic effects applied to the beam. Some practical limitations such as transmission distance, minimal strain resolution and sensor's lifetime remain as open questions.

The same concept of self-powered sensor is being explored at the Siemens R&D center near Munich, Germany. A team headed by Wolf-Eckhart Bulst has developed an entirely autonomous sensor mounted on car tires in order to provide the information about road condition, traction and pressure. The developed sensor exploits the piezo and pyroelectric effects to provide the power required to transmit a radio signal [Illinger (2001)]. This "smart tire" contains tiny piezoelectric crystals that vibrate when an alternating voltage is applied. The speed at which vibrations travels depends on temperature and pressure, so the embedded sensor can reveal precisely how the tires are "rolling". This sensed information is transmitted through a RF signals to an on-board computer.

Major progress in low power very large scale integration (VLSI) technologies has occurred in the last years pushed by the continuous demand of long battery life in portable systems and heat removal in larger, non portable ones. This progress in VLSI technologies has enabled the possibility of using ambient energy to power future digital systems. A last publication concerning the actual research review in power harvesting is the article written by Amirtharajah and Chandrakasan (1998). In this publication the authors prototyped a Digital Signal Processor (DSP) system powered by its own generator. The DSP and the low power voltage regulator were implemented on a single chip. Amirtharajah and Chandrakasan (1998) modeled and developed an inertial electromechanical generator which was able to produce an average output of $400 \mu W$ from a parasitic vibrations induced by human walking which was sufficient to power DSP application and its power regulating circuit.

1.1.2 Power flow Analysis

Development of regenerative systems is based on the understanding of the power flow between the different parts of the system. Power flow in mechanical structures and in electro-mechanical systems have been widely studied and analyzed. A few related publications are cited in the following.

Power flow in Structures

One of the early references in the power flow in structures is an article written by Lyon and Maidanik (1962) at the origin of the well-known Statistical Energy Analysis (SEA) approach. For a more recent reference on power flow in structures, Miller et al. (1990), performed control optimization analysis in order to minimize power at structural junctions. A thermodynamic approach for analyzing power flow through coupled oscillators has been derived by Kishimoto and Bernstein (1995). The authors showed that the energy flow models based upon thermodynamic energy can be used to predict power flow in mechanical structures. They compared their model to a SEA approach for mechanical systems and demonstrate the flow estimation on system involving three coupled oscillators. In our concept we are interested in regenerating mechanical energy absorbed by the structure and transformed and transferred through an electromechanical actuator into electrical energy. The following section is about the literature on power flow in electromechanical systems.

Power flow in Electromechanical systems

The analysis of power flow through the amplifier and actuator has been discussed by Warkentin and Crawley (1995), Leo (1999), and Zvonar and Lindner (1999). Warkentin shows that actively damping the structure with a controlled piezoelectric actuator causes the mechanical power injected into the structure by the external disturbance source to be absorbed by the structure and funneled to the electrical source. Similar results were presented by Lindner and Chandrasekaran and Lindner (2000) that show that the electrical power at the actuator terminals has a negative real component, which indicate that the actuator feeds electrical power back to the source. Recent work by Chandrasekaran et al. (2000) has demonstrated that the type of feedback control is a factor in determining the real and reactive power flow for a controlled system. An important element in the defined

regenerative control in closed loop is the electrical driver.

1.1.3 Electrical driver, a key element in regenerative systems

Electrical drivers, also called amplifiers, play an important role in electromechanical regenerative systems. Even if design of electrical drivers is out of the scope of this thesis, it is important to understand actual issues and limitations in power electronics. Lindner et al. (2002) discuss the power requirements imposed on four different electrical drivers including switching and linear topologies. As explained later in Section 2.4 only switching type electrical drivers can be used in regenerative systems. A good introduction and explanation of the different switching amplifier topologies for driving electromagnetic based actuators is found in “Fundamentals of Power electronics” by Erickson and Maksimovic (1999). The literature concerning design of switching drives for piezoelectric actuator is more rare. Main et al. (1996) highlights the advantage of using switching amplifier topologies and proposes three different control topologies for driving capacitive-type loads based on pulse-width-modulation (PWM) amplifier scheme. Main et al. (1996) shows direct charge control of piezoelectric actuators removes much of the hysteresis that is inherent in voltage control. Paine et al. (2000) highlights the importance of using bi-directional systems and compares the efficiency of different switching and hybrid topologies for driving a piezoelectric load of $40 \mu F$. Recent work by Chandrasekaran et al. (2001) formulates and solves an optimization problem for the design of a current controlled switching power amplifier. The objective function of the optimization problem is chosen to be the weight of the inductor. The optimized design procedures developed by Chandrasekaran and Lindner takes into account actuator characteristics with its coupling to the mechanical structure.

1.1.4 Actively controlled Vibration Isolation Systems

Actual Active-Passive technology for vibration isolator

In this part of the literature survey, we focused on the systems developed for vibration suppression in space truss structures. With the progress in development of the optical technologies, the issue of parasitic vibrations and micro vibration in satellites carrying this precious equipment is critical for proper operation. Several publications concerning the design of vibration isolator are present in literature. Foshage et al. (1996) developed an

active/passive hybrid actuator for multi-axis isolation and positioning of optical spacecraft payloads that they named Vibration Isolation, Steering, and Suspension (VISS) system. VISS has a complementary active and passive elements to provide passive broadband isolation. The active actuator is a voice coil motor which enables the low-frequency and transmissibility to be reduced with feedback control. Other similar hybrid active systems were developed for similar applications by Vailon et al. (1999) and Anderson et al. (1999). Those systems uses a piezoelectric stack actuator for active vibration suppression. Another hybrid topology is analyzed and prototyped by Sciulli and Griffin (1999). This design incorporates the active components in parallel to the passive design. This is done in the case of a failure of the active system (electrical break down or control instability), the passive system would be able to provide a backup isolation.

Regenerative systems

With respect to the modeling of regenerative system, the only document found was the Ph.D. thesis of Jolly (1993) titled “Passive and Regenerative Solutions for Vibration Control”. In his dissertation, the author developed a general analysis and derived mathematical tools for identifying or incorporating passive and regenerative elements. Jolly’s theory is based on Bond Graph Theory, a graphical based generalized notation which objective is to normalize dynamic system representation [Karnopp and Rosenberg (1968)]. The proposed mathematical approach for system categorization (active, passive or regenerative) is based on the analysis of the impedance matrix of the system[Jolly and Margolis (1997a)]. In order to differentiate the three categories of systems or subsystems, Jolly derives a general expression for power absorption in case of a single input systems and multiple input systems. The theory is applied to few examples such as control of wind response of multi-story structures and vibration control of distributed systems. In a journal publication Jolly and Margolis (1997b) applied the regenerative force actuator to vehicle seat suspension and to a control of vibrations in a lateral elevator. The results showed that for the vehicle seat suspension application, the regenerative force actuator exhibits positive average energy absorption regardless of the nature of the excitation. Furthermore it is shown that the ability to isolate a suspended mass greatly exceeded that of a passive system.

Self-powered Regenerative Control Systems

Nakano et al. (2000) proposed a new method to achieve self-powered active vibration control. The proposed system produces continuous control input using energy absorbed by a damper and does not require external energy. This self-powered control strategy is applied to a two degree of freedom suspension system. The DC motor in the primary suspension is a energy regenerative damper which generates electricity from vibration and charges a condenser. The DC motor in the secondary suspension is an actuator which produces control input using the energy stored in the condenser by the first DC motor. The experimental setup used by Nakano et al. is shown on Figure 1.3.

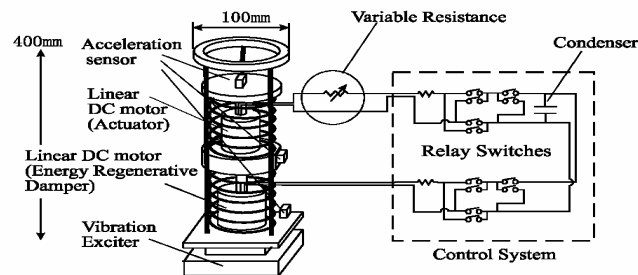


Figure 1.3: Experimental setup developed by Nakano et al. (2000)

The authors propose a control scheme depending on the energy available in the condenser. The mode in which the regenerative damper regenerates vibration energy is called regeneration mode. However, when the magnitude of the induced voltage is less than the voltage of the condenser, the energy-regenerative damper cannot transfer the vibration induced energy to the condenser. In this mode, the energy-regenerative damper halts energy. It is connected to the short circuit and operated as a typical damper, which doesn't regenerate energy. For the motor in the secondary suspension, a skyhook control scheme is applied. In this case the actuator is connected to the condenser and produces control input using the accumulated energy. Through simulation and experiments, Nakano et al. shown that regenerative control scheme achieves better performance than those of the semi-active and passive control.

Nakano et al. (1999) applied the previously described control strategy to cab suspension of a heavy duty truck. As in a previous system an electric generator that is installed

in the suspension of the chassis regenerates vibration energy and stores it in the condenser. An actuator in a cab suspension achieves active vibration control using the energy stored in the condenser. Since the weight of the chassis of a typical heavy duty truck is greater than that of the cabin, vibration energy in suspension of the chassis is expected to be greater than in the cab suspension. Nakano et al. confirmed through simulation that the self-powered active control could be applied to heavy-duty truck and would have better isolation performance than with a semi-active or passive control systems.

The same group of authors also applied their self-powered active control topology to a case of an anti-rolling system for ships [Nakano et al. (2001)]. In order to suppress the rolling motion of a research vessel the authors propose an active system composed of a mass damper with pendulum suspension mechanism. This damper reduces a rolling motion of the ship by the movement of the mass controlled by an electrical motor. In the previous two articles, the self-powered active control systems have two actuators: one actuator produces control force while the other actuator regenerates vibration energy. However, in this article, the proposed anti-rolling system contains only one motor. A trade-off between the closed loop damping and the input energy from a wave-exciting moment is established through simulation. The article concludes with results from an experimental system which confirmed the performance of the simulated system.

1.2 Energy regeneration for active vibration suppression

When addressing the problem of vibration control, the designer is confronted with several fundamental trade-offs. In the case of vibration absorber, improvement in isolation is achieved over a narrow frequency band and usually comes at the expense of increased system weight and size [Inman (2000)]. Active control of vibration represents an important increase in system cost and complexity compared to corresponding passive solutions. While the aforementioned tradeoffs still exist, they are reduced and better performance is obtained with active control. A new trade-off inherent to active control presents itself: power requirement versus level of performance. Also, correlated with power requirements is the size of hardware for power generation or energy storage.

Hence the power requirements imposed on an active vibration isolation systems are quite important to the overall system design. For example active suspension for automobiles

capable of controlling low frequency body motion and higher frequency transmission require power and power generating equipment comparable to that required for the air conditioning [Sharp and Crolla (1987)]. Similarly active noise and vibration control systems designed for space application have the same critical trade-off with power requirements and especially weight and volume requirements. In structural aerospace applications weight and volume are major critical parameters in the overall aircraft or spacecraft design. Therefore, there is a major advantage of using regenerative concepts in active systems designed, associated with weight reduction of heavy and often bulky generators and electrical storage elements. Also the overall energetic efficiency of a vibration isolator is improved since a part of a disturbance input is used for system powering.

Another good reason for using regenerative systems is in suppressing the need for electro-chemical storage devices such as rechargeable batteries. The difficultly controllable risks of leakage or explosions of electrochemical batteries within an extreme temperature variation environment is another issue for implementing active systems for payloads. As the payloads are very sensitive and expensive devices as well as the cost of their launching on orbit, safety conditions and norms on all equipment surrounding the payload are very severe. Avoiding the necessity to use rechargeable batteries by a set of capacitors which will be recharged by a regenerative vibration system will make the actual active systems safer and acceptable in the payload environment.

Energy regeneration technology has been successfully implemented in the case of electrically propelled vehicles which have the ability to feed the kinetic energy occurring during the breaking back into the electrical network using regenerative breaking concept. A comprehensive experimental activity conducted on a electrified subway line of the city of Rome, Italy has permitted to evaluate the energy savings obtained with trains equipped with drives providing regenerative breaking. The obtained measurement recorded significant energy savings: about 19% during the traffic peak, with peak values of 21% [Adinolfi et al. (1988)]

The motivation for regenerative control in the scope of this research was exploring the regenerative possibilities applied to a rocket payload vibration protection. The concept of a regenerative vibration isolator for rocket payloads is illustrated on Figure 1.4. During the take of the transmitted amount of vibrations is not critical. Hence the active actuator is driven in a “regenerative control” mode. In this mode the parasitic vibration energy is

a rectifying circuit. We name this concept “passive” type regeneration due to the fact that the actuator operates in its open loop dynamics. In this case, the regenerative power flow is influenced by the boundary conditions of the electrical circuit which are in this case the rectifying circuit and the storage capacitor. This configuration will not necessarily provide the maximum energy regeneration. The second concept, the one analyzed and discussed in this thesis is a control-based regeneration. In this case a feedback control is applied to the actuator. Structural and electrical parameters are fed back into the control signal of the electrical driver through a regenerative control. The regenerative control concept is illustrated on Figure 1.5. It is important to notice that the electrical driver must have the ability to transfer energy to the batteries. Figure 1.5 also shows the energy losses in each part of the system. In the following analysis we assume an ideal behavior for the electrical driver which implies that all the energy flowing back into the driver is transferred to the storage elements. We also consider a structure without damping in order to simplify the analytical derivations. The regenerated power is analyzed in the case of a single tone (harmonic) vibration disturbance.

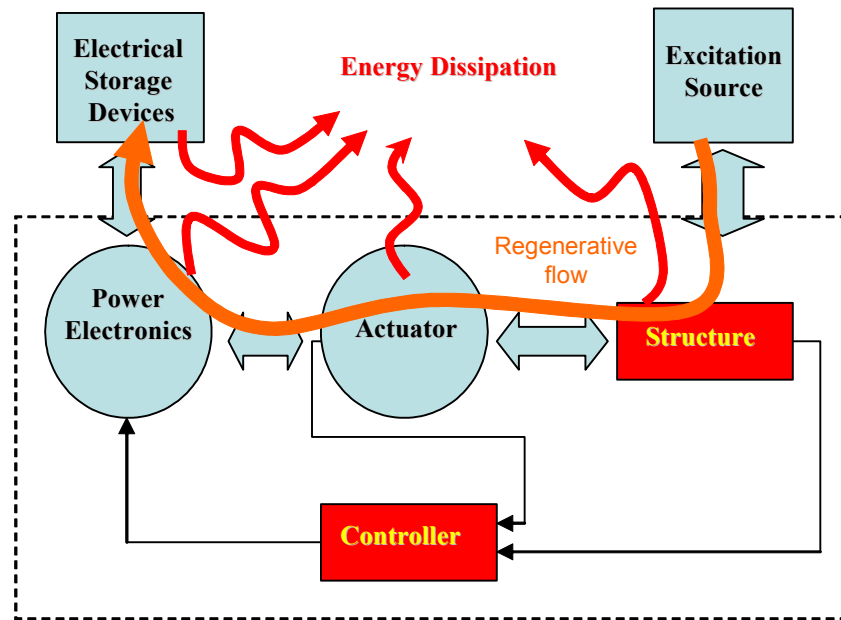


Figure 1.5: Regenerative Control Concept

Several fundamental questions to be answered through this work can now be stated:

- Can we harvest(regenerate) energy from a vibration isolation system in closed loop?
- How should we tune the controller such that the disturbance input energy is transferred through the electromechanical actuator to the electrical driver?
- Is it possible to design a regenerative controller such that we guarantee a maximum energy regeneration?

1.3 Overview of thesis

1.3.1 Research Objectives

The objective of this research is to understand how feedback control applied to an active vibration isolation system influences energy regeneration from disturbance vibrations. Two simplified linear state-space models of a vibration isolator, first-one using electromagnetic actuator technologies and the second one using a piezoelectric based actuator technology are developed. These models assume an ideal behavior of the electrical driver. The reasoning behind it was that once a optimal regenerative control is analyzed, the amount of the maximum regenerative power without the losses in the switching amplifier and storage devices could be estimated as well an initial regenerative efficiency. In order to understand better the influence of feedback control on the regenerated power, a harmonic analysis (single frequency excitation) is performed.

1.3.2 Contributions

In this thesis a 1-DOF electromechanical model for an active vibration isolation system is developed in order to understand the feasibility of regenerative control and its implementation. What differentiates this study from the analysis found in literature is the fact that energy regeneration is done in closed loop and a control problem is formulated in order to optimize energy regeneration. The estimations of efficiency on the amount of input disturbance energy and the output required energy for active control will tell a designer whether the system could be regenerative or will require an external power sources. Also, the simulated regenerated voltage and current quantities provide the design specifications for optimized switching amplifier and electrical storage devices.

An active one degree of freedom (1-DOF) vibration isolation system using a linear electromagnetic (EM) actuator is derived and simulated. An experimental setup using a electromagnetic shaker as actuator was built to demonstrate the regenerative control concept. Following the research trends in development of active structures using piezoelectric-based actuators, a equivalent 1-DOF isolation system with a piezoelectric stack actuator is modeled and simulated.

The two models for the piezoelectric-based and linear electromagnetic (EM) actuator are developed in state-space form, which eventually takes advantage of the software simulation tools that are provided by Matlab. Thus, it is possible to simulate the amount of regenerated power to the vibration disturbance input and quantify the regenerated voltage and current quantities. Also, the state-space model formulation in Matlab enables the future design and estimation of a required power for operation of an active vibration suppression. The fundamental tradeoff for a design of a regenerative system which is the required energy for proper vibration suppression versus the amount of regenerated energy can then be predicted.

1.3.3 Approach

Chapter 2 is a general introduction to regenerative dynamic systems. All the elements of the defined regenerative active vibration system are presented. Two different types of electromechanical actuators: electromagnetic linear motor and a piezoelectric stack actuator are presented and modeled. The constraints on a electrical driver for a regenerative system are defined. Furthermore a generalized state-space model of a piezostructure is derived. The chapter ends with a generalized definition of power and its normalization.

Chapter 3 applies the developed theory to two different type of vibration isolation systems. The only difference between the two systems is the in type of electromagnetic actuator used: voice-coil actuator and PZT stack actuator. After the modeling and comparison of both systems, a normalized expression for electrical power in closed loop is derived and analyzed. The chapter concludes with the derivation of regenerative control laws and their influence on the performance of a vibration isolator.

Chapter 4 is devoted to the design of an experimental setup and to the experimentally obtained results in closed loop. The obtained experimental results are analyzed, compared with simulation and tradeoffs are outlined.

Finally, *Chapter 5* summarizes conclusions, proposes future work and formulates the corresponding recommendations.

Chapter 2

Electromechanical regenerative systems for vibration suppression

2.1 Introduction

This chapter is a general introduction to regenerative dynamic systems. Two different types of electromechanical actuators are presented and modeled. Then the issue of electrical drives is also discussed, specifically for regenerative applications. The last part defines a general expression for power in case of any dynamic system and defines system classification based on their power consumption. The extensive application of regenerative control on two different examples is performed in the following chapter.

2.2 Model of a Piezoelectric stack actuator

This part provides some background information on the piezoelectric effect and how it is used for actuation. The second part is a brief overview of the actual PZT (Lead Zirconate Titanate ceramic) stack actuator technology.

2.2.1 About the piezoelectricity

Definition

A piezoelectric substance is one that produces an electric charge when a mechanical stress is applied. Conversely a mechanical deformation is produced when an electrical field is applied.

The first piezoelectric phenomenon was observed in a quartz colorless crystals such as the “Rochelle salt” (sodium potassium tartrate tetrahydrate, $KNaC_4H_4O_6 - 4H_2O$) by Pierre Curie and his brother Jacques in 1880. They named the effect piezoelectricity (from Greek piezein, “to press”). While the Curies correctly predicted that a voltage difference could be produced from an applied stress on piezoelectric materials, they did not predict the reciprocal behavior of the materials. The reciprocal behavior is just a mechanical stress in response to a voltage difference. This property of reciprocity was mathematically produced from thermodynamic principles by Nobel physicist Gabriel Lippmann in 1881.

Material Properties

Modern piezoceramics capable of greater motion replace the natural material used by the Curies with a ceramic. The most commonly used type of piezoceramics, Lead Zirconate Titanates (PZTs) are solid solutions of lead zirconate and lead titanate, often doped with other elements to obtain specific properties. These ceramics are manufactured by mixing together proportional amounts of lead, zirconium and titanium oxide powders and heating the mixture to around 800 - 1000 °C. They then react to form the perovskite PZT powder. This powder is mixed with a binder and sintered into the desired shape. During the cooling process, the material undergoes a paraelectric to ferroelectric phase transition and the cubic unit cell becomes tetragonal. As a result, the unit cell becomes elongated in one direction and has a permanent dipole moment oriented along its long axis (3-axis) [Jaffe et al. (1954)]. A typical PZT crystal in a raw PZT material is shown on shown on Figure 2.1-(A)

In order to produce the piezoelectric effect, the polycrystal is heated (over the Curie temperature) under the application of a strong electric field ($> 2000 \frac{V}{mm}$). The heat allows the molecules to move more freely and the electric field forces all of the dipoles in the crystal to line up and face in nearly the same direction, see Figure 2.2. This is phenomenon is also called poling. After the application of the high voltage the piezoelectric effect is observed in the crystal and the molecule is poled as shown on Figure 2.1-(B). If the material is compressed, then the voltage of the same polarity as the poling voltage will appear between the electrodes. If stretched, a voltage of opposite polarity will appear (direct piezoelectric effect). Conversely, if a voltage is applied the material will deform. A voltage with the opposite polarity as the poling voltage will cause the material to expand, and a voltage with the same polarity will cause the material to compress (converse piezoelectric effect).

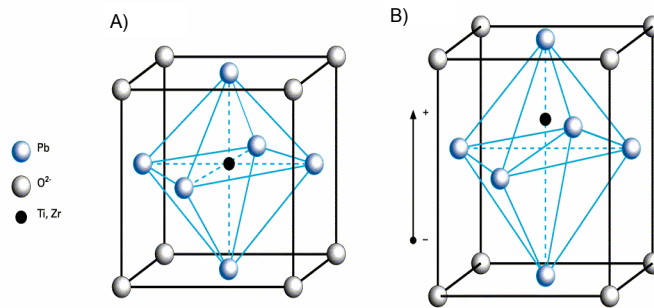


Figure 2.1: Typical PZT crystal: A) before poling B) after poling [Physik Instrumente (2002)]

If alternative and continuous (AC) signal is applied then the material will vibrate.

2.2.2 PZT Stack Actuators (Translators)

PZT stack actuators are composed of thin PZT wafers mechanically connected in series and electrically connected in parallel as represented in Figure 2.3. Two main types of piezo actuators are commercially available: low voltage (LVPZT) devices requiring about 100 V for full motion and high voltage devices requiring about 1000 V for full extension (LHPZT). The main difference between the LVPZT and LHPZT is that low voltage are composed of thin wafers and the high voltage actuators are composed of thicker PZT wafers which require more voltage for extension. HVPZT are constructed from 0.5 to 1.0 mm layers while low voltage piezo actuators are monolithic (diffusion bonded) multilayer designs constructed from 20 to 100 μm layers. Driving HVPZT requires high voltage electrical devices which implies the necessity to use semiconductor components with higher internal resistance. As a consequence, this induces higher losses in the electrical driver.

Model of the Piezoelectric Stack as an electromechanical actuator

In most of the cases the piezoelectric actuator is used in systems where the mechanical system is controlled through the actuator with an electrical system which generates control

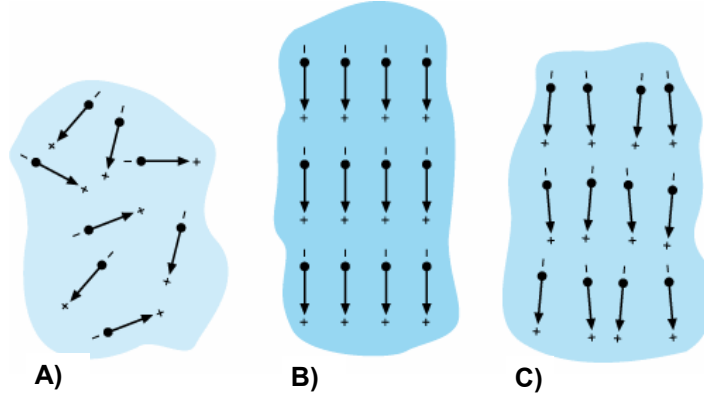


Figure 2.2: Electrical dipole in Weiss domains:(A) unpoled ferroelectric ceramic, (B) during and (C) after polling [Physik Instrumente (2002)]

current or voltage. This is the case in most of the commercially available micro positioning and micro vibration suppression systems using PZT stacks. This section is devoted to the analysis of the electromechanical phenomenon described by the coupled electrical and mechanical constitutive equations. Practical introduction to piezoceramic elements can be found in the catalogs of piezoceramics manufactures such us [Piezo Systems (2000)] and [Physik Instrumente (2002)]. A general scientific analysis of the fundamentals of piezoelectric phenomena is performed by [Ikeda (1990)]. Furthermore, the standards conventions and constitutive equations on piezoelectricity have been established in ANSI/IEEE Standard 176 (1987).

A piezoelectric stack consists of a stack of thin piezoceramic wafers (disks) as shown in Figure 2.3. Various shapes of piezoelectric designs exists, depending on the shape of the wafer and can be found in the [Physik Instrumente (2002)] and [Piezomechanik GmbH (2001)]. The wafers are stacked together in series such that two following wafers are stacked in opposite polling directions. When a positive voltage (in the same direction as the polarization vector) is applied, all the wafers are expanding and similarly, when negative voltage (opposite to the polling vector) is applied all the wafers are contracting. A typical design of a PZT stack actuator and its electrical wiring is shown in Figure 2.3. As an individual PZT wafer the obtained stack of wafers have the same piezoelectric properties. When the stack is mechanically stressed by a force, it generates an electric charge and when voltage

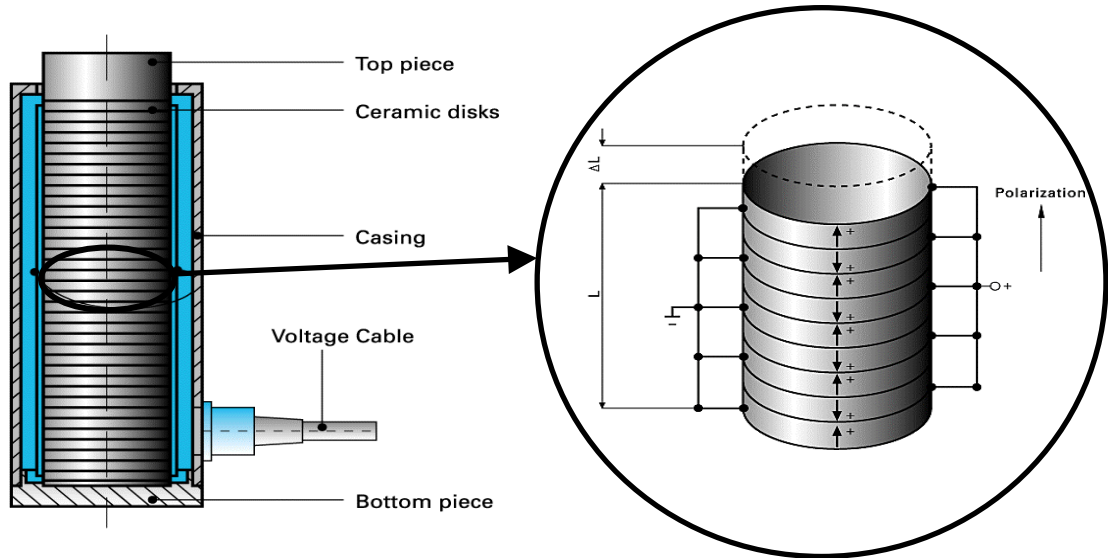


Figure 2.3: Stack design and wafers wiring [Physik Instrumente (2002)]

is applied, the piezoceramic element is “stressed electrically” and its dimension changes. In piezoelectricity standards ANSI/IEEE Standard 176 (1987), properties have subscripts and superscripts, or both. A single subscript gives the direction of the axis of interest. “Piezoelectric coefficient with double subscripts link electrical and mechanical quantities. The first subscript gives the direction of the electrical field associated with the voltage applied, or the charge produced. The second subscript gives the direction of the mechanical stress or strain.” Piezo Systems (2000). For the piezoelectric stack voltage as well as force are applied in the 3 direction. Thus any coefficient x , relating piezoelectric properties will be denoted as X_{33} . Following the standards notation given in Piezo Systems (2000), the following superscripts are used:

T = constant stress = mechanically free

E = constant electrical field = short circuit

D = constant electrical displacement = open circuit

S = constant strain = mechanically clamped

In the case of a piezoelectric stack we assume that the strain in PZT actuator exists only in one direction. Thus, the constitutive equations for a one-dimensional excitation and deformation of a piezoelectric wafer in consistency with [ANSI/IEEE Standard 176 (1987)]

standards are:

$$D_3 = \epsilon_3^T E_3 + d_{33} T_3 \quad (2.1)$$

$$S_3 = d_{33} E_3 + s_3^E T_3 \quad (2.2)$$

where:	D = Electric Density or Flux Density	$\left[\frac{C}{m^2}\right]$
	E = Electric Field	$\left[\frac{V}{m}\right]$
	T = Mechanical Stress	$\left[\frac{N}{m^2}\right]$
	S = Mechanical Strain	$\left[\frac{m}{m}\right]$
	ϵ = Dielectric Permittivity of the Material	$\left[\frac{F}{m} = \frac{C^2}{Nm^2}\right]$
	d = Piezoelectric d-constant	$\left[\frac{m}{V} = \frac{C}{N}\right]$
	s = Mechanical Compliance	$\left[\frac{m^2}{N}\right]$

This two constitutive equations represents the equation of motion of the piezo wafer. They are expressed in the “material coordinates” (strain-charge form) which describes the physical phenomenon of the material. In this approach we are interested in coupling the actuator with a mechanical load and an electrical driver. Therefore, it is very convenient to express equations (2.1) and (2.2) in the conventional electromechanical variables such as voltage/current at the terminals of the stack and force exerted by the actuator and its displacement. In the following the constitutive equations are rewritten in “actuator coordinates”. This approach is brief derivation which is described in details in [Nasser (2000)].

As D_3 represents a charge per area, the electric density will be referred to as the surface charge density, which in Serway (1994) is defined as:

$$\sigma_q = \frac{Q}{A} \quad (2.3)$$

where a uniformly distributed charge Q , on surface area A has been assumed. The subscript “ q ” has been added to distinguish from the mechanical stress “ m ”. The dielectric permittivity of a material, ϵ , is related to the constant of permittivity of free space, ϵ_o , by the dielectric constant [Ikeda (1990)],

$$K = \frac{\epsilon}{\epsilon_o} \quad (2.4)$$

Assuming that the actuator displacement is defined positive when the actuator expands (which also means that positive voltage is applied on the terminals of the stack), the mechanical strain, ϵ_m is defined as,

$$\epsilon_m = S_3 = + \frac{\Delta L}{L}. \quad (2.5)$$

Furthermore, the mechanical stress is defined as:

$$\sigma_m = \frac{F}{A} = \frac{-F_{wafer}}{A} \quad (2.6)$$

and it is negative because F_{wafer} represents the force exerted by single piezoelectric wafer on the element it is acting on.

The electric potential difference between two points, is related to an induced electric field [Serway (1994)]. As a result, then the potential difference and the electric field, can be expressed as:

$$V_{wafer} = E L \quad \Rightarrow \quad E = \frac{V_{wafer}}{L} \quad (2.7)$$

Substituting equations (2.3),(2.4), (2.5), (2.6) and (2.7) into the constitutive equations (2.1) and (2.2) we obtain the new equation of motion for a single wafer,

$$\frac{Q_{wafer}}{A} = k \epsilon_o \frac{V_{wafer}}{L} - d_{33} \frac{F_{wafer}}{A} \quad (2.8)$$

$$\frac{\Delta L}{L} = d_{33} \frac{V_{wafer}}{L} - s_{33}^E \frac{F_{wafer}}{A}. \quad (2.9)$$

Assuming that the stack actuator is composed of n identical PZT wafers as shown on Figure 2.3, the previous set of electromechanical equations of motions can be integrated for the full PZT actuator,

$$Q_{pzt} = n Q_{wafer} = \frac{n k \epsilon_o A}{L} V_{pzt} - n d_{33} F_{pzt} \quad (2.10)$$

$$x_{pzt} = n \Delta L = n d_{33} V_{pzt} - \frac{n s_{33}^E L}{A} F_{pzt}. \quad (2.11)$$

By inspection, the expression $\left(\frac{n k \epsilon_o A}{L}\right)$ represents the capacitance of the PZT stack C_{pzt} in stress-free configuration and $\left(\frac{n s_{33}^E L}{A}\right)$ represents the compliance of the stack actuator

$\frac{1}{k_a}$ in short circuit condition. Finally, the new piezoelectric coefficient $n d_{33}$ is renamed by x_o . This coefficient represents the “strain constant” of the hole actuator and its units are $[\frac{V}{m}]$. The previous equations (2.10) and (2.11) are rewritten with the new constants and the desired constitutive equations are obtained,

$$Q_{pzt} = C_{pzt} V_{pzt} - x_o F_{pzt} \quad (2.12)$$

$$x_{pzt} = x_o V_{pzt} - \frac{1}{k_a} F_{pzt}. \quad (2.13)$$

The obtained set of equations sacrifices the physical aspects of the IEEE constitutive equations for a more convenient set of constants and variables. The advantage of this representation of constitutive equations for a stack actuator are that for a given actuator all its characteristic coefficients can be obtained experimentally. For example the capacitance of the stack C_{pzt} actuator can be obtained by a simple electrical measurement. The stiff-

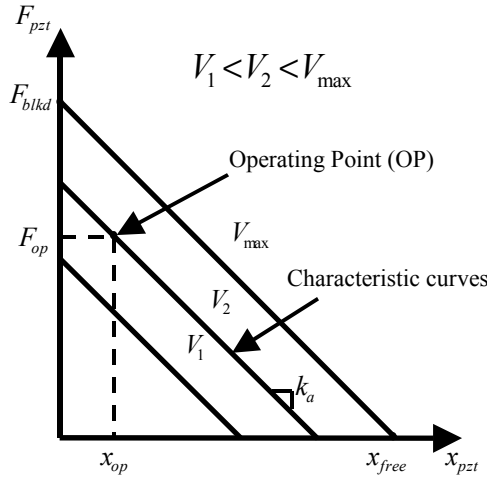


Figure 2.4: Force-stroke characteristic curves

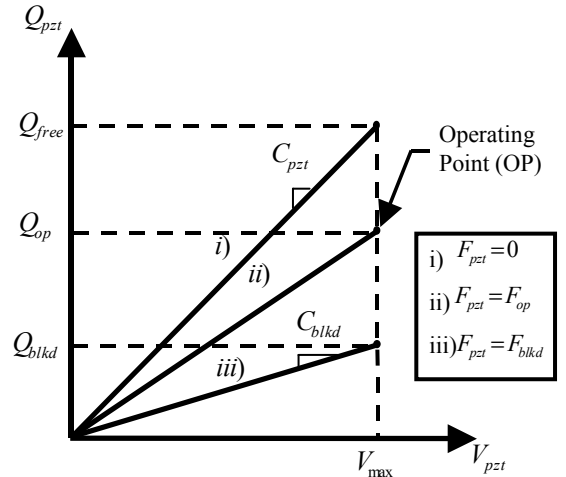


Figure 2.5: Charge-voltage characteristic curves

ness of the actuator k_a can be determined, for example from a frequency response function analysis. Finally the new strain constant x_o is obtained by taking the ratio of the free displacement (no load on the actuator) and the applied voltage. Assuming that the stack actuator operates in its linear region, we can plot the force-displacement characteristic curve and the charge-voltage characteristic curve for the stack. Under free operation, or no load,

the stack doesn't exert any force and equation (2.13) reduces to $x_{pzt} = x_o V_{pzt}$. Thus, this represents the free displacement of the stack denoted as x_{free} . Similarly, if the stack operates under a load such that the displacement is x_{pzt} is zero then equation (2.13) reduces to $F_{pzt} = k_a x_o V_{pzt}$. This expression represents the blocked force of the PZT stack and it is denoted F_{blkd} . The force-displacement and charge-voltage characteristic curves are shown respectively on figures 2.4 and 2.5

2.3 Linear Electromagnetic actuators

In this part we will briefly introduce the permanent magnet linear DC electromechanical actuator. The following section discusses the basics of the magnetic circuit configurations and the electromechanical coupling equations with the assumed linear behavior. The goal is to provide a basic understanding of how voice coil actuators work and then derive the electromechanical equations. More detailed analysis of this type of actuator are done by Beranek (1954).

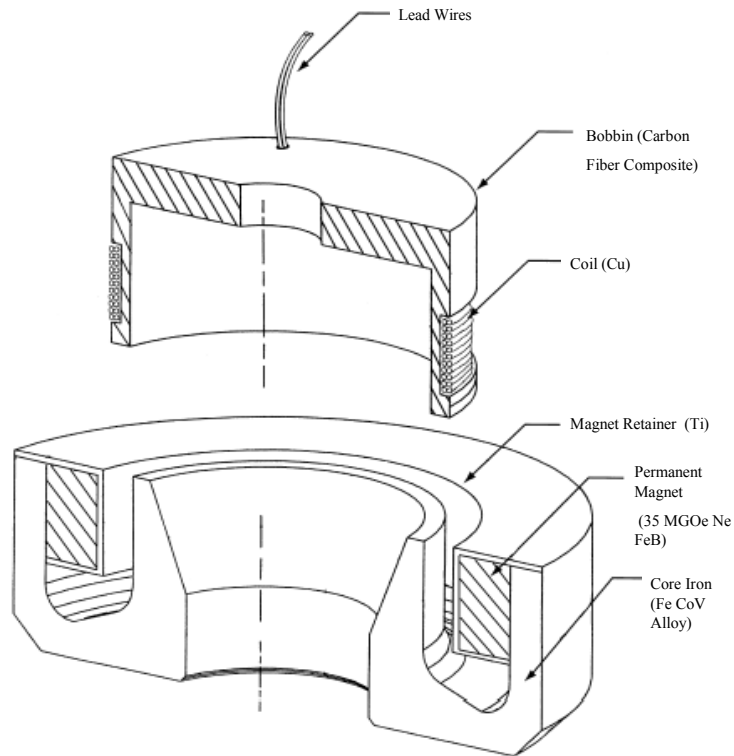


Figure 2.6: Voice Coil Motor Cross-section (Honeywell)

In its simplest form, a linear voice coil actuator is a tubular coil of wire situated

within a radially-oriented constant magnetic field as shown in Figure 2.6. This magnetic field is produced by permanent magnets embedded on the inside diameter of a ferromagnetic cylinder. This cylinder is arranged so that the magnets facing the coil are all of the same polarity. When current is applied to the circumferentially-wound coil, it interacts with the radial magnetic field of the permanent magnet assembly via the Lorentz Force Principle to create an axial force. The Lorentz force relation is represented by the cross product,

$$\vec{F}_{vc} = \vec{i}L \times \vec{B} = B L i \cos(\theta), \quad (2.14)$$

where B represents magnetic flux density, L the length of the conductor, i conductor current and θ is the angle between the direction of magnetic flux and conductor current. For the general case, the voice-coil linear actuators are designed such that θ is equal to 90° . This relationship described in equation (2.14) is a simplest view of the phenomenon. In reality, the force constant ($Bl i$) is dependant upon current and stroke but in the following we assume an ideal linear behavior. Applying the Lorentz force to the case of a voice coil actuator, the force developed by the actuator is,

$$\vec{F}_{vc} = \pi D_c N B i = Bl i, \quad (2.15)$$

where, D_c represents the diameter of the coil, N number of turns per coil, i coil current and $Bl = \pi D_c N B$ is the electromagnetic constant of the actuator. Conversely, forcing the coil to move in the magnetic field with velocity $\frac{dx}{dt}$ induces a voltage also called back electromotive force $V_{bemf}(t)$ in the coil,

$$V_{bemf}(t) = Bl \frac{dx}{dt}. \quad (2.16)$$

The mechanical equation of motion of the electrical actuator is,

$$M\ddot{x} = -k_a x - c_a \dot{x} + Bl i = F_{EM}, \quad (2.17)$$

where M is the mass of the moving member, k_a the equivalent stiffness of the actuator, c_a friction coefficient. Assuming the moving mass is negligible compared to the driven load and neglecting the friction, the displacement of the actuator x_{EM} of the actuator is[Nasar and Boldea (1987)],

$$x_{EM} = -\frac{1}{k_a} F_{EM} + \frac{Bl}{k_a} i. \quad (2.18)$$

The voltage equation for the coil is,

$$V = Ri + L_c \frac{di}{dt} + Bl \dot{x}_{EM}, \quad (2.19)$$

where R and L_c are respectively the resistance and the inductance of the coil. As the $R \gg L_c$ the equation (2.19) reduces to [Nasar and Boldea (1987)],

$$i = \frac{V}{R} - \frac{Bl}{R} \dot{x}_{EM}. \quad (2.20)$$

2.4 Electrical Power Supplies

Electrical power supplies and amplifiers (also called electrical drivers) are crucial components in electromechanical actuation systems. Their role consists of adapting the electrical network input power into the desired voltage and current waveforms required by the actuator for proper operation. They process the controlled low power command signal and transform the input electrical power waveforms into the commanded output power signal. In the closed loop feedback systems, the low power command input signal is amplified by the controller, when in the open loop case the command signal is determined by the user through appropriate signal generation.

In regenerative applications it is important to have an electrical amplifier which will allow the current to flow not only from the network source to the actuator but also from the actuator through the amplifier back to the input source. An important characteristic of an electrical amplifier is its efficiency which is defined as a ratio of input and output power provided to the actuator. In particular for regenerative applications, efficiency is an important issue due to the fact that the goal is to recover as much energy as possible and minimize energy dissipation. In the next two sections, two different topologies of electrical supplies are presented and discussed. Characteristics, limitations and losses estimation are specifically developed with the respect to a regenerative application.

2.4.1 Power Operational Amplifiers

The simplest way to envision a Power-Operational amplifier is to think of it as a conventional operational amplifier (op amp) built with high voltage transistors and physically large output devices. In fact, some of the earliest power operational amplifiers were built by combining a high voltage, low current op amp with an output stage made from high

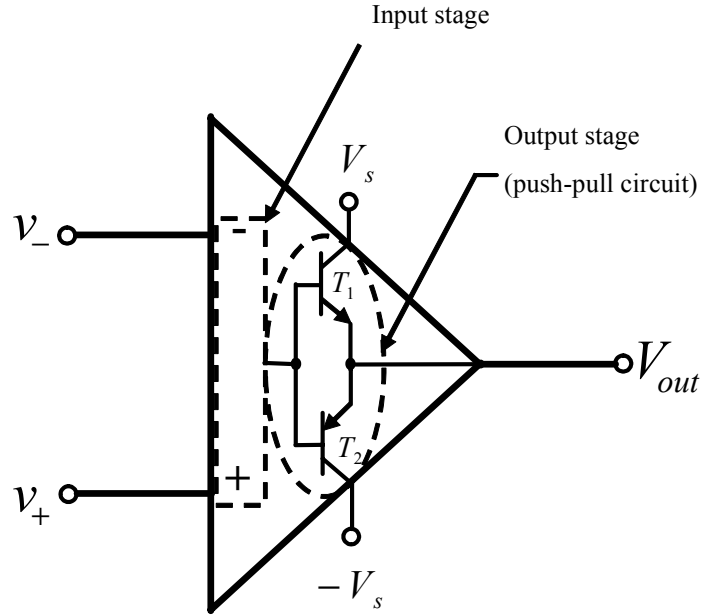


Figure 2.7: Power Operational Amplifier

current Darlington transistors. In this analysis we assume that the op amp is operating in its linear region (not saturated) and we want to determine an expression for dissipated power. The output stage is assumed as in Figure 2.7, to be a push-pull stage composed of two power transistors. Dissipations due to the base-emitter voltage drops, base currents of the transistors and dissipation in earlier stages are orders of magnitude less compared to those in the power stage. They are then neglected and considered as quiescent power dissipations which means independent of the output conditions of the amplifier driving a given load.

The operation of the output push-pull stage is shown on Figure 2.8. Depending on the sign of the voltage across the load, either T_1 or T_2 are allowing the flow of current from the source. When voltage across the load is positive T_1 is activated (T_2 is off) and a pass is established between the load and the source V_S . In the same manner when the voltage across the load is negative, T_2 is activated (T_1 is off) and the pass between the current sink $-V_S$ and the load is established. Figure 2.8 summarizes the operation of the push-pull circuit.

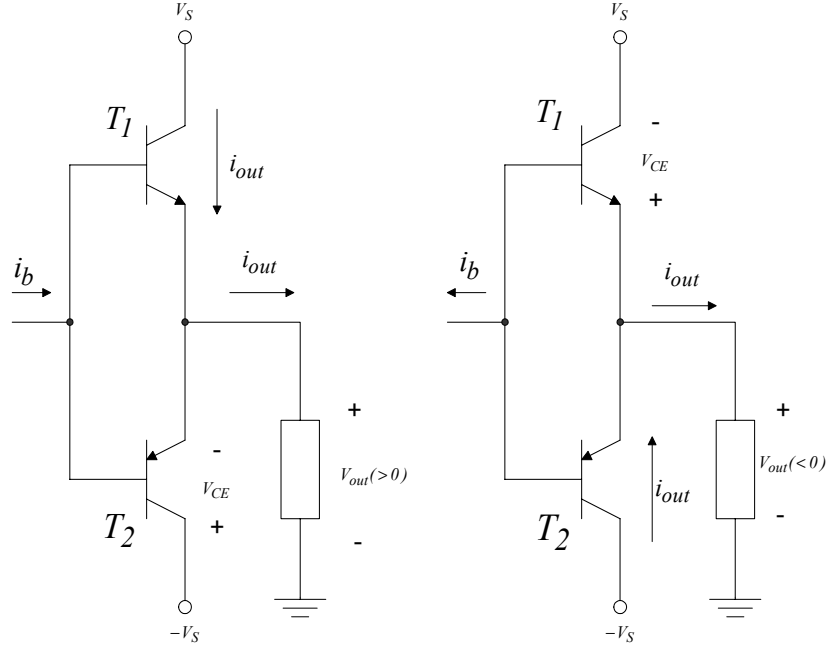


Figure 2.8: Push-pull circuit

The expression of dissipated power is then [Warkentin and Crawley (1995)],

$$\begin{aligned}
 P_{T_1} &= \begin{cases} (V_s - V_{out})i_{out}(t), & i_{out}(t) > 0 \\ 0, & i_{out}(t) < 0 \end{cases} \\
 P_{T_2} &= \begin{cases} 0, & i_{out}(t) > 0 \\ (-V_s - V_{out})i_{out}(t), & i_{out}(t) < 0. \end{cases}
 \end{aligned} \tag{2.21}$$

Then the total power dissipated by the amplifier is given by,

$$P_{amp}(t) = -i_{out}(t)V_{out} + |i_{out}|V_s, \tag{2.22}$$

where the first term represents the power flow to the actuator and the second is power drawn from the actuator. From this expression we notice that in the linear operational amplifier power sources even when the load is reactive (pure capacitor or inductor) the amplifier dissipates the energy due to the reactive current flow. The losses in the linear amplifier could be minimized when the amplifier supply voltage V_s is nearly equal to the voltage V_{out} supplied to the load [Leo (1999)].

2.4.2 Switching amplifiers

The second type of amplifier are switching amplifiers. In recent years, this type of amplifier has experienced large growth and development due to the confluence of several factors but

in most due to the progress in semiconductor industry. A switching amplifier is composed of a constant DC source, switching circuit and an output filter. The DC source can be a battery or rectifier stage (AC to DC converter). The DC source is connected to a switching circuit which is composed of controlled switches such as MOSFETs, IGBTs, BJTs, GTOs or thyristor depending of the type of the converter. During the operation the switches are actuated with a control signal at very high frequency compared to the frequency of the desired output signal as shown on Figure 2.9. This type of switching operation is called Pulse Width Modulation (PWM). In most of the cases the switching frequency is constant and fixed. If the high output is commanded, the switch is held on most of the period. As less output is commanded, the duty cycle or percent of time on is reduced. The switch is usually both on and off once during each cycle of the switching frequency.

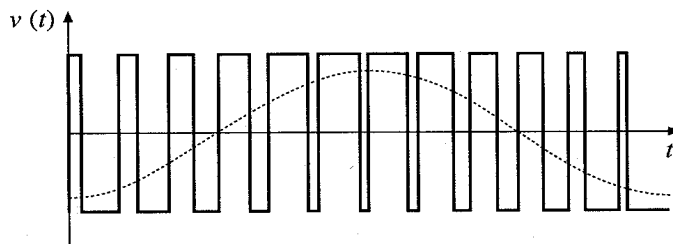


Figure 2.9: Typical pulse-width-modulated switch voltage waveform [Erickson and Maksimovic (1999)]

The output filter is in most cases composed of an inductor. The function of the inductor is both storing energy during the off portion of the cycle and for filtering. As an inductor require continuous current flow, they become the energy sources during the off time. In this manner the load “sees very little” of the switching significantly below the switching frequency.

As the switching amplifiers are composed of switches and reactive components the losses are theoretically equal to zero. As all real electrical components have a resistive part, the losses in switching amplifiers exist and are mostly due to resistance of the inductor and switches. Also each switch requires a turn-on and turn-off time which also generates power losses. Efficiency of PWM circuits may reach efficiencies up to 90% [Mohan et al. (1989)].

There is no universal expression for a dissipated power in a switching amplifier

because the losses are dependent on the type of switches, inductors and control electronics. A good estimation can be obtained by computing the switching losses per switch $P_{switching}$ and the “on time” losses per switch, P_{on} which can be defined per switch [Mohan et al. (1989)],

$$P_{switching} = \frac{1}{2} V_{ds} I_{ds} (t_{rise} + t_{fall}), \quad (2.23)$$

$$P_{on} = V_{ds} I_{ds} d, \quad (2.24)$$

with V_{ds} , I_{ds} , t_{on} and t_{off} respectively switch voltage, current, turn on and turn off time and d duty ratio defined as the ratio of time at which the switch is on and the switching frequency of the amplifier. The rough estimation of the losses is obtained by adding the switching and on time losses and multiplying them by the number of switches.

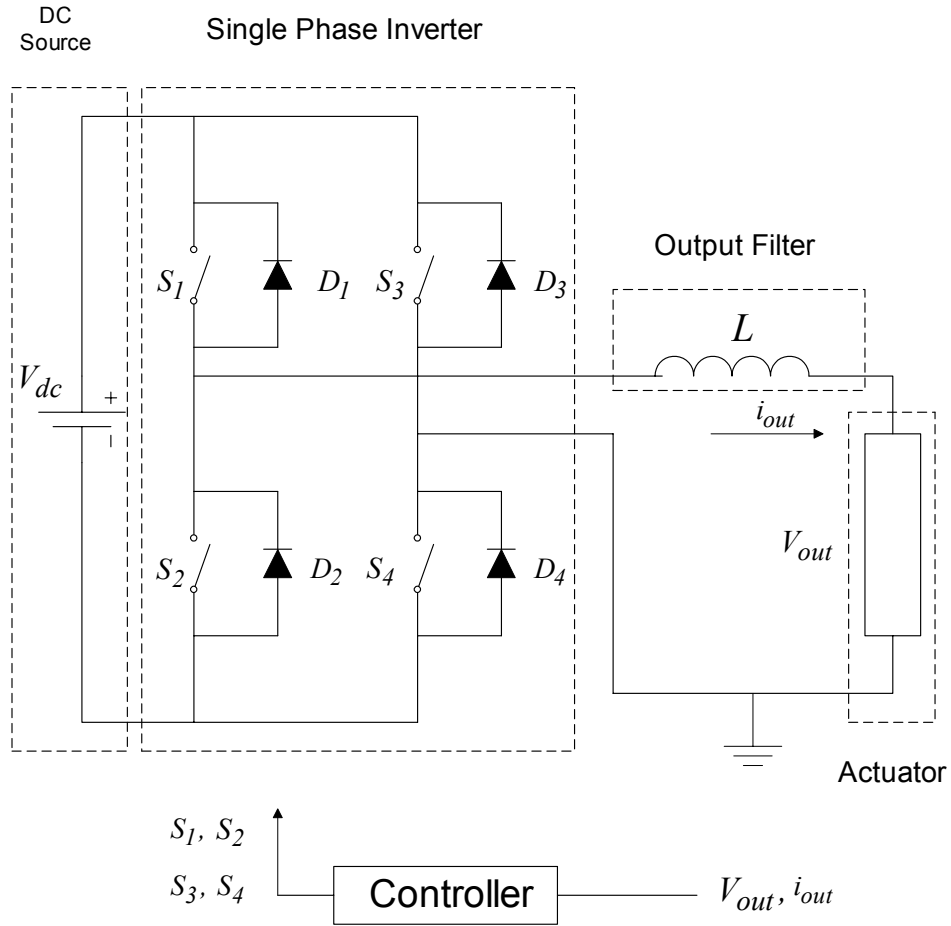


Figure 2.10: Bi-Directional Single Phase Inverter

An interesting family of switching amplifiers are current bi-directional switching amplifiers. In regenerative operation electromechanical actuators are generating power. By using current bi-directional amplifiers the generated power from the source can be used for charging the battery (DC source). A typical current bi-directional switching H-bridge inverter(converts DC to AC) is shown on Figure 2.10. When switches S_1 and S_2 are turned on simultaneously(S_2 and S_3 are turned off), the positive voltage appears at the load terminals. Similarly, when S_2 and S_3 are simultaneously turned on (S_1 and S_2 are turned off), negative voltage appears on the load terminals. If the load is unipolar then a half of the H-bridge (S_1 and S_2) is enough to drive the circuit. The diodes connected in parallel with the switches allows the current to flow from the load (actuator) to the source (battery) as shown on Figure 2.11.

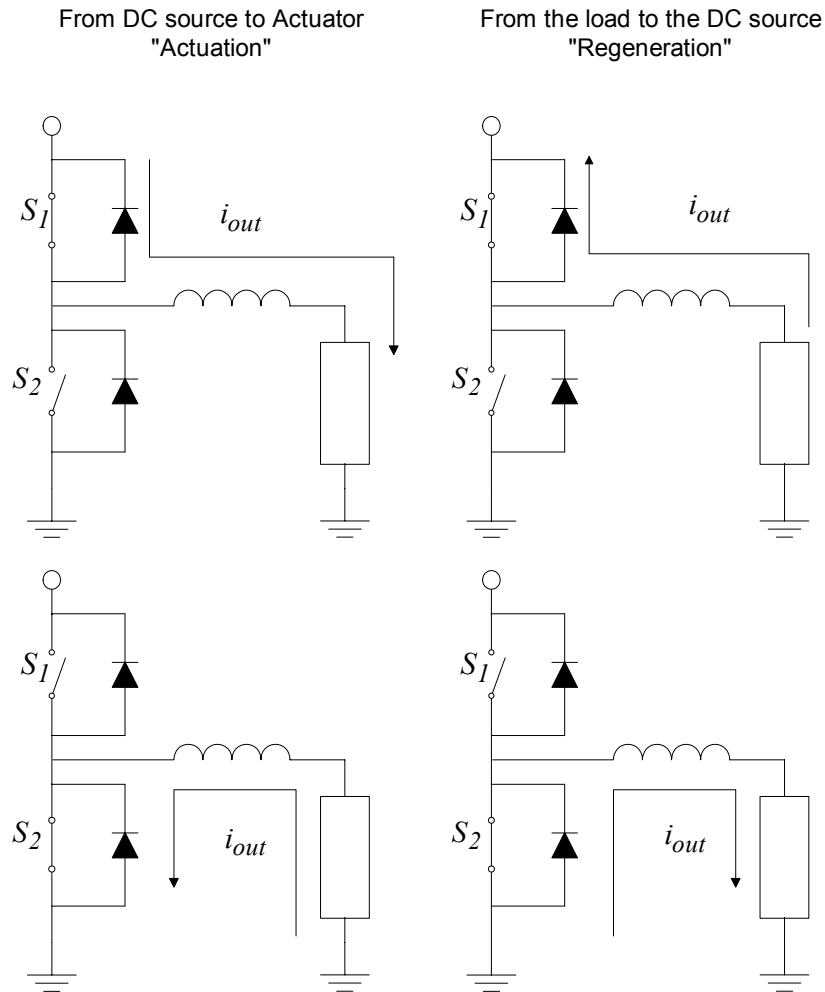


Figure 2.11: Operational Principle of a Bi-Directional current inverter

2.4.3 Conclusion on Electrical Power Supplies

This analysis shows that energy regeneration is possible only if bidirectional switching amplifier topology is used for driving the actuator. In the case of the linear power amplifiers the regenerative flow will be dissipated in the amplifier to a permitted level and after that level the back flow will permanently damage the operational amplifier. Therefore by using an amplifier based on bi-directional switching topology will allow the system to recover a part of energy when the external disturbance is transformed by the way of an electromechanical actuator into electrical energy and then transmitted through the amplifier into the battery or set of capacitors. Although switching amplifiers are very efficient compared to power op amps they have some drawbacks. The disadvantage of using switching amplifiers is in their complexity and dependence on the actuator electrical load. They also induce distortions into a desired signal due to the high frequency noise that can not be completely filtered out. The good indicator of the switching amplifier distortion is the total harmonic distortion (THD) index defined for current as [Mohan et al. (1989)],

$$THD_i = \sqrt{\sum_{h \neq 1} \left(\frac{I_{sh}}{I_{s1}} \right)^2}, \quad (2.25)$$

where I_{s1} is the magnitude of the fundamental and I_{sh} are the magnitudes of the harmonics. A similar index THD_v can be expressed by using voltage components in equation (2.25).

2.5 Power absorption in a single input system

This part defines the theory on system classification. In the first part the general expression for power for any physical system is presented and discussed. Then depending on the power properties of a system a classification is established.

2.5.1 Generalized definition of Power and system classification

In this section the basic modeling tools for analyzing power absorption are described. From an analysis standpoint, systems, subsystems and components are defined by a series of nodes (ports) on which the environment can act. Karnopp and Rosenberg (1968) normalized the system representation with the use of Bond Graph method. This graphical modeling technique provides a uniform mechanism for the description of a wide variety of physical

Table 2.1: Effort and flow quantities for various dynamic systems.

Domain	Effort, $e(t)$	Flow, $f(t)$
Mechanical translation	Force component, $F(t)$	Velocity component, $v(t)$
Mechanical rotation	Torque component, $\tau(t)$	Angular velocity, $\omega(t)$
Electrical circuit	Voltage, $v(t)$	Current, $i(t)$
Hydraulic systems	Pressure, $P(t)$	Volume flow rate, $q(t)$

systems. Bond Graph representation highlights the power and energy exchanges between systems and subsystems. In order to represent the power flow the choice of variables to be chosen in the input and output ports of the system are very important. Karnopp and Rosenberg (1974) also normalized the port variables to be represented. The variables for any ports are forced to be identical when two multiports are connected and are called power variables because the product of two variables considered as function of time is the instantaneous power flowing between the two ports. The generalized names and notation for the two variables have been defined as effort $e(t)$ and flow $f(t)$. Table 2.1 lists effort and flow quantities for a variety of dynamic systems. The instantaneous power, $p(t)$ flowing into or out of a port can be expressed as product of an effort and a flow variable, and thus in general notation is given by the following expression,

$$p(t) = e(t)f(t). \quad (2.26)$$

When effort and flow are periodic variables in time, it is common to define the average instantaneous power in time denoted P ,

$$P = \frac{1}{T} \int_0^T e(t)f(t)dt = \frac{1}{T} \int_0^T p(t)dt, \quad (2.27)$$

where T represents the period of the effort and flow variables. In frequency domain, equation (2.27) becomes [Hambley (1997)],

$$P(j\omega) = \frac{1}{2} \text{Re} [e(j\omega)^* f(j\omega)] = \frac{1}{2} \text{Re} [e(j\omega) f(j\omega)^*]. \quad (2.28)$$

Depending on the sign of the scalar P a direction of the power flow can be deduced. It is also important to specify if either generator or load convention is used to define the port in order to define the flow of power. In generator convention effort and flow are in the same directions while in load convention the effort and flow are in opposite directions.

This convention arises from the fact that the scientific community wanted to avoid negative values for power which may introduce confusion. If the power is a positive scalar then it means that the effort and flow variables are in the same direction and the power is being delivered in a generator convention and being absorbed in a load convention. Likewise when the power is an negative scalar that means that the power is being absorbed in the generator convention and being delivered in load convention.

As a general expression of power has been defined a system classification based on energetic properties can now be established. In the following section a system classification based on their energy absorption or generation is presented.

2.5.2 System classification

A dynamic system is a collection of components that change with time in response to environmental inputs which are external to a system. The analyst has a liberty to define what is called the environment, the dynamic system and the components. In other words, it is the analysts job to break up large systems hierarchically based on the scope of information desired. Usually, the system lives in an environment, but is assumed dynamically separable from the environment. A system might be composed of multiple subsystems which as well as a simple system are composed of fundamental elements called components. In each analysis hierarchies between all this elements are defined to yield specific information. Nevertheless this hierarchy and the system breakup is never absolute, what might be a component to one analyst may be a subsystem to another analyst. Components are traditionally broken into three categories: passive, active and regenerative components.

It is intuitively known that the average power absorption in a passive subsystem is always positive regardless of the input. A very common example of passive mechanical components are springs, masses and dampers. Active components are those which require power from an external, dynamically separate source. Systems composed of only passive elements are called passive systems and those which consist at least of one active component are called active systems or subsystems.

Regenerative system are more difficult to define. In a regenerative component net power that flows in, is stored rather than dissipated (passively or actively) and stored power is drawn on to create efforts of which passive components are incapable. A very important characteristic of a regenerative system is that during operation more energy, on average,

flows into the component then flows out. A system or subsystem which consists of at least one regenerative component is called regenerative system or subsystem. A mathematical approach for system classification is developed by Jolly (1993). This analysis is based on a analysis of the impedance matrix Z which maps nodal flows f into corresponding nodal efforts e . In order to distinguish the difference between regenerative and passive systems the average power absorption of the analyzed system has to be performed. In our approach we do not follow the theory developed by Jolly since we decided to keep a modern (state-space) control approach.

2.6 Summary

Two different types of electromagnetic linear actuators have been presented along with two different types of electrical drivers. It was shown that only switching amplifier topologies can be used in regenerative systems. A general expression for power determination in frequency domain has been established and then a system classification based on power absorption/generation was deduced.

In the next chapter an active vibration isolation system is modeled for a case of an electromagnetic and piezoelectric actuator and electrical power flow in closed loop is analyzed.

Chapter 3

Two examples of active vibration isolator and their power flow analysis in closed loop

3.1 Introduction

The purpose of this chapter is to apply the theory developed in the previous chapter to two different examples. In both cases an active vibration isolation problem is considered. In the first example the active system is realized through a linear electromagnetic (EM) actuator (voice-coil actuator). The second example uses the same system but with a piezoelectric stack actuator instead of an EM actuator. In both cases the influence of feedback control is studied in order to obtain a regenerative power flow through feedback control for a harmonic vibration disturbance. Different control strategies are analyzed and the analysis is focused on determining control law which will “force” the flow to be regenerative and find a law which maximizes energy regeneration. First a set of numerical simulation with a single frequency disturbance were performed using pole placement and Linear Quadratic Optimum Control (LQR) algorithms [Friedland (1986)]. As both of this techniques were not ensuring regenerative power flows, a need for derivation of an analytical expression of electrical power is necessary for understanding how the feedback control influences the power flow. Hence in the following a case of vibration isolation is studied but the applied control strategy is examined and evaluated from the power regeneration point of view. In

fact our first objective is to understand how feedback control can obtain a regenerative flow and how can we maximize this regeneration of energy.

The first two parts of this chapters derive a normalized electromechanical state-space equation for both vibration isolation cases. Then the two normalized state-space models are compared and the normalized electrical power expression is derived and analyzed. From this analysis, four different regenerative control strategies (cases) are examined. The chapter concludes with the influence of the regenerative control on the performance of a vibration isolator.

3.2 Example of an active vibration isolation system realized with an Electromagnetic (EM) actuator

An active vibration isolation system is composed of a base connected to the payload by the way of a voice-coil actuator and an additional spring in parallel with the actuator (see Figure 3.1). In the ideal situation an external disturbance excites the base, the voice-coil counteracts the disturbance and cancels the disturbance. This prediction and counteraction of the disturbance is obtained by sensing a set of parameters such us displacement, velocity, coil current and feeding those back through voltage.

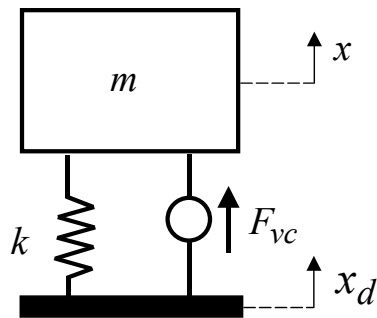


Figure 3.1: Vibration isolation system

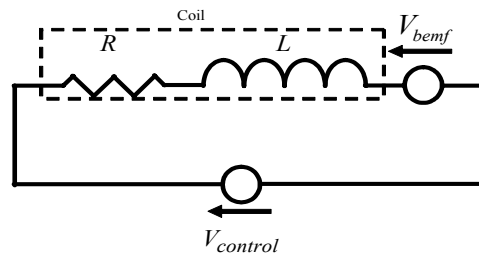


Figure 3.2: Electrical circuit in a case of a EM actuator

3.2.1 Modeling of the electromagnetic system

The modeling of the linear electromagnetic actuator is described in Section 2.3. In the case of an ideal voice-coil translator, the force is linearly proportional to applied current over a wide frequency range. If the structure is assumed to be without damping then the system

represented on Figure 3.1 has the following equation of motion,

$$m\ddot{x} = -kx + kx_d + F_{vc}. \quad (3.1)$$

By defining a relative coordinate system x_r which represents the stroke of the actuator,

$$x_r = x - x_d, \quad (3.2)$$

and combining equations (3.1) and (3.2) we obtain the equation of motion,

$$\ddot{x}_r = -\frac{k}{m}x_r + \frac{Bl}{m}i - \ddot{x}_d. \quad (3.3)$$

Applying the second Kirchoff law on the circuit shown on Figure 3.2, we obtain the second differential equation,

$$\frac{di}{dt} = -\frac{R}{L}i + \frac{V}{L} - \frac{Bl}{L}\dot{x}_r. \quad (3.4)$$

In order to study the influence of the feedback control on the power flow in this system equations (3.3) and (3.4) are normalized with non dimensional quantities. This will make the system of equations (3.3) and (3.4) easier to manipulate.

3.2.2 Normalization of the differential equations in the case of a linear electromagnetic actuator

In non dimensional variables, equation (3.3) is rewritten as,

$$\zeta_m'' = -\zeta_m - \phi_m + \Omega \tilde{x}_d. \quad (3.5)$$

The disturbance x_d is assumed to be harmonic for this analysis. Hence, x_d is defined as,

$$x_d = X_{od} \tilde{x}_d, \quad (3.6)$$

where X_{od} is the amplitude of the harmonic function and $\|\tilde{x}_d\| = 1$. The normalized displacement ζ_m is then defined as $x_r = X_{od} \zeta_m$. The disturbance frequency ω is normalized by the mechanical natural frequency defined as $\omega_n = \sqrt{k/m}$ such that $\omega = \Omega \omega_n$. The normalized voltage \tilde{v} and current ϕ_m are respectively defined as $\tilde{v} = \frac{V}{V_n}$ and $\phi_m = \frac{Bl}{kX_{od}}i$ with $V_n = \frac{kLX_{od}\omega_n}{Bl}$. Also, a new differential operator $d/d\tau$ defined as

$$\frac{d}{dt} = \frac{1}{\omega_n} \frac{d}{d\tau} = \frac{1}{\omega_n} (\cdot)'. \quad (3.7)$$

Substituting the normalized quantities into equation (3.4) we obtain the normalized electrical equation,

$$\phi'_m = -\beta\phi_m - \psi_m\zeta'_m + \tilde{v}. \quad (3.8)$$

The coupling coefficient ψ appears in this normalized electrical equation as,

$$\psi_m = \frac{(Bl)^2}{kL}. \quad (3.9)$$

The time constant τ_{el}^m , defined as $\tau_{el}^m = R/L$, and the natural frequency are combined in the new constant β_m such that $\beta_m = \frac{1}{\tau_{el}^m\omega_n}$. The equations (3.6) and (3.8) can be cast in a first order state-space equation,

$$x'_m = A_m x_m + B_m u_m + F_m x_d, \quad (3.10)$$

where x_m is a state vector defined as $x^T = [\phi_m \ \zeta_m \ \zeta'_m]$. The normalized voltage and current output are formulated through two output equations,

$$\phi_m = C_{\phi_m} x_m, \quad (3.11)$$

$$\tilde{v} = C_{\tilde{v}} x_m, \quad (3.12)$$

where A_m , B_m , $C_{\tilde{v}}$, C_{ϕ_m} and F_m are time invariant coefficient matrices defined as,

$$A_m = \begin{bmatrix} -\beta_m & 0 & -\psi_m \\ 0 & 0 & 1 \\ 1 & -1 & 0 \end{bmatrix}, \quad B_m = \begin{bmatrix} 1 \\ 0 \\ 0 \end{bmatrix}, \quad F_m = \begin{bmatrix} 0 \\ 0 \\ \Omega \end{bmatrix}, \\ C_{\phi_m} = \begin{bmatrix} 1 & 0 & 0 \end{bmatrix}, \quad C_{\tilde{v}} = \begin{bmatrix} -\tilde{g}_1^m & -\tilde{g}_2^m & -\tilde{g}_3^m \end{bmatrix}. \quad (3.13)$$

Assuming full state feedback control, the closed loop control law is defined as

$$u_m = \tilde{v} = -\tilde{G}_m x, \quad (3.14)$$

where $\tilde{G}_m = [\tilde{g}_1^m \ \tilde{g}_2^m \ \tilde{g}_3^m]$. Then, the normalized voltage and current transfer functions in closed loop can be computed by the following matrix transformations,

$$\frac{\tilde{v}}{\tilde{x}_d} = C_{\tilde{v}} \left((j\Omega)I - A_m + B_m\tilde{G}_m \right)^{-1} F_m \quad (3.15)$$

$$\frac{\phi_m}{\tilde{x}_d} = C_{\phi_m} \left((j\Omega)I - A_m + B_m \tilde{G}_m \right)^{-1} F_m, \quad (3.16)$$

where I is the identity matrix.

In this section the normalized state-space model of an active vibration isolation system using a electromagnetic actuator is derived. From this model normalized voltage and current are expressed through two output equations. Before computing the power in closed loop a second example of an active vibration isolation system using piezoelectric actuator is modeled in a similar way.

3.3 Example of an active vibration isolation system realized with a Piezoelectric (PZT) actuator

In this case, the active vibration isolation system is composed of a base connected to the payload by the way of a piezoelectric stack actuator. As in the previous case, when a disturbance excites the base, the stack actuator counteracts and cancels the disturbance. Prediction and counteraction of the disturbance is obtained by a feedback control law where relative displacement and velocity are fed back through current.

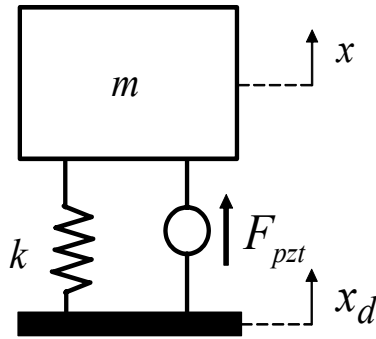


Figure 3.3: Vibration isolation system

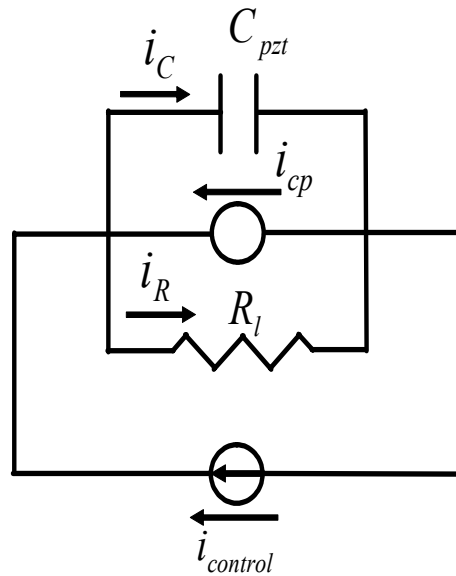


Figure 3.4: Electrical circuit in a case of a PZT actuator

3.3.1 Modeling of the piezo-based vibration isolation system

Electromechanical equations in the case of a piezoelectric actuator are derived in Section 2.2.2. Assuming a 1-DOF mechanical system without damping as represented on Figure 3.3, the equation of motion can be written as,

$$m\ddot{x} = -kx + kx_d + F_{pzt}. \quad (3.17)$$

Defining the same relative coordinate system as in the equation (3.2), the output force of the stack actuator can be derived from Equation (2.13) as,

$$F_{pzt} = k_a x_o V - k_a x_r. \quad (3.18)$$

Equation (3.17) we obtain an expression of the equation of motion in the relative coordinates,

$$\ddot{x}_r = -\frac{k + k_a}{m} x_r + \frac{k_a x_o}{m} V - \ddot{x}_d. \quad (3.19)$$

The next step consists in defining the electrical differential equation of the system. Equation (2.12) in the previous chapter defines the electrical equation of the stack actuator. In this equation the stack is modeled electrically as ideal capacitor. In reality piezoelectric ceramics have very small resistance which is electrically observed as a current leakage across the actuator [Physik Instrumente (2002)]. As we are interested in analyzing electrical power regeneration and the efficiency of energy regeneration we have to consider this phenomenon in order to better estimate power losses in the actuator. In the same manner as for an electrical capacitor the current leakage can be modeled as a resistor R_l connected in parallel with the equivalent stack capacitance C_{pzt} . The equivalent electrical network is obtained from the combination of the equation (2.12) and the leakage resistance added in parallel with equivalent capacitance of the stack actuator as shown on Figure 3.4.

Applying the first Kirchoff law to the circuit shown on Figure 3.4,

$$i_{control} = i_c + i_{R_l} - i_{cp}, \quad (3.20)$$

with $i_{control}$ is the controlled current, i_c current across the capacitor C_{pzt} , i_{R_l} the leakage current and i_{cp} the current generated through the converse piezoelectric effect. The converse piezoelectric current effect is defined as,

$$i_{cp} = x_o \frac{d}{dt} F_{pzt} = k_a x_o^2 \dot{V} - k_a \dot{x}_r, \quad (3.21)$$

where V is applied voltage to the terminals of the stack. Replacing the expressions for the three different currents in equation (3.20) we obtain the first order differential equation of the equivalent electrical circuit,

$$\dot{V} = -\frac{1}{R_l C_{blk}} V - \frac{k_a x_o}{C_{blk}} \dot{x}_r + \frac{1}{C_{blk}} i, \quad (3.22)$$

where $C_{blk} = C - k_a x_o^2$ is the equivalent capacitance of the stack actuator in blocked mechanical boundary condition. In order to study the influence of the feedback control on the power flow in this system equations (3.19) and (3.22) are normalized with non dimensional quantities.

3.3.2 Normalization of the differential equations in the case of a PZT actuator

With non-dimensional variables, equation (3.19) is rewritten as,

$$\zeta_p'' = -\zeta_p - \phi_p + \Omega \tilde{x}_d. \quad (3.23)$$

As in the case of the electromagnetic actuator the base disturbance is assumed to be harmonic and is defined in equation (3.6). The disturbance frequency is normalized by the mechanical natural frequency defined as $\omega_n = \sqrt{(k + k_a)/m}$ such that $\omega = \Omega \omega_n$. The normalized displacement ζ_p is then defined as $x_r = X_{od} \zeta_p$. Normalized voltage ϕ_p and current \tilde{i} are respectively defined as $\phi_p = \frac{k_a x_o}{(k+k_a)X_{od}} V$ and $\tilde{i} = \frac{k_a x_o}{(k+k_a)\omega_n C_{blk}} i$. The same differential operator defined in equation (3.7) is used for this case as well.

Substituting the defined quantities into equation 3.22 the normalized electrical equation is obtained,

$$\phi_p' = -\beta_p \phi_p - \psi_p \zeta_p' + \tilde{i}. \quad (3.24)$$

The coupling coefficient ψ_p in the case of the piezoelectric actuator appears in the normalized electrical differential equation as,

$$\psi_p = \frac{(k_a x_o)^2}{C_{blk} (k + k_a)}. \quad (3.25)$$

The time constant, τ_{el}^p defined in this case as $\tau_{el}^p = R_l C_{blk}$, and the natural frequency are combined in the new constant β_p such that $\beta_p = \frac{1}{\tau_{el}^p \omega_n}$. The equations (3.23) and (3.24)

can be cast in a first order state-space equation,

$$x_p' = A_p x_p + B_p u_p + F_p x_d, \quad (3.26)$$

where x_p is a state vector defined as $x_p^T = [\phi_p \ \zeta_p \ \zeta_p']$. The normalized current and voltage output are formulated through two output equations,

$$\phi_p = C_{\phi_p} x_p, \quad (3.27)$$

$$\tilde{i} = C_{\tilde{i}} x_p, \quad (3.28)$$

where A_p , B_p , $C_{\tilde{i}}$, C_{ϕ_p} and F_p are time invariant matrices defined as,

$$A_p = \begin{bmatrix} -\beta_p & 0 & -\psi_p \\ 0 & 0 & 1 \\ 1 & -1 & 0 \end{bmatrix}, \quad B_p = \begin{bmatrix} 1 \\ 0 \\ 0 \end{bmatrix}, \quad F_p = \begin{bmatrix} 0 \\ 0 \\ \Omega \end{bmatrix}, \\ C_{\phi_p} = \begin{bmatrix} 1 & 0 & 0 \end{bmatrix}, \quad C_{\tilde{i}} = \begin{bmatrix} -\tilde{g}_1^p & -\tilde{g}_2^p & -\tilde{g}_3^p \end{bmatrix}. \quad (3.29)$$

Assuming full state feedback, the closed loop control law is defined as,

$$u_p = \tilde{i} = -\tilde{G}_p x_p, \quad (3.30)$$

where the feedback gain vector is defined as $\tilde{G}_p = [\tilde{g}_1^p \ \tilde{g}_2^p \ \tilde{g}_3^p]$. Then, the normalized voltage and current transfer functions can be computed by the following matrix transformations,

$$\frac{\tilde{i}}{\tilde{x}_d} = C_{\tilde{i}} \left((j\Omega)I - A_p + B_p \tilde{G}_p \right)^{-1} F_p \quad (3.31)$$

$$\frac{\phi_p}{\tilde{x}_d} = C_{\phi_p} \left((j\Omega)I - A_p + B_p \tilde{G}_p \right)^{-1} F_p, \quad (3.32)$$

where I is the identity matrix.

The electromechanical state-space model of an active vibration isolation system with PZT stack actuator is derived along with the voltage and current outputs. Before proceeding with the details on power flow in closed loop, the two examples are compared in the next section.

Table 3.1: State-space matrix coefficients comparison for two active vibration system using two different actuators

Quantities / System	EM actuator	PZT stack actuator
State vector	$x_m = [\phi_m \zeta_m \dot{\zeta}_m]^T$	$x_p = [\phi_p \zeta_p \dot{\zeta}_p]^T$
Input u	\tilde{v}	i
A matrix	$A_m = \begin{bmatrix} -\beta_m & 0 & -\psi_m \\ 0 & 0 & 1 \\ 1 & -1 & 0 \end{bmatrix}$	$A_p = \begin{bmatrix} -\beta_p & 0 & -\psi_p \\ 0 & 0 & 1 \\ 1 & -1 & 0 \end{bmatrix}$
B matrix	$B_m = \begin{bmatrix} 1 \\ 0 \\ 0 \end{bmatrix}$	$B_p = \begin{bmatrix} 1 \\ 0 \\ 0 \end{bmatrix}$
F matrix	$F_m = \begin{bmatrix} 0 \\ 0 \\ \Omega \end{bmatrix}$	$F_p = \begin{bmatrix} 0 \\ 0 \\ \Omega \end{bmatrix}$
Current C Matrix	$C_{\phi_m} = \begin{bmatrix} 1 & 0 & 0 \end{bmatrix}$	$C_i = \begin{bmatrix} -\tilde{g}_1^p & -\tilde{g}_2^p & -\tilde{g}_3^p \end{bmatrix}$
Voltage C Matrix	$C_{\tilde{v}} = \begin{bmatrix} -\tilde{g}_1^m & -\tilde{g}_2^m & -\tilde{g}_3^m \end{bmatrix}$	$C_{\phi_p} = \begin{bmatrix} 1 & 0 & 0 \end{bmatrix}$

3.3.3 Comparison of the two active control vibration isolation systems

Electromechanical state-space model for both examples has been developed in normalized coordinates. Now we will compare these two systems before analyzing the power flow. In both cases the mechanical coordinates and the disturbance are identical due to the fact that both systems are active-based 1-DOF active vibration isolation systems. Although the mechanical coordinates are identical, the electrical coordinates are different. By inspection of the system the fundamental difference of this two system is in the actuator used to implement active vibration control. In the case of an electromagnetic actuator the control input is voltage while in the case of the piezoelectric stack actuator the control input is current. This difference influences the choice of the electrical driver. Using an EM actuator, a voltage controlled electrical driver is necessary while in the case of a PZT stack a current controlled electrical driver is required. Another fundamental difference is in the electrical properties of the actuators. Electromagnetic actuators are mostly inductive and resistive loads while the actual PZT actuators are assumed to be capacitive electrical loads. This is very important in the case of a switching topology actuator. The type of electrical, influences the design of the output filter of the switching amplifier [Erickson and Maksimovic (1999)].

Table 3.1 compares the state-space matrix coefficients and the defined state vectors for both systems. It can be easily observed that the normalized matrix coefficients of the

state equation are identical. Thus the two systems are equivalent from the mathematical point of view and by analyzing the closed-loop power flow for one normalized example will also apply to the other. In fact performing one power flow analysis in closed loop will be valid for both systems. In the next section an analytical regenerative power flow analysis in closed loop is performed. Due to the fact that the two systems are equivalent, the subscripts and superscripts m and p , which were used to differentiate respectively the case of an electromagnetic and piezoelectric actuator are removed.

3.3.4 Analytical expression for electrical power in closed loop

Replacing the electrical effort and flow variables in equation (2.28) with the corresponding electrical voltage and current variables we recover the well-known expression for electrical power P_{el} in frequency domain,

$$P_{el}(j\omega) = \frac{1}{2} \text{Re} [v(j\omega)i(j\omega)^*]. \quad (3.33)$$

Replacing the voltage v and current i with their normalized variables, respectively \tilde{v} and ϕ in equation (3.33), we obtain the relationship between the normalized power \tilde{P}_{el} and the normalized voltage and current quantities,

$$\tilde{P}_{el} = \text{Re} [\tilde{v}\phi^*]. \quad (3.34)$$

Normalized electrical power \tilde{P}_{el} is related to the electrical power P through,

$$\tilde{P}_{el} = \frac{P}{\frac{1}{2}\omega_n k X_{od}^2} \psi. \quad (3.35)$$

By observing the expression of normalized electrical power \tilde{P}_{el} a physical interpretation to this normalized quantity can be drawn. P_{el} represents the rate of energy exchange between the regenerated energy and energy stored in the spring. Finally, by substituting the normalized voltage and current by their transfer functions equations (3.15) and (3.16) we obtain the analytical expression for the normalized power,

$$\tilde{P}_{el} = \frac{\Omega^4}{|\Delta|^2} ((a_1 b_1 - a_0 b_2) \Omega^2 + a_0 b_0), \quad (3.36)$$

where a_0 , a_1 , b_0 , b_1 and b_2 are functions of the control gains and system parameters and Δ is the determinant of the 3×3 matrix defined as,

$$\Delta(\tilde{g}_1, \tilde{g}_2, \tilde{g}_3, \Omega) = \det(j\Omega - A + BG). \quad (3.37)$$

The complete expression of \tilde{P}_{el} in terms of the physical parameters and normalized gains is shown in Appendix B. By computing the roots of the polynomial $\Delta(j\Omega)$ or by finding the eigenvalues of $A - BG$ we obtain the stability criteria. The closed loop system will be stable if all the poles (eigenvalues or roots of $\Delta(j\Omega)$) are located in the left hand side of the s-plane.

The obtained analytical expression in equation (3.36) is function of the system parameters, normalized frequency Ω and normalized gains \tilde{g}_1 , \tilde{g}_2 and \tilde{g}_3 . The advantage of deriving an analytical expression of the normalized electrical power is in performing an optimal analysis of the influence of feedback gains on the power flow for a given disturbance frequency.

As the analytical expression of the electrical power (equation (3.36)) is obtained, we can perform a mathematical analysis of the influence of the feedback gains on the power flow in the voice-coil actuator. The following shows four different cases where particular settings of control parameters influence the power flow between the mechanical disturbance and the electrical (control) source.

Case 1: $\tilde{g}_2 = \tilde{g}_3 = 0$

In this case only current is fed back and the control law is similar to a “resistive law” ($u = -\tilde{g}_1 \phi$). The current flowing in the coil is sensed and fed back into control voltage through the gain \tilde{g}_1 . We notice that the stability criteria is satisfied only for positive \tilde{g}_1 ,

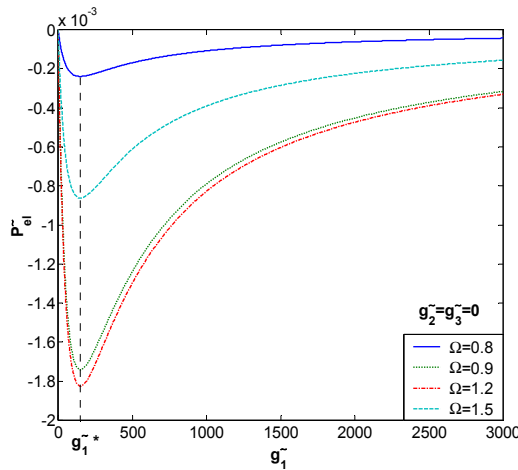


Figure 3.5: Regenerative electrical power flow vs \tilde{g}_1 and $\tilde{g}_2 = \tilde{g}_3 = 0$ for three different values of Ω

$$\tilde{P}_{el\ g_2=g_3=0} = -\frac{\psi^2\Omega^6}{|\Delta|^2}\tilde{g}_1. \quad (3.38)$$

The expression of power in equation (3.38) shows that the power is always negative for any \tilde{g}_1 in the stability region. The negative sign represents regenerative power flow. This means that the power is flowing from the disturbance source through the voice-coil to its electrical source. As the stability region for this control law is for $\tilde{g}_1 > 0$, applying a resistive control law ($\tilde{g}_2 = \tilde{g}_3 = 0$) will always lead to a regenerative flow. It is also interesting to examine the existence of a gain which maximizes the regenerative flow. By deriving the equation (3.38) towards \tilde{g}_1 and solving for \tilde{g}_1 ,

$$\frac{d\tilde{P}_{el\ \tilde{g}_2=\tilde{g}_3=0}}{d\tilde{g}_1} = 0, \quad (3.39)$$

we obtain the optimal gain \tilde{g}_1^* which maximizes the regenerative power flow in the Case 1. Figure 3.5 shows the normalized power and the existence of a minimum (maximum regeneration) for three different normalized frequencies. This optimum normalized gain \tilde{g}_1^* is unique for all normalized frequency Ω . In the physical model g_1^* is only unique for the case where the mechanical harmonic disturbance is defined in terms of displacement amplitude. This property comes from the relationship between the two gains,

$$\frac{g_1}{\tilde{g}_1} = \frac{Bl^2}{k^2 X_{od}^2 L\omega_n}, \quad (3.40)$$

and

$$X_{od} = \frac{\ddot{X}_{od}}{\omega^2} = \frac{\dot{X}_{od}}{\omega}. \quad (3.41)$$

We also notice that the amount of regenerated power increases with an increase in the normalized frequency Ω .

Case 2: $\tilde{g}_3 = 0$

In this case the current in the coil and the relative displacement are sensed and fed back through control voltage. The analytical expression of the electrical power may be written as

$$\tilde{P}_{el\ g_3=0} = \frac{\Omega^4}{|\Delta|^2} f(\tilde{g}_1, \tilde{g}_2, \Omega), \quad (3.42)$$

where f is a function also depending on \tilde{g}_1 , \tilde{g}_2 and Ω . Figure 3.6 shows the regenerated electrical power for different combinations of gains \tilde{g}_1 and \tilde{g}_2 for a harmonic excitation of the base at $\Omega = 1.5$. We also notice from this surface plot that the surface representing the regenerated flow exhibits a maximum. In fact, this maximum corresponds to the maximum from the previous case (Case 1) which means that the optimal regenerative flow is located in the plane where $\tilde{g}_2 = \tilde{g}_3 = 0$. The projection of the regenerative area on the surface

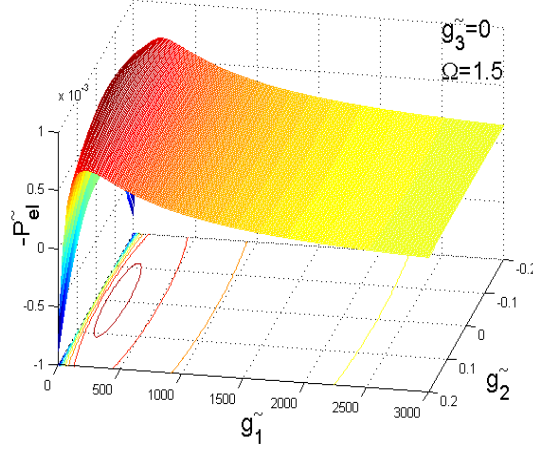


Figure 3.6: Regenerated Electrical power vs \tilde{g}_1 and \tilde{g}_2 for the case where $\Omega = 1.5$ and $\tilde{g}_3 = 0$

defined by $(\tilde{g}_2, \tilde{g}_3)$ is shown on Figure 3.7. This regenerative area matches the stability region for the given normalized gains. Choosing \tilde{g}_1 and \tilde{g}_2 inside the area delimited by the parabola, the power will flow from the disturbance source to electrical source (regenerative flow). In the situation where \tilde{g}_1 and \tilde{g}_2 are chosen outside of the parabolic area, the flow will go from the electrical source to the mechanical system (discharging flow). Also, with the increase of Ω , the parabolic areas shown on Figure 3.7 are expanding. The set of curves shown on Figure 3.8 is cut of Figure 3.6 for three different values of \tilde{g}_2 . From this plots we notice that if $\tilde{g}_2 \neq 0$ the nature of the flow is controlled by the choice of \tilde{g}_1 .

Case 3: $\tilde{g}_1 = 0$

In this case the relative displacement and the relative velocity are sensed and fed back through control voltage. The analytical expression of the electrical power is then,

$$\tilde{P}_{el_{g_1=0}} = \frac{\Omega^4}{|\Delta|^2} f(\tilde{g}_2, \tilde{g}_3, \Omega), \quad (3.43)$$

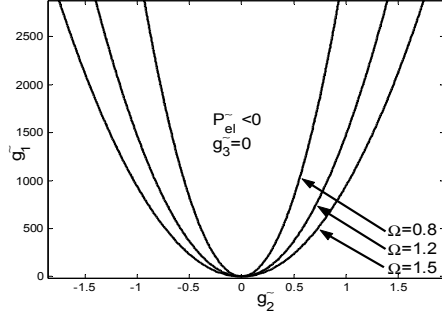


Figure 3.7: Regenerative area vs \tilde{g}_1 and \tilde{g}_2 for three different values of Ω and $\tilde{g}_3 = 0$

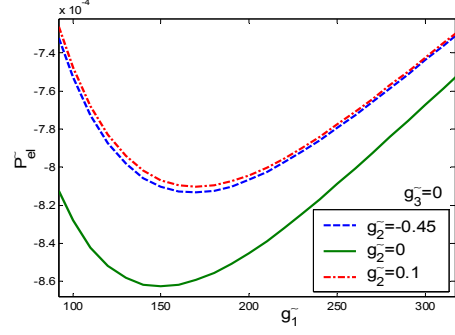


Figure 3.8: Curves of \tilde{P}_{el} vs \tilde{g}_1 for three different values of \tilde{g}_2 at $\Omega = 1.5$ and $\tilde{g}_3 = 0$

where f is a function depending on \tilde{g}_2 , \tilde{g}_3 and Ω . The electromechanical system is then

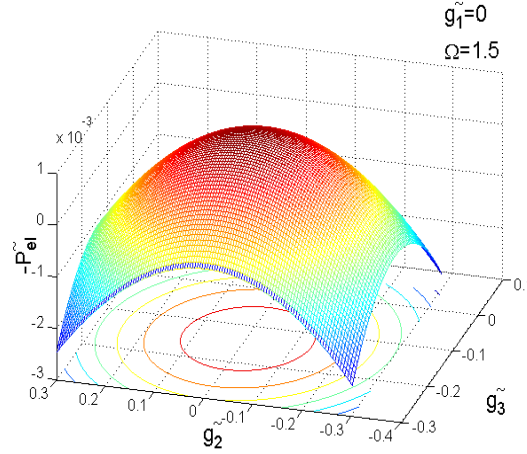


Figure 3.9: Regenerated Electrical power vs \tilde{g}_2 and \tilde{g}_3 for the case where $\Omega = 1.5$ and $\tilde{g}_1 = 0$

controlled only from its mechanical part. This is similar to traditional controls problem in structural dynamics, where a 1-DOF freedom mechanical system has its open loop characteristics (natural frequency and damping) changed in some required closed loop characteristics. In most of the control problems achieving the closed loop characteristics require the control source to provide a given effort. The following analysis shows that with the usual feedback states (displacement and velocity), the power flow in a electromechanical system can be regenerative as well as in the previous two cases. Figure 3.9 shows the surface of $-\tilde{P}_{el}(\tilde{g}_2, \tilde{g}_3, \Omega = 1.5)$ representing different values (magnitudes) and types of electrical power flow for a given harmonic excitation of the base. As in the previous case the elec-

trical power exhibits a regenerative area. It is also interesting to notice that the optimal (maximal) regenerative power flow is obtained with a control law defined such that $\tilde{g}_2 = 0$ and $\tilde{g}_3 = \tilde{g}_3^*$. This particular case is similar to the “resistive control” due to the fact that

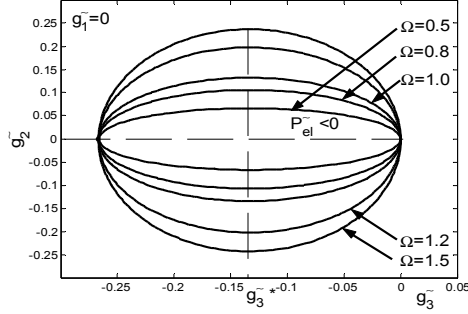


Figure 3.10: Regenerative area vs \tilde{g}_2 and \tilde{g}_3 for different values of Ω and $\tilde{g}_1 = 0$

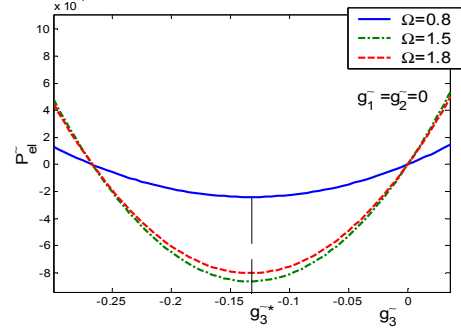


Figure 3.11: Curves of \tilde{P}_{el} vs \tilde{g}_3 for three different values of Ω ($\tilde{g}_1 = \tilde{g}_2 = 0$)

\tilde{g}_3 is controlling velocity which is a flow variable and corresponds to current in a electrical system. The projections of regenerative areas on the plane defined by $(\tilde{g}_2, \tilde{g}_3)$ are shown on Figure 3.10. The regenerative electrical power flow is obtained by choosing \tilde{g}_2, \tilde{g}_3 inside the area delimited by the ellipse. It is easy to notice from Figure 3.10 that with the increase of frequency Ω the regenerative area expands. For each driving frequency the optimum regenerative flow is in the center of the elliptic area ($\tilde{g}_2 = 0$ and $\tilde{g}_3 = \tilde{g}_3^*$), independently of Ω . This shrinkage of the regenerative domain is also noticed in Figure 3.11. This plot represents a 2-D plot in the plane where $\tilde{g}_2 = 0$. As the disturbance frequency ω approaches the resonant frequency ($\Omega = 1$), the maximum power flow increase and is infinite at the resonant frequency.

Case 4: $\tilde{g}_2 = 0$

In this case the current and the velocity are sensed and fed back through control voltage. This control law may be named as “flow control law” due to the fact that both electrical and mechanical flow quantities, current and velocity are tuned respectively with \tilde{g}_1 and \tilde{g}_3 . The analytical expression of the electrical power is,

$$\tilde{P}_{el, g_2=0} = \frac{\Omega^4}{|\Delta|^2} f(\tilde{g}_1, \tilde{g}_3, \Omega), \quad (3.44)$$

where f is a function depending on \tilde{g}_1, \tilde{g}_3 and Ω .

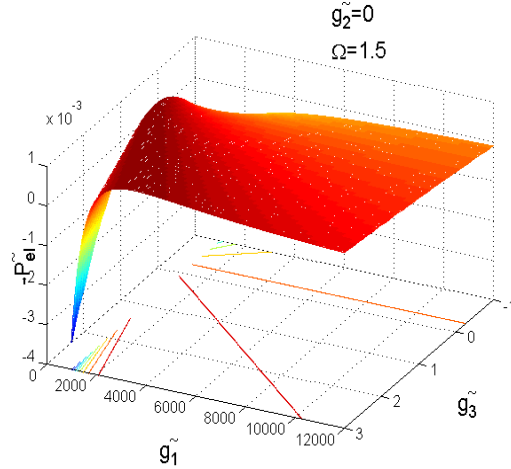


Figure 3.12: Regenerated Electrical power vs \tilde{g}_2 and \tilde{g}_3 for the case where $\Omega = 1.5$ and $\tilde{g}_2 = 0$

From the surface plot shown on Figure 3.12 we notice that the surface does not exhibit a maximum regenerative power flow value but the regenerative flow is constantly increasing with the increase of \tilde{g}_1 and \tilde{g}_3 . The projection of the regenerative area ($\tilde{P}_{el} < 0$) on the $(\tilde{g}_1, \tilde{g}_2)$ surface shown on Figure 3.13 also exhibits the infinite regenerative area. As the driving frequency increase, the regenerative set of values of \tilde{g}_3 decreases but still extends towards infinity for the positive values of \tilde{g}_1 . For each value of \tilde{g}_3 an optimal value of \tilde{g}_1 exists and is increasing as \tilde{g}_3 increase. Figure 3.14 shows a set of curves of \tilde{P}_{el} for

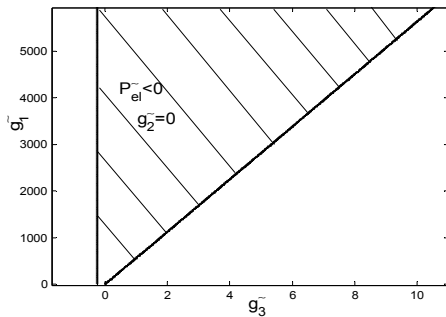


Figure 3.13: Regenerative area vs \tilde{g}_2 and \tilde{g}_3 for different values of Ω and $\tilde{g}_1 = 0$

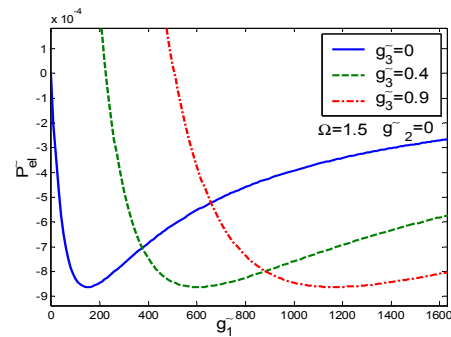


Figure 3.14: Curves of \tilde{P}_{el} vs \tilde{g}_1 for three different values of \tilde{g}_3 ($\Omega = 1.5$ and $\tilde{g}_2 = 0$)

different values of \tilde{g}_3 . The regenerative electrical flow increases very slowly with an increase in the two flow gains. That means that in the ideal case, with a infinitely big flow control gains, any regenerative flow can be obtained if stability criteria is still satisfied. Choosing

a flow control law will allow the actuator to transfer and regenerate as much energy as the disturbance source is able to provide. In reality this infinite regenerative flow is limited by the actuator and disturbance source physical limits.

3.4 Summary on the regenerative control topologies and their influence on the vibration of the payload

A voice-coil actuator integrated in an active vibration isolation system with feedback control was modeled and normalized. The normalized set of non dimensional equations of motions were integrated in a state-space model with the normalized electrical effort and flow outputs. An analytical non dimensional expression of the electrical power was obtained and then analyzed in function of the normalized control parameters and non dimensional frequency. This analysis lead us into four different control strategies that exhibits the power to flow from disturbance to the electrical source (regenerative flow). In the Case 1, that we also named as “resistive control”, the power flow is always regenerative for any positive value of \tilde{g}_1 . The maximum flow is obtained by choosing a control law such that $\tilde{g}_1 = \tilde{g}_1^*$. In the Case 2, we showed that a the regenerative flow exists if the two control parameters (\tilde{g}_1 and \tilde{g}_2) are chosen inside the parabolic area. The flow is maximized for $\tilde{g}_2 = 0$, which bring us back to Case 1. The optimal energy regeneration is obtained again for $\tilde{g}_1 = \tilde{g}_1^*$. Case 3 also exhibits a regenerative region for its control parameters.

In a conclusion to these analysis, in order to obtain regenerative control through feedback, at least one flow variable (current or velocities) has to be sensed and fed back.

3.4.1 Influence of regenerative control on the isolator dynamics

In the previous sections we were interested in maximizing the regenerative power flow through full-state feedback. It is important to determine the influence of the optimum regenerative control on the dynamics of the mechanical system. We want to know how well the isolation system protects the load from vibrations in the case of a regenerative control scheme. A good indicator of the “quality” of the vibration isolator is the determination of the transmissibility ratio $T.R.$ [Inman (2000)]. Following the same notation as in Figures 3.1

and 3.3 the $T.R.$ is defined in frequency domains as,

$$T.R. = (j\omega) = \frac{x(j\omega)}{x_d(j\omega)}. \quad (3.45)$$

A magnitude plot of $T.R.$ in the case of resistive topology and its zoom around the resonance are shown respectively on Figure 3.15 and 3.16. From the magnitude plot we notice that

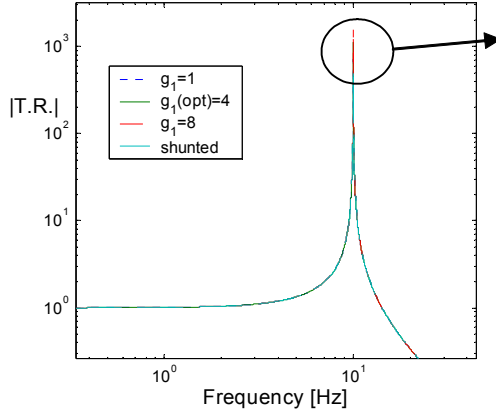


Figure 3.15: $|T.R.|$ in the case of the resistive control

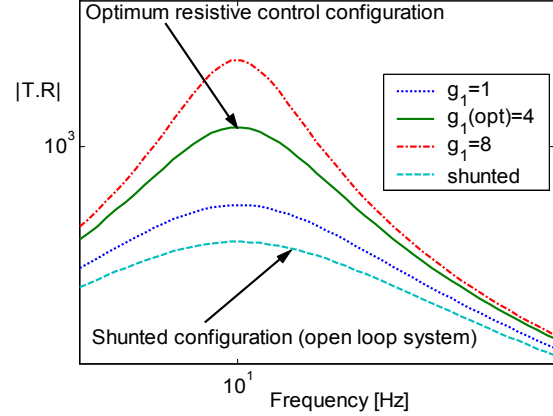


Figure 3.16: $|T.R.|$ around the mechanical resonance

the level of vibration at resonances increases compared to the open loop system. With the increase of resistive gain g_1 , the level of vibration increase. It is important to understand that the open loop system represents the shunted configuration (short circuit electrical boundary condition). Also the high magnitude values of the $T.R.$ are due to the fact that the structure is modeled without any structural damping. Although at resonance the $T.R.$ is higher than in the shunted configuration also called semi-active control [Nakano et al. (2000)], at lower frequencies the $T.R.$ is lower in resistive control topology. Magnitude and phase plots in the case of velocity control have the identical behavior and are shown on Figure 3.17 and 3.18. In conclusion to the analysis of different regenerative control topologies, the influence of regenerative control on closed loop topologies is performed. Figure 3.19 is schematic representation of the open and closed loop poles of the voice-coil actuator. It is important to remind the reader that open loop configuration represents the short circuit electrical boundary condition and that the two conjugate poles represent the 1-DOF mechanical system and the real pole represents the time constant of the electrical circuit. Hence, in closed loop the complex conjugate poles are being moved from their open loop location towards the imaginary axis along the circle of radius ω_n . That means

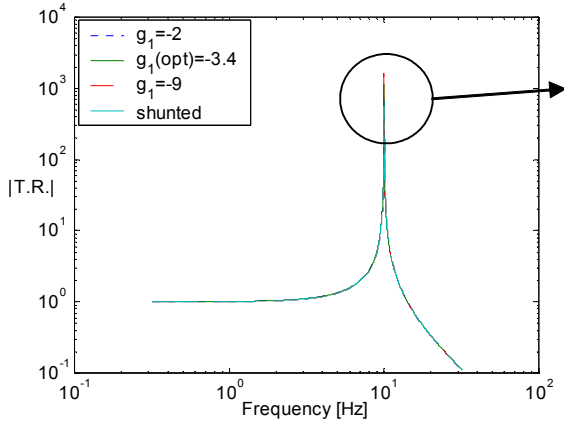


Figure 3.17: $|T.R.|$ in the case of the velocity control

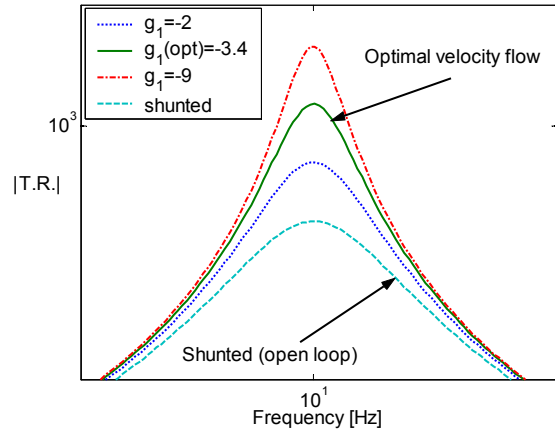


Figure 3.18: $|T.R.|$ around the mechanical resonance

that in the closed loop, the damping is decreased compared to the short circuit electrical configuration. The real pole representing the electrical time constant is shifted on the

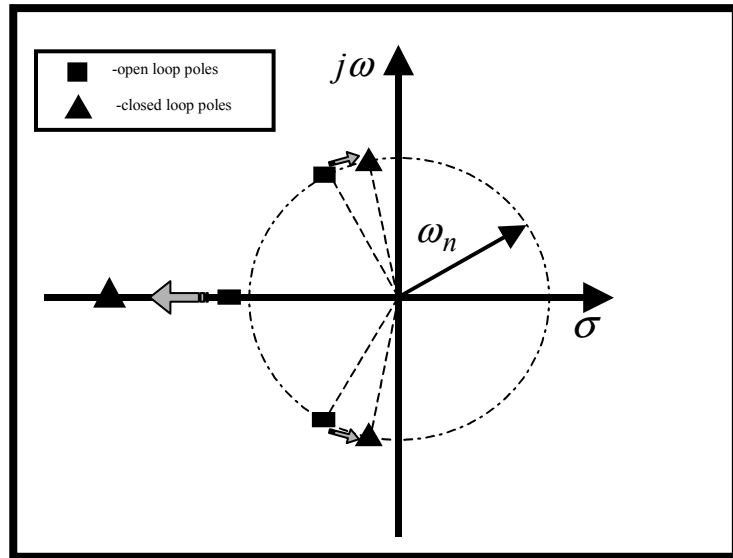


Figure 3.19: Open and closed loop poles location for regenerative control

real axis of the s-plane towards minus infinity which makes the electrical system faster in closed-loop. In the case of a EM actuator the closed loop system has a tendency to oscillate more than in the shunted configuration. Hence this control strategy is less efficient than the short circuit configuration for vibration suppression also called semi-active control. Although the regenerative control increases the level of vibration, a trade off may exist in a way of regenerating the “allowed” level of vibration using a regenerative control law and

suppressing the vibration when they become critical with active vibration control strategy.

Chapter 4

Measurements and simulation

4.1 Introduction

This chapter presents the experimental verification of the previously developed control strategies in the case of electro-magnetic linear actuator. The experimental system is different from the system analyzed in the previous chapter. The setup is equivalent to a single degree of freedom mass connected to a ground through a spring, damper and electromagnetic actuator. This modification was done in order to obtain a simpler mechanical system and also in order to ensure a measurable quantities such as induced voltage and current. Although the two system are different from a mechanical point of view, from the mathe-

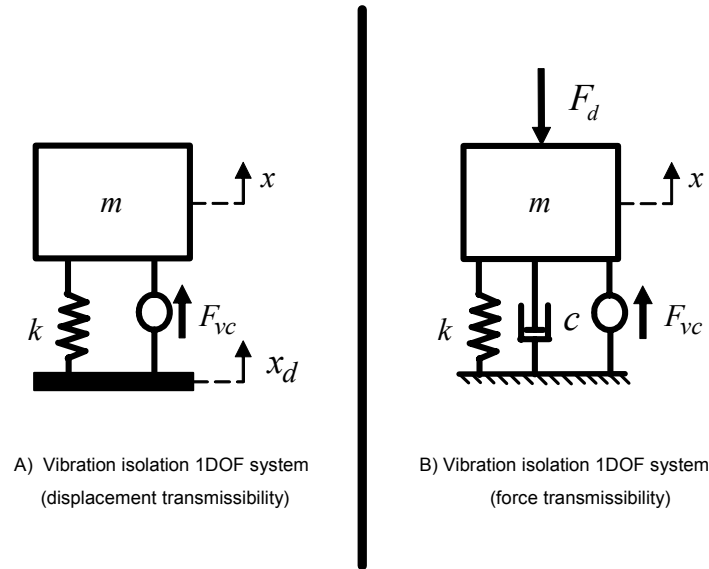


Figure 4.1: Difference between the analyzed and experimental system

Table 4.1: System comparison

Quantities Models	Vibration Isolation	Force Isolation
State vector	$x = [i \ x_r \ \dot{x}_r]^T$	$x = [i \ x \ \dot{x}]^T$
Me. Diff. Equation	$\ddot{x}_r = \frac{Bl}{m}i - \frac{k}{m}x_r - c\dot{x}_r - x_d$	$\ddot{x}_r = \frac{Bl}{m}i - \frac{k}{m}x - c\dot{x} - \frac{1}{m}F_d$
El. Diff. Equation	$\frac{d}{dt}i = -\frac{R}{L}i - \frac{Bl}{m}\dot{x}_r + V_c$	$\frac{d}{dt}i = -\frac{R}{L}i - \frac{Bl}{m}\dot{x} + V_c$
A matrix	$A = \begin{bmatrix} -\frac{R}{L} & 0 & -\frac{Bl}{m} \\ 0 & 0 & 1 \\ \frac{Bl}{m} & -\frac{k}{m} & \frac{c}{m} \end{bmatrix}$	$A = \begin{bmatrix} -\frac{R}{L} & 0 & -\frac{Bl}{m} \\ 0 & 0 & 1 \\ \frac{Bl}{m} & -\frac{k}{m} & \frac{c}{m} \end{bmatrix}$
B matrix	$B = \begin{bmatrix} \frac{1}{L} \\ 0 \\ 0 \end{bmatrix}$	$B = \begin{bmatrix} \frac{1}{L} \\ 0 \\ 0 \end{bmatrix}$
F matrix	$F = \begin{bmatrix} 0 \\ 0 \\ -1 \end{bmatrix}$	$F = \begin{bmatrix} 0 \\ 0 \\ -\frac{1}{m} \end{bmatrix}$

mathematical point of view they are identical. The fundamental difference of this two systems is in the disturbance and mechanical coordinates as shown in Figure 4.1. In the case of the vibration isolation system the disturbance is the acceleration and the mechanical coordinates are relative to the motion of the base ($x_r = x - x_b$) while, in the case of the “fixed” base system the disturbance is force and the mechanical coordinate is absolute displacement x and velocity of the moving mass. The comparison of the two state-space models are shown in Table 4.1.

Another difference with the previously described system is in the choice of the electrical driver. Energy regeneration is only possible if a switching current bi-directional amplifier is used (see section). Switching amplifiers are complex and expensive devices and are designed for a particular load. As the goal of this experimental approach is to verify the concept of optimal regenerative control, we decided not invest into a design of a switching amplifier. Instead of using switching amplifier, which function is to adapt current and voltage waveforms and transfer regenerated electrical energy towards electrical storage devices, we are using a linear amplifier which is sinking the regenerated current and dissipating all the regenerated energy into heat. The energy which would be regenerated in the case of a system with a switching amplifier is estimated by measuring the sunked current and voltage at the output of the operational amplifier. This measurement will provide a good estimation of the amount of energy that could be regenerated.

The purpose of this chapter is to experimentally demonstrate the behavior of the power flow in three different control strategies. In the first part of this chapter we identify

the necessary open loop mechanical and electrical parameters. Then resistive, velocity and flow control implementation is discussed respectively, as well as the comparison of the experimentally obtained and predicted phenomenon. The last part provides a comparison between the measured and simulated optimal gains as well as a discussion of to several practical issues associated with regenerative control.

4.2 Experimental Setup

The experimental setup consists of a mechanically constrained shaker connected through a stinger to a suspended shaker. The constrained shaker is a Brüel & Kjær Type 4810 mini-shaker. The constrained actuator, approximated as one degree of freedom (1-DOF) electromechanical system is used to test different regenerative control strategies. The second shaker, suspended Ling Dynamic System electromagnetic actuator, is used as force disturbance. Both shakers are connected to a linear amplifier HP model 62825A and controlled through a dSpace DS 1104 board. A simplified schematics of the experimental setup is shown on Figure 4.2.

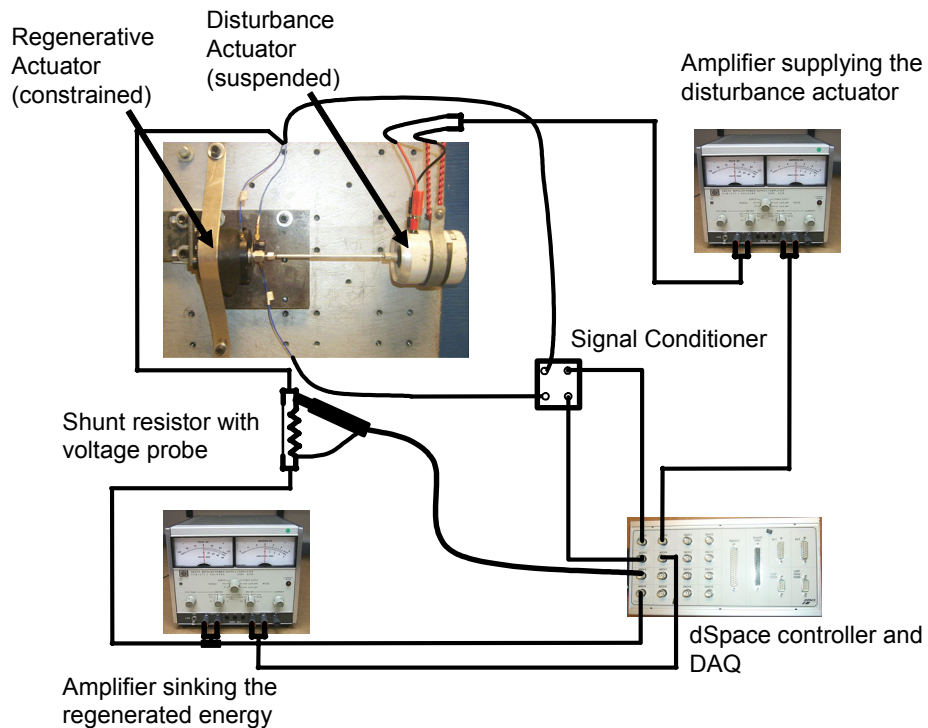


Figure 4.2: Simplified schematics of the experimental setup

The current flowing between the regenerative actuator and the linear amplifier is measured through a shunt resistor. Shunt resistors have a very small and accurate value of resistance (in our setup $R_{sh} = 0.2\Omega$ with 1% precision). In the experimental setup shown on Figure 4.2, the shunt resistor is placed in between the regenerative actuator and the amplifier on the low side. As the resistance of the shunt is an order of magnitude less than the resistance of the inductor, the influence of the shunt on the dynamics of the electrical system is negligible. The measurement of current flowing in the coil is obtained by measuring the voltage across the shunt resistor and corrected with a factor of $\frac{1}{R_{sh}}$. It is very important to connect the ground of the probe used to measure the voltage across the shunt, to the ground of the amplifier in order to measure the current as in a generator convention and also avoid a short-circuit.

Acceleration of the moving mass and the input force to the regenerative actuator are measured respectively with an accelerometer and a force sensor connected to the ADC (Analog to Digital Converter) board of the dSpace through a signal conditioner. The velocity is obtained by digitally integrating the acceleration signal (ref. Section 4.5.1).

The different control strategies are designed using Matlab/Simulink and then loaded into the dSpace board. Once a desired control law is loaded into the board the experiment is performed by varying the desired gains g_1 , g_3 or both g_1 and g_3 . The data acquisition of acceleration, voltage across the shunt (current), regenerated voltage and input force is realized using the ADC dSpace board.

4.3 Open loop Results

The system is characterized in open loop before performing closed loop tests. Frequency response function (FRF) tests are performed in order to determine the open-loop mechanical and electrical parameters such as moving mass, stiffness, damping, resistance and inductance of the coil. The following two sections describe the experimental analysis performed in order to obtain mechanical and electrical open-loop parameters.

4.3.1 Mechanical parameters

In the developed model described in previous chapter the open loop system is equivalent to a short circuit condition. The transfer function between the acceleration and force is

then taken with the regenerative actuator shunted. Figure 4.3 shows the transfer function between displacement of the moving mass of the actuator and input force. In the frequency range of 0 – 300 Hz the system can be approximated to a second order system which can be modeled as one degree of freedom mass spring damper system.

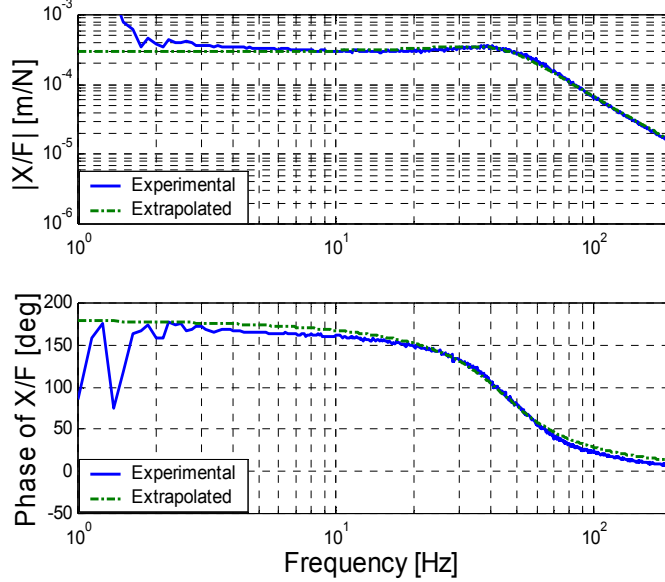


Figure 4.3: Open loop transfer function between displacement and input force (short circuit boundary condition)

The experimentally obtained data is then extrapolated to the assumed second order transfer function defined as,

$$\frac{x}{F} = \frac{-\frac{1}{m}}{s^2 + 2\zeta\omega_n s + \omega_n^2}. \quad (4.1)$$

The extrapolation is realized with an optimized numerical algorithm. The desired polynomial degree of the numerator and denominator are inputted to the algorithm along with the experimentally obtained frequency domain data. The algorithm provides the optimally fitted polynomial coefficients and by identification with equation (4.1) we obtain the desired open loop mechanical parameters. The extrapolated equivalent mass, spring and damper values are:

$$\begin{aligned} M &= 41.40 \text{ g}, \\ k &= 3.35 \frac{kN}{m}, \end{aligned}$$

$$c = 1.37 \frac{Ns}{m},$$

and the open loop natural frequency of the system is 45.3 Hz. Figure 4.3 shows the extrapolated transfer function and the experimental data. The experimental and fitted magnitudes are well matched but the phase plots diverges at low frequency and at higher frequencies above resonance due to non-linear behavior of the shaker at low frequencies and the influence of the other modes at higher frequencies. This phase difference will introduce a difference between the simulated and measured mechanical powers.

The next section describes the similar analysis performed to obtain the electrical parameters of the coil and the Bl coupling coefficient.

4.3.2 Electrical Parameters

In order to estimate the electrical parameters a FRF test between the voltage and current of the regenerative shaker is performed using an impedance analyzer. For this test, the shaker is decoupled from the disturbance input (the suspended shaker) to avoid the influence through electromagnetic coupling. The measured impedance is shown in Figure 4.4.

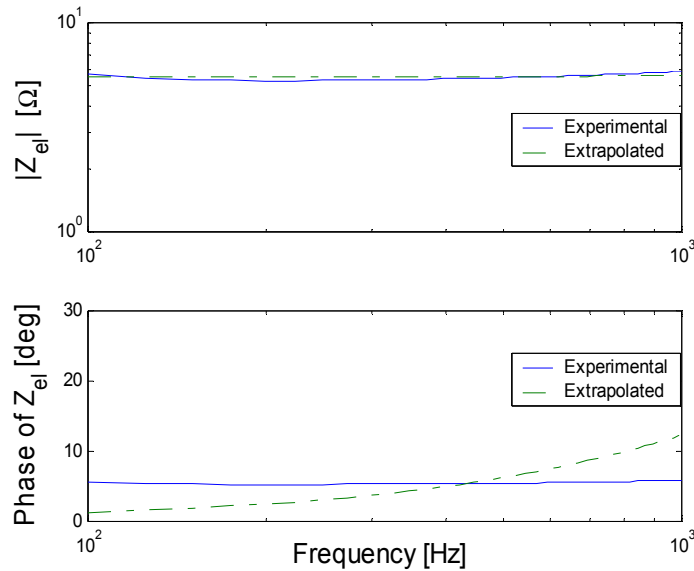


Figure 4.4: Open loop electrical impedance Z_{el} (mechanically unconstrained shaker)

We assumed that the actuator is composed of a coil which is modeled as an inductor

L in series with a resistance R representing equivalent resistance part of the coil. The analytical expression of the electrical impedance is then,

$$Z = R + sL. \quad (4.2)$$

Figure 4.4 shows the extrapolated and experimentally obtained impedance plot. The extrapolated electrical parameters are:

$$\begin{aligned} R &= 5.48 \, \Omega, \\ L &= 0.19 \, mH. \end{aligned}$$

From Figure 4.4 we notice that in the frequency range of interest, the electrical impedance is mostly resistive. As in the case of a the transfer function between displacement and force, the magnitude values are well matched but the phase is not well correlated. This may introduce some differences between the estimated and measured regenerated power. The last open loop parameters to be identified is the electromagnetic coupling coefficient Bl . This parameter is known to vary with frequency of actuation and stroke of the actuator [Foshage et al. (1996)]. In order to estimate this parameter, we measured the force exerted by the actuator and the input current at different frequencies of interest. Knowing the amplitude of the input current and the measured force the coupling coefficient is estimated from the following relationship,

$$Bl = \frac{F}{i}. \quad (4.3)$$

The average Bl in the frequency range of 0–300 Hz is $4.1 \frac{N}{m}$. As all the open loop parameters are identified, different closed loop regenerative control topologies can now be implemented. Experimental and predicted results for the three different control strategies are presented and discussed in the following sections.

4.4 Resistive Control

This section discusses the implementation and the obtained experimental results of the resistive control law. The simplified schematics of the resistive feedback law is shown on Figure 4.5.

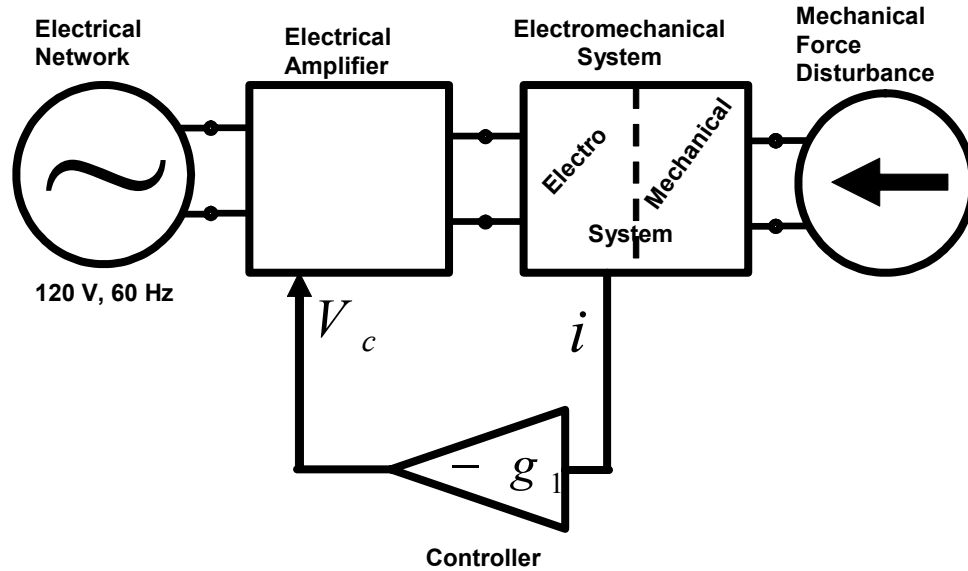


Figure 4.5: Resistive control schematics

4.4.1 Implementation of the Resistive Control

The regenerated current is sensed through the shunt resistor. The control law,

$$V_c = -g_1 i, \quad (4.4)$$

is implemented digitally with the dSpace board. The digital controller has a sampling frequency of $f_s = 30$ kHz. During the tests, the frequency of the disturbance signal is fixed by setting the input voltage and the frequency of the input signal (generated through the DAC of dSpace) to the disturbance linear amplifier. Data acquisition of the regenerated voltage as well as force and acceleration of the moving mass is realized with the ADC of dSpace. For a given harmonic disturbance excitation, different values of resistive gain g_1 are tested. The obtained time data is then processed to compute the regenerated input power and the input mechanical power. Next section discusses measured power quantities and their comparison with the predicted results.

4.4.2 Results and their comparison with estimated results

The experimental results of measured and simulated regenerated power, input mechanical power and the regeneration efficiency are shown respectively on Figure 4.6, Figure 4.7, Figure 4.8 on the following three pages. From Figure 4.6 we can notice that the experimental set of data exhibits an optimum resistive gain value for the regenerated power flow. Power magnitudes are negative due to the fact that generator convention was kept for the simulated and experimental results. Negative power values in the case of generator convention mean that the power flow is going from the disturbance input into the amplifier and is being dissipated by the linear amplifier. In the case of an ideal switching amplifier this same amount of power will be transferred and stored in condenser elements.

Although the experimental data exhibits the same phenomenon the measured power values are not matching well for all frequencies. This is especially the case for the mechanical input power. Reasons for these discrepancies will be discussed later in the chapter.

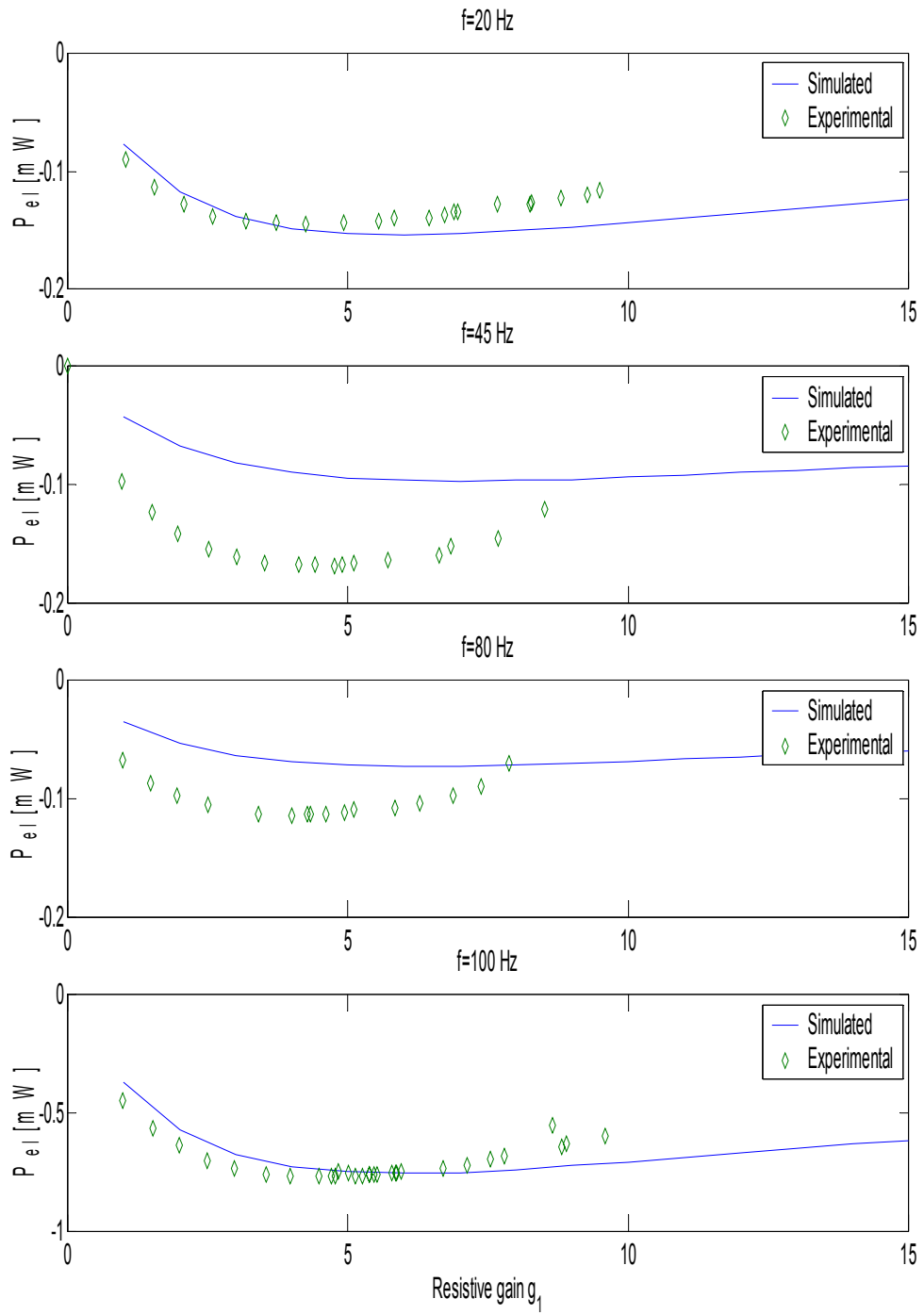


Figure 4.6: Regenerated simulated and measured powers in resistive control configuration

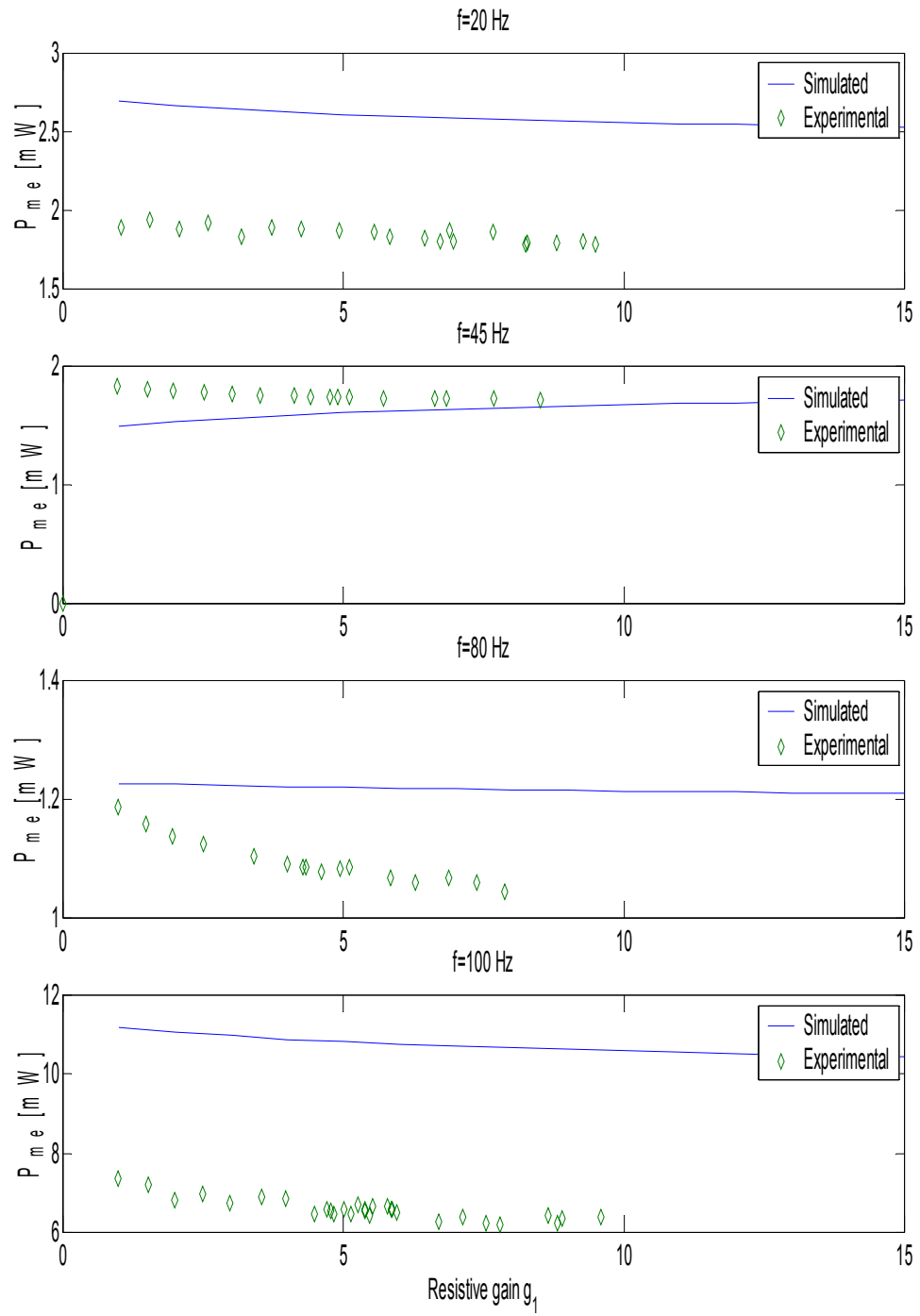


Figure 4.7: Input mechanical simulated and measured powers in resistive control configuration

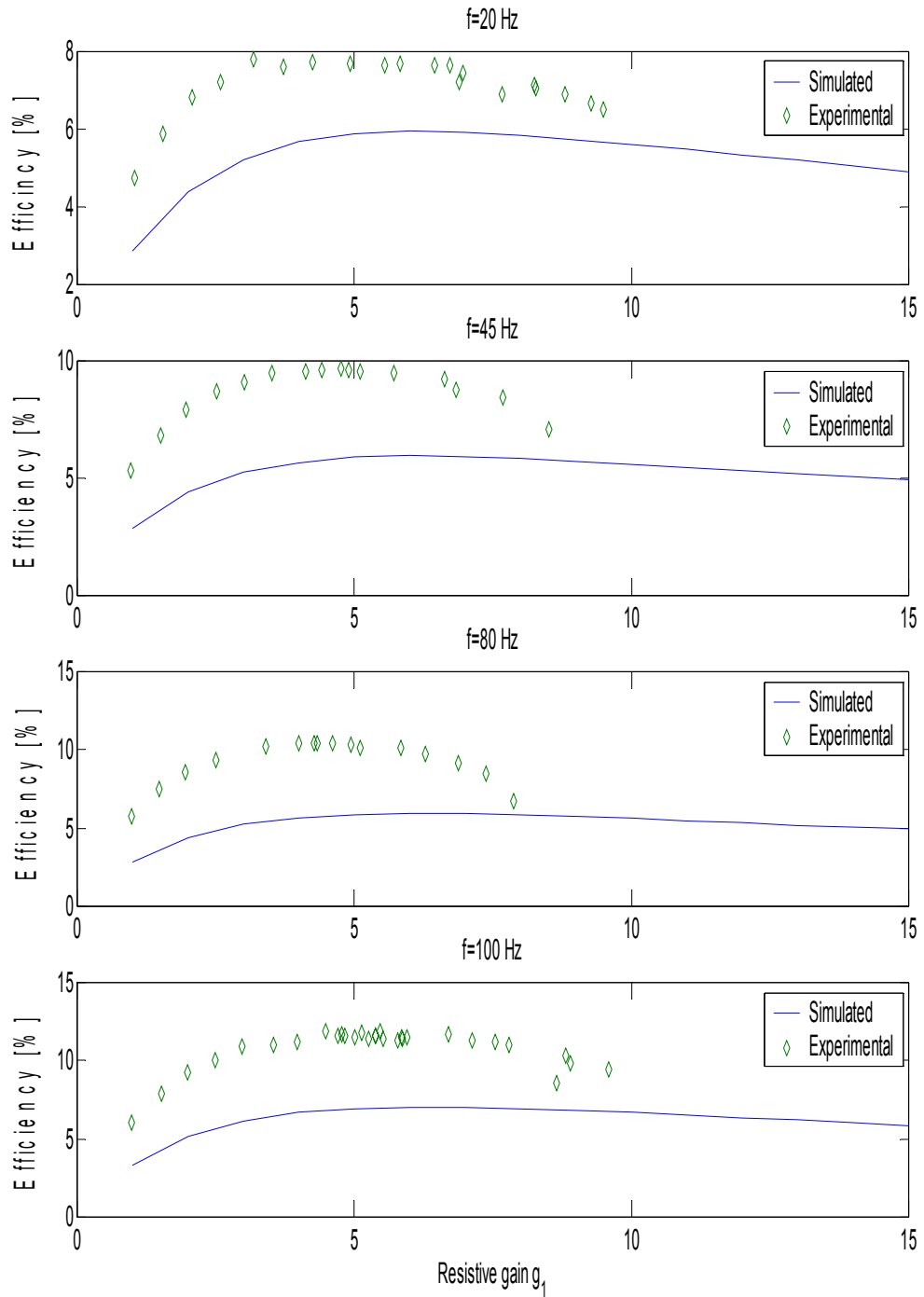


Figure 4.8: Simulated and experimental efficiencies in resistive control configuration

4.5 Velocity Control

This section discusses the implementation of the velocity type control law. The simplified schematics of this feedback law is shown on Figure 4.9. In this case velocity is fed back

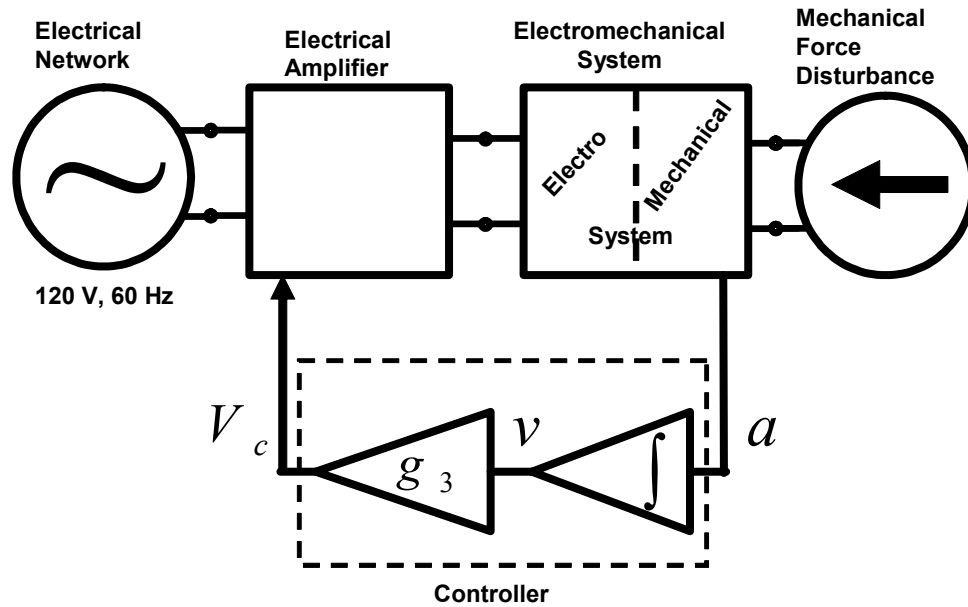


Figure 4.9: Velocity control schematics

through the following control law,

$$V_c = -g_3 \dot{x}. \quad (4.5)$$

As simulated and analyzed in previous section, velocity feedback with negative g_3 we want to experimentally verify the existence of the optimal velocity regenerative gain.

4.5.1 Implementation of the Velocity feedback Control

In the experimental setup the velocity can not be measured directly. Velocity is obtained after integrating the acceleration signal obtained from the accelerometer. The accelerometer signal is integrated through a digital filter designed with dSpace. For practical reasons a ideal integrator can not be implemented. An ideal integrator will provide infinite values for any small DC values and in particular for any signal with offset. To avoid this problem a

“pseudo integrator” is implemented. A pseudo integrator has a derivative properties (High Pass filter) below the break frequency ω_n and over the break frequency has the behavior of an integrator. The breaking frequency should be as low as possible to avoid the influence of the derivator on the magnitude and phase of the integrator. A transfer function $H(s)$ between the input and output signal of pseudo integrator is,

$$H(s) = \frac{s}{s^2 + 2\zeta\omega_n s + \omega_n^2}, \quad (4.6)$$

where ω_n is the break frequency and ζ the damping ratio of the second order Low Pass Filter (LPF). Figure 4.10 shows the transfer function of the pseudo integrator and of the ideal integrator. The break frequency of 1 Hz is chosen because that was the lowest frequency that could be implemented digitally with a sampling frequency of 30 kHz. Decreasing the breaking frequency under 1 Hz will make the digital filter unstable. From the transfer function plot on Figure 4.10 it can be easily observed that the implemented digital filter acts as an ideal integrator a decade above its breaking frequency (around 10 Hz).

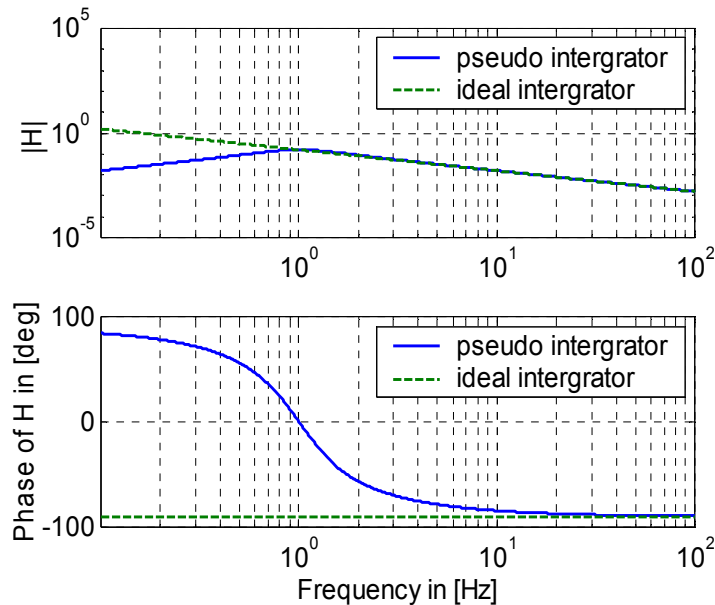


Figure 4.10: Bode plot of an pseudo integrator and an ideal integrator

Once the digital integrator is designed, the velocity feedback control is implemented with a variable g_3 velocity gain. For each tested harmonic disturbance the velocity gain is changed in the range from -5 to 0 where the simulation predicted the exitance of an optimum power flow.

4.5.2 Results and their comparison with estimated results

The experimentally obtained and simulated regenerated electrical power, input mechanical powers and regeneration efficiencies are plotted on the following next three pages (Figure 4.11, Figure 4.12 and Figure 4.13). The experimental power values are obtained after averaging the instantaneous power signals for mechanical and electrical subsystems.

Figure 4.11 shows a good correlation between the estimated and experimentally obtained results. The regenerative phenomenon is exhibited with the existence of an optimal gain for all frequencies under on and above the mechanical system resonance. The maximum regenerated electrical energy is obtained for a mechanical disturbance at resonance with an optimal gain of $g_3 = -2.2$. As predicted when the magnitude of the velocity gain g_3 is increased the regenerative electrical energy increase up to the optimal point where it reaches its maximum regenerative flow. After the optimal point the regenerated power decreases with the parabolic behavior up to the point the power flow (pure reactive flow). Over this point the flow is not anymore regenerative (P_{el} is positive) and the amplifier is then acting as energy source.

The mechanical input powers are not as well correlated with the experiment. Amplitudes of the measured and simulated velocities are matched within the range of 5 – 10 % but as in the previous case the power computation is very sensitive to the error on phase.

The efficiency plot shows that the maximum efficiency is around 10%. Due to an important error on mechanical input power the simulated and experimentally measured efficiencies are not well correlated in magnitudes. The predication of the optimal gains for different frequencies of the mechanical disturbance are matched within 5%.

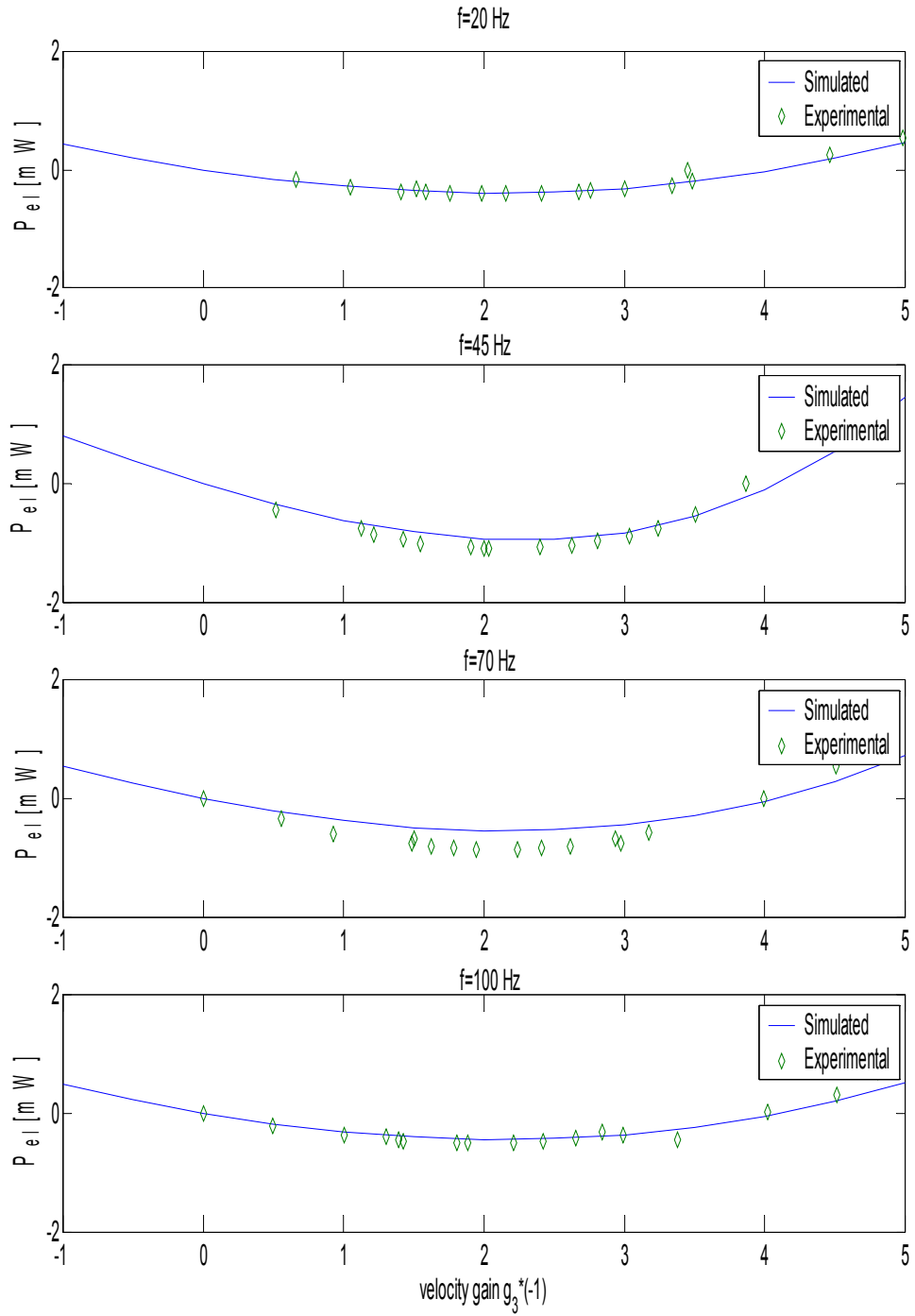


Figure 4.11: Regenerated simulated and measured powers in resistive control configuration

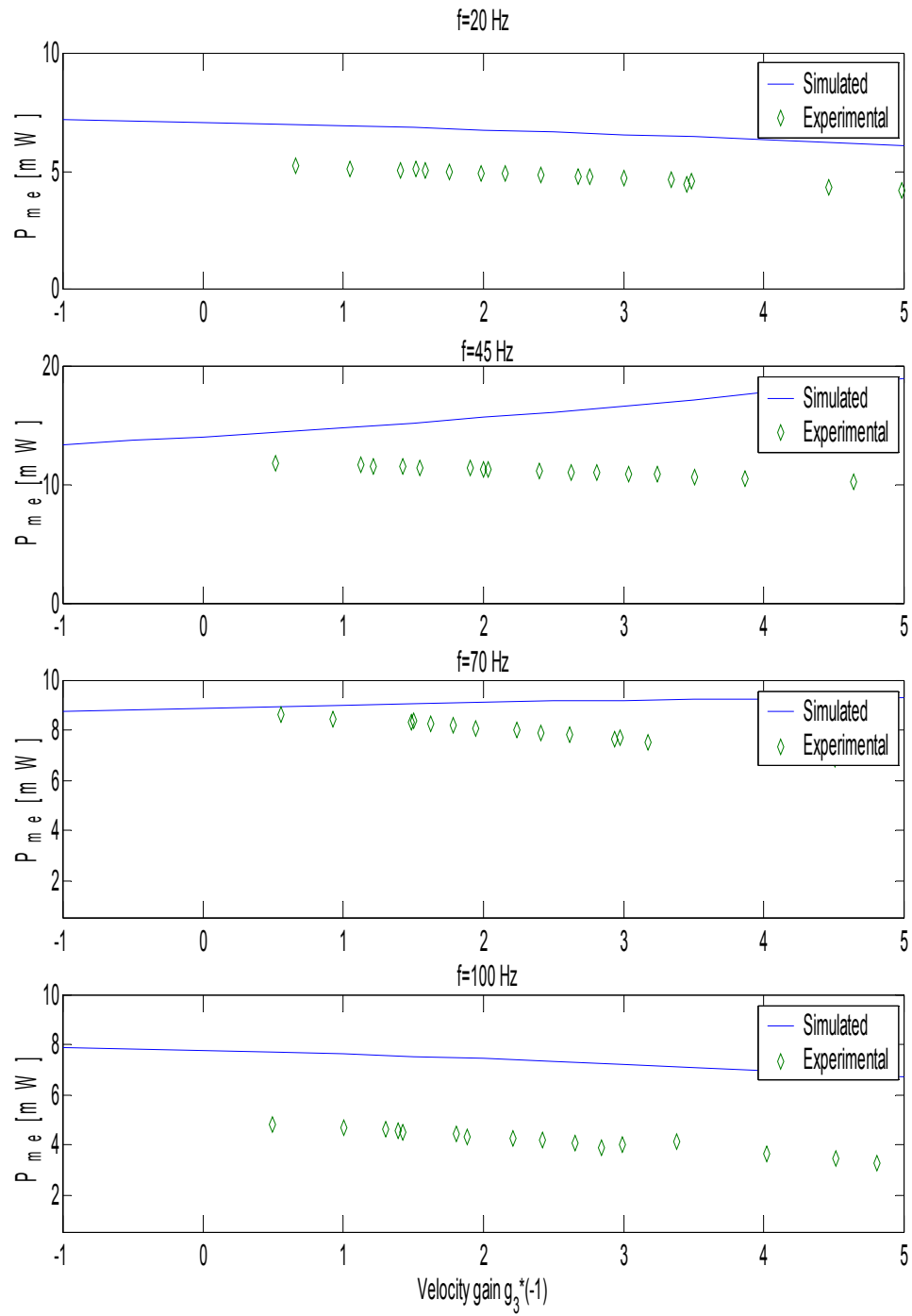


Figure 4.12: Input mechanical simulated and measured powers in velocity control configuration

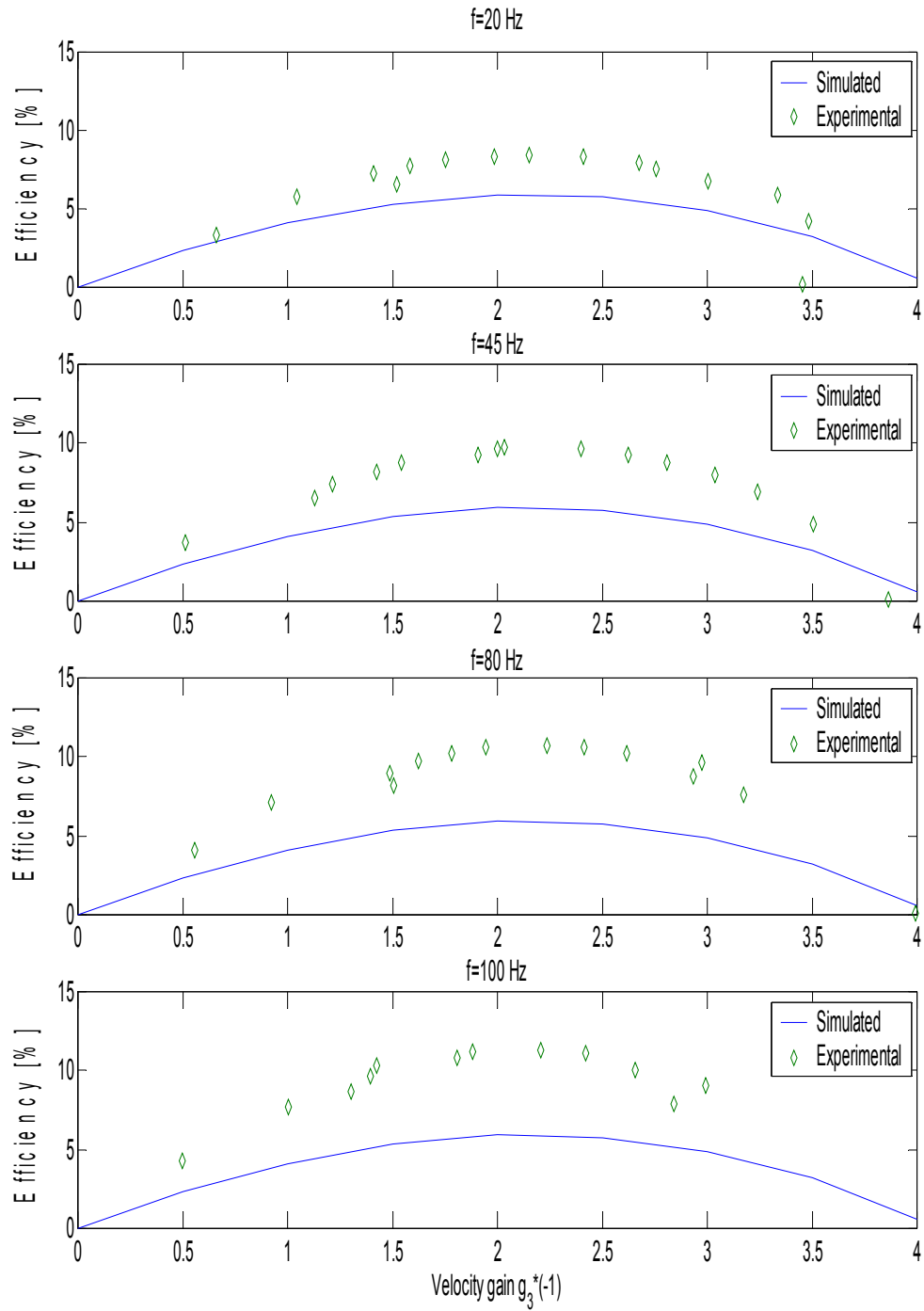


Figure 4.13: Simulated and experimental efficiencies in velocity control configuration

4.6 Flow Control

This section discusses the implementation and the measured results of the flow type control law. In the flow type control law current and velocity are fed back with the resistive and velocity gains respectively g_1 and g_3 . The simplified schematics of system in closed loop is shown on Figure 4.14. The control law is,

$$V_c = -g_1 i - g_3 \dot{x}. \quad (4.7)$$

From the previous analysis it was shown that in order to obtain the regenerative flow we have to have g_1 positive and a defined interval of negative values for g_3 .

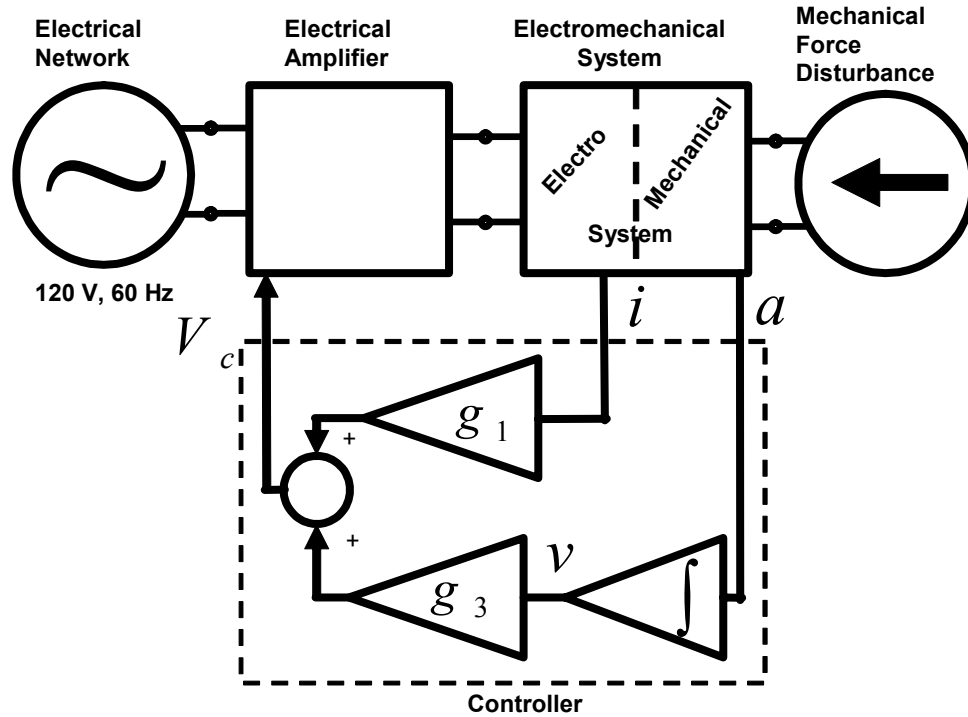


Figure 4.14: Flow control schematics

4.6.1 Results and their comparison with estimated results

The implementation of flow control law is very similar to the two previous cases. In fact flow control is the combination of both resistive and velocity control. As in the previous cases the current is sensed through a shunt resistor and velocity is obtained by digitally integrating the signal from the accelerometer with pseudo integrator which transfer function is shown

on Figure 4.10. During the experiment, for a given harmonic disturbance the resistive gain g_1 is fixed to 2 and then to 4. Data is taken by changing the velocity gain in the range of interested values (where the optimum flow is located). In the next three pages Figure 4.15, 4.16, and 4.17 show the experimental and predicted electrical regenerated power, mechanical input power and regenerative efficiencies for four different frequencies of harmonic force disturbance in the case of flow control with $g_1 = 2$.

The plots for the case where $g_1 = 4$ are shown in Appendix A. From Figure 4.15 we notice the existence of an interval of gains g_3 for which the electrical power flow is regenerative. This interval also contains an optimum value of gain g_3 for which the regenerative flow is maximized for $g_1 = 2$. The estimated and measured optimal gains are well correlated. Again the mechanical input power values are not well correlated due to the same issues explained in the next section.

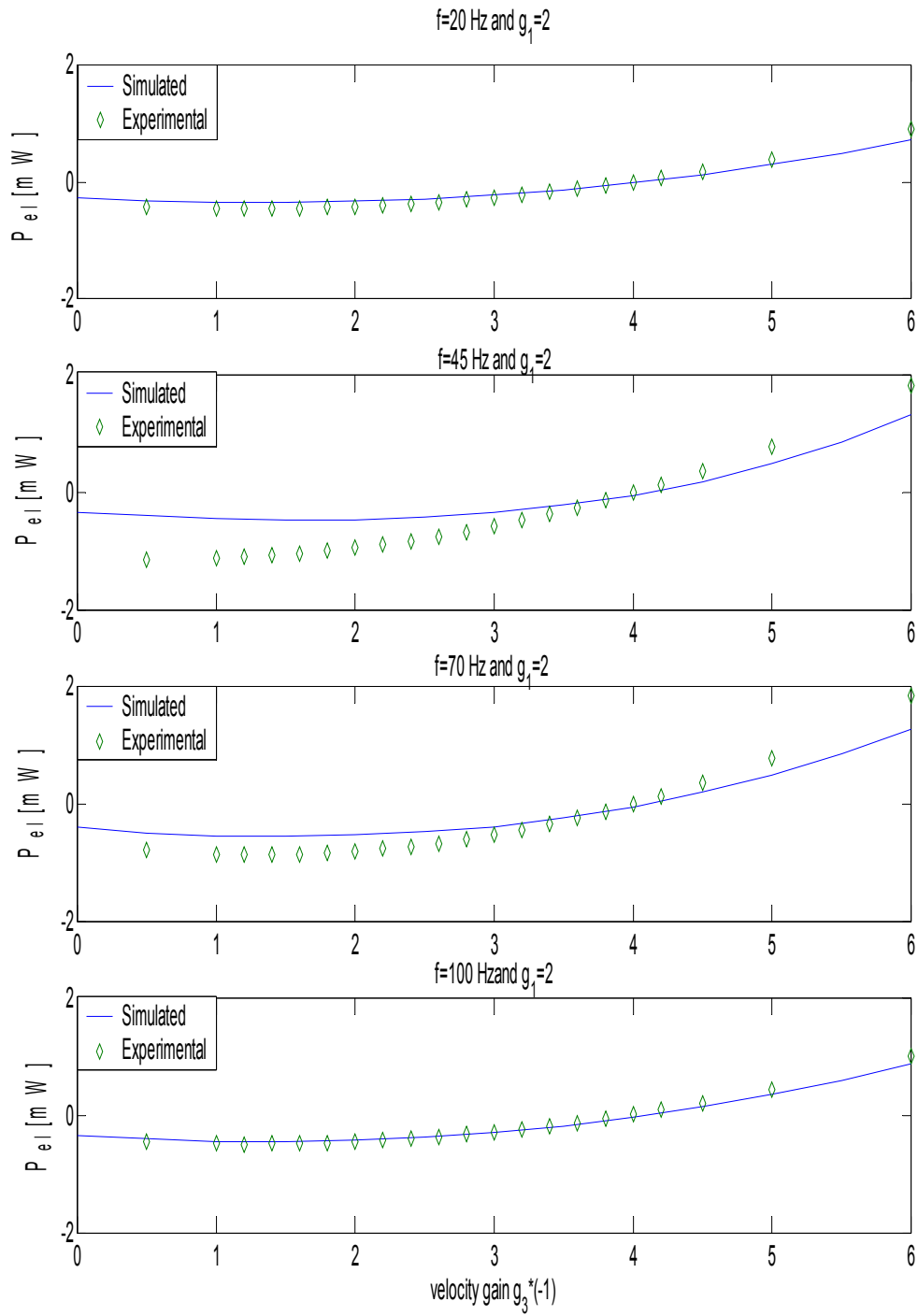


Figure 4.15: Regenerated simulated and measured powers in flow control configuration

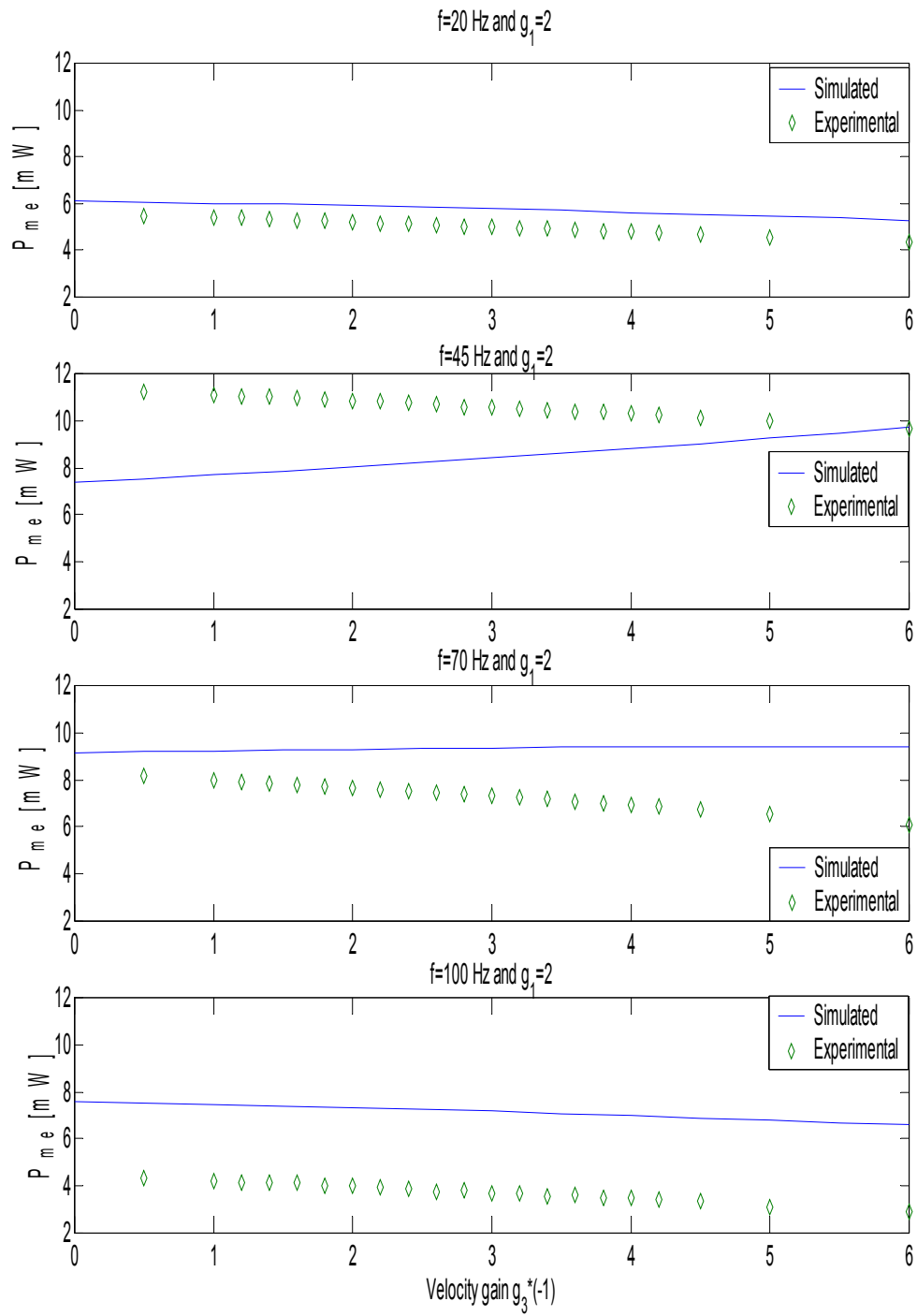


Figure 4.16: Input mechanical simulated and measured powers in flow control configuration

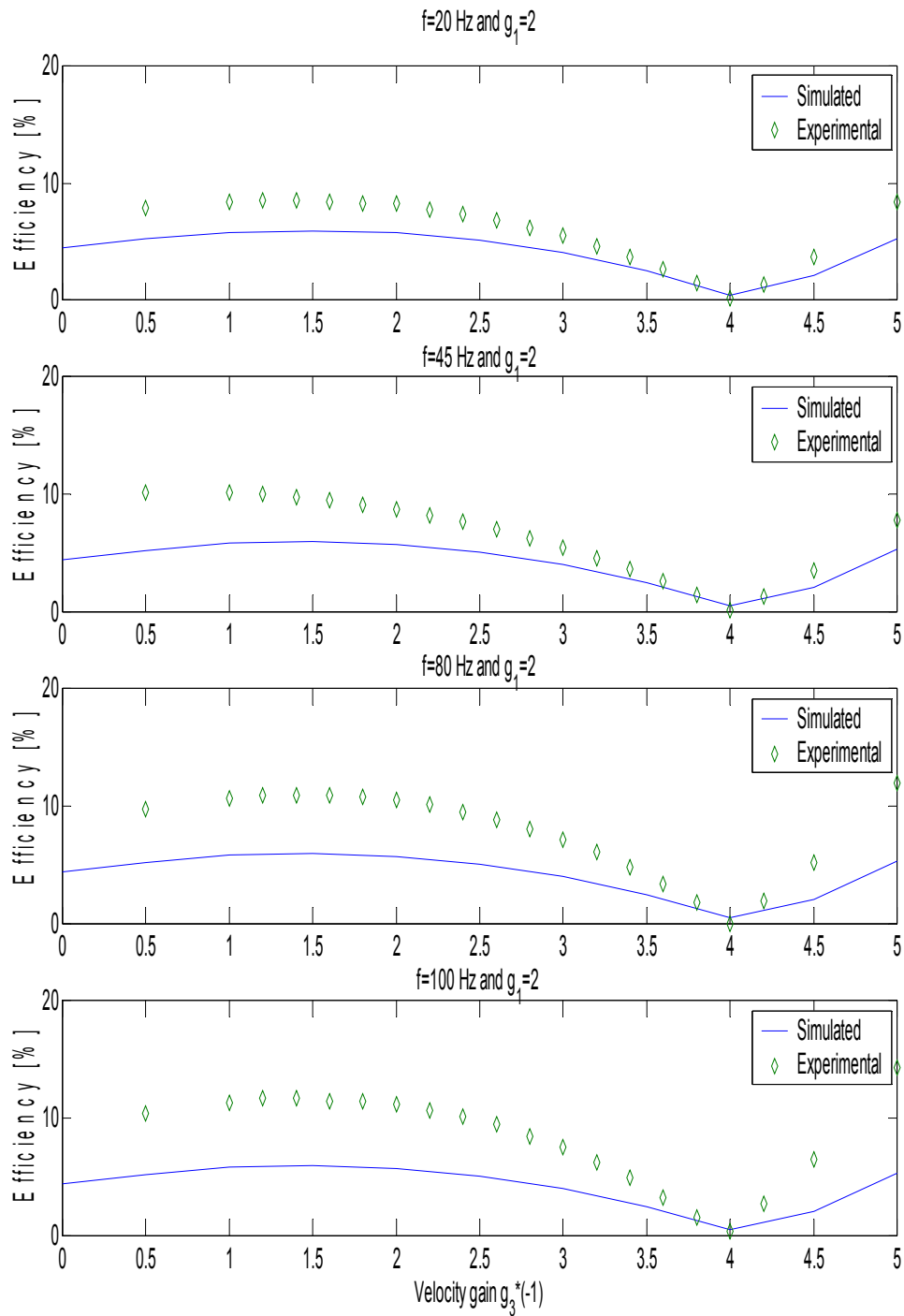


Figure 4.17: Simulated and experimental efficiencies in flow control configuration

4.7 Summary on the experimental verification

Closed loop measurements for three different closed loop cases have been presented. In all closed loop cases the regenerated power had the predicted behavior. In the case of the resistive control with g_1 positive, the power flow was always regenerative in the stability region. For each frequency of the harmonic disturbance excitation, the existence of an optimum regenerative gain g_1^* was experimentally confirmed. The maximum power flow is obtained in the case of the disturbance excitation at the open loop resonance (45 Hz) and the maximum error in the prediction of the optimal gain is 32 %.

Magnitudes of the power quantities are not very well correlated due to several reasons. Power determination from time domain flow and effort quantities is sensitive to phase variation. It is important to notice that there is already a not negligible phase difference between the simulated and experimental open loop systems as shown on Figure 4.3 and Figure 4.4. Another phenomena related to phase, is the stability issue in closed loop. Increasing the resistive gain over 10 will lead the closed loop system into instability. This instability limitation which doesn't appear in the model is mostly due to the digital controller and the internal dynamics of the linear amplifier. Increasing the sampling frequency of the controller will increase the stability region. This instability region makes an important influence on the stability region. We observed during the experiment, for higher values of resistive 5 – 10 the waveform started to be modulated with higher frequency phenomenon and the magnitudes of the electrical quantities where then corrupted.

Another important issue in the experimental setup was the harmonic distortion of the disturbance and measured acceleration. In the other words input force waveform is not a perfect harmonic function. The computed Total Harmonic Distortion (THD) indices of force and acceleration are in the order of 12 % at low frequencies (around 20 Hz) and in the order of 18 % at higher frequencies (100 Hz and above). As the power is computed from time signals the nonlinearity of the time waveform will corrupt the computed values of power. The comparison between the predicted and experimentally obtained optimal gains are shown on Table 4.2.

Another sensitive parameter for power estimation from time flow/effort data is the phase between them. Although the input simulated and experimentally obtained velocities are matched within 5 – 10 % and the input force is estimated from the experiment and

Table 4.2: Experimentally obtained and simulated optimum regenerative flow gains comparison

f in [Hz]	Flow cont.			Velocity cont.		
	$g_3^*(sim)$	$g_3^*(exp)$	<i>Error</i>	$g_3^*(sim)$	$g_3^*(exp)$	<i>Error</i>
20	-1.4	-1.5	7 %	-2.1	-2.15	2.8 %
45	-1.40	-1.20	14 %	-2.3	-2.2	4 %
70	-1.5	-1.35	10 %	-2.2	-2.1	4 %
100	-1.4	-1.2	14 %	-2.1	-2.0	5 %

f in [Hz]	Resistive cont.		
	$g_1^*(sim)$	$g_1^*(exp)$	<i>Error</i>
20	5.85	4.6	21 %
45	6.95	4.98	28 %
80	6.1	4.07	32 %
100	5.9	5	15.25 %

then plugged into the model (force is an input to the state-space model), the amplitude of measured power quantities are not well correlated. This error is due to an important difference in the phase of the assumed open loop system and the simulated system. Equation (2.27) can be expressed in terms of amplitudes of effort and flow E , and F and phase between this two quantities ϕ ,

$$P = \frac{1}{2} E F \cos(\phi). \quad (4.8)$$

The angle ϕ is the phase difference between the two time signals. From Equation (4.8) we notice the computation of power is sensitive to the error on phase. In the actual experimental system the difference of phase in the open loop mechanical transfer function between force and velocity and the simulated second order mechanical system is increasing with frequency, see Section 4.3.1.

In the case of velocity control with negative gain g_3 , the obtained experimental power confirmed an existence of a regenerative area. This area has a parabolic behavior. With the increase of $|g_3|$ the regenerated power increases up to the point where it reaches its maximum for $|g_3^*|$. When the magnitude of the velocity gain is increased over the optimum point, the regenerative flow decreases parabolically up to a point where it disappears. At this point the power flow is purely reactive. Increasing g_3 over the reactive point, the flow is

inversed which means that energy is transferred from the electrical source to the mechanical disturbance. The experimentally obtained optimal gains g_3^* for different force disturbance are well correlated with the predicted optimal gains (prediction within 5%). For the same reasons as in the case of resistive control there is a non negligible difference between the predicted and experimentally obtained powers.

In the third case (flow control) the predicted behavior is experimentally confirmed with an existence of optimum flow (case where g_1 is fixed). This case is a combination of the two previous cases and as in the velocity control this case also exhibits an interval of gains g_3 , $\forall g_1 > 0$ in which the flow is regenerative and a particular optimum value exists for each set of control laws with fixed g_1 . Out of this interval the flow is not anymore regenerative. The optimum predicted and experimentally obtained gains for all three different control topologies are summarized in Table 4.2.

Chapter 5

Conclusions

A regenerative control topology for an active vibration isolation system has been demonstrated. From the analysis performed in this research, the following conclusion are made:

- A generalized concept of regenerative vibration isolation has been defined. The major difference of this concept with the regenerative systems found in literature is that in our case energy regeneration is performed in closed loop. Two different technologies of linear electromechanical actuators have been defined and modeled. The necessary requirements on the electrical driver have been established and discussed. It has been determined that only a switching bidirectional driver can satisfy the requirements in the case of regenerative control is closed loop.
- For both different actuator technologies a corresponding electromechanical state-space model have been derived. The two obtained state-space models were then normalized and compared. The comparison showed that both systems were mathematically identical. From the controls point of view, the major difference was in the control input. This difference impacted the switching amplifier topology. In the case of an EM actuator a voltage control amplifier is required while in the case of a PZT actuator a current control is necessary. As both systems are mathematically identical, one analytical analysis of regenerated power was sufficient and valid for both systems.
- The analysis of the analytical expression of electrical power in closed loop showed that there is three different regenerative control topologies. Feeding back any flow type parameter such as current, velocity or a linear combination of both may exhibit

regenerative flow. These three control laws are named: resistive control, velocity feedback and flow control whether respectively current or velocity or both current and velocity were fed back. The maximum value of regenerative power flow is obtained in resistive control. Conversely, feeding back the displacement through a constant control gain will either decrease the amount of regenerated power or make the system dissipative depending on the value of the applied gain.

- An analysis of the closed loop poles locations indicated that the regenerative control is reducing the amount of damping in closed loop. It is important to remember that the open loop in the case of an EM actuator represents a short-circuit boundary condition (shunted actuator) while in the case of an PZT actuator it represents an open circuit electrical boundary condition. Also, the optimum regenerative control does not correspond to the maximum damping reduction.
- A simple experimental setup in force isolation configuration have been implemented and tested in closed loop. The regenerative flow was observed and the simulated optimum control law were experimentally confirmed. Thus the concept of regenerative control was proved and demonstrated.
- For each of this control strategy an optimal operation point could be determined and experimentally verified. An important unpredicted practical issue observed in the experimental setup was the instability of the electrical driver in the closed loop.
- Finally, a good estimate of regenerative efficiency in the case of an EM actuator was obtained. For the simulated vibration isolation system representing the prototype at the AFRL the maximum regenerative efficiencies were in the order of 35 %. In the case of the developed experimental setup (force isolation) the measured and simulated efficiencies were in the order of 10 %. In the case of the vibration isolation system with a piezoelectric actuator the regenerative efficiencies were in the order of 90 %. It is important to remember that an important dissipative phenomenon, the hysteresis the stack actuator, was not taken into account in the model. Taking into account this phenomenon may considerably reduce the obtained regenerative efficiencies.

5.1 Recommendations and Future Work

From the experience of this research, the following recommendation on future work are suggested:

- As the developed model estimates the electrical quantities and the maximum regenerative efficiency, a set of specification for the design of the electrical driver and energy storage elements can be established. The design of the power electronics (switching amplifier) will have a enormous impact on the efficiency of the overall regenerative vibration isolator. As switching amplifiers already require voltage and current feedback control loops for their proper operation [Chandrasekaran et al. (2001)], the same voltage or current sensor could be used for implementation of the resistive control topologies. Using the same sensor will reduce the losses induced by the controller and increase the overall efficiency.
- Following the idea of sensor combination, an observer based control strategy could be analyzed. In this case the only sensed parameter will be current or voltage for the same reason as mentioned previously. The observer will estimate all the other necessary quantities such us displacement and velocity and then provide a control input in both regenerative and vibration control modes. Using an observer based control will increase the complexity of the control electronics but will simplify and reduce the cost of the overall system. The need for accelerometers which require associated electronics for signal conditioning and the digital or analog filters necessary for estimating velocity and displacement signals will be then eliminated.
- Since the fundamental tradeoff in the design of a regenerative active vibration system is the amount of regenerated energy towards the required energy for active control a system composed of two actuators one driven in regenerative mode and the other in vibration control mode can be explored. Figure 5.1 illustrates a 2-DOF active vibration system where the first stage is connected to the base through a regenerative actuator. The second stage consists of the payload connected through the second actuator driven in typical vibration suppression control mode. This concept is similar to the one developed by Nakano et al. (2000), where a 2-DOF vibration isolator is used but the regeneration is realized in open loop mode.

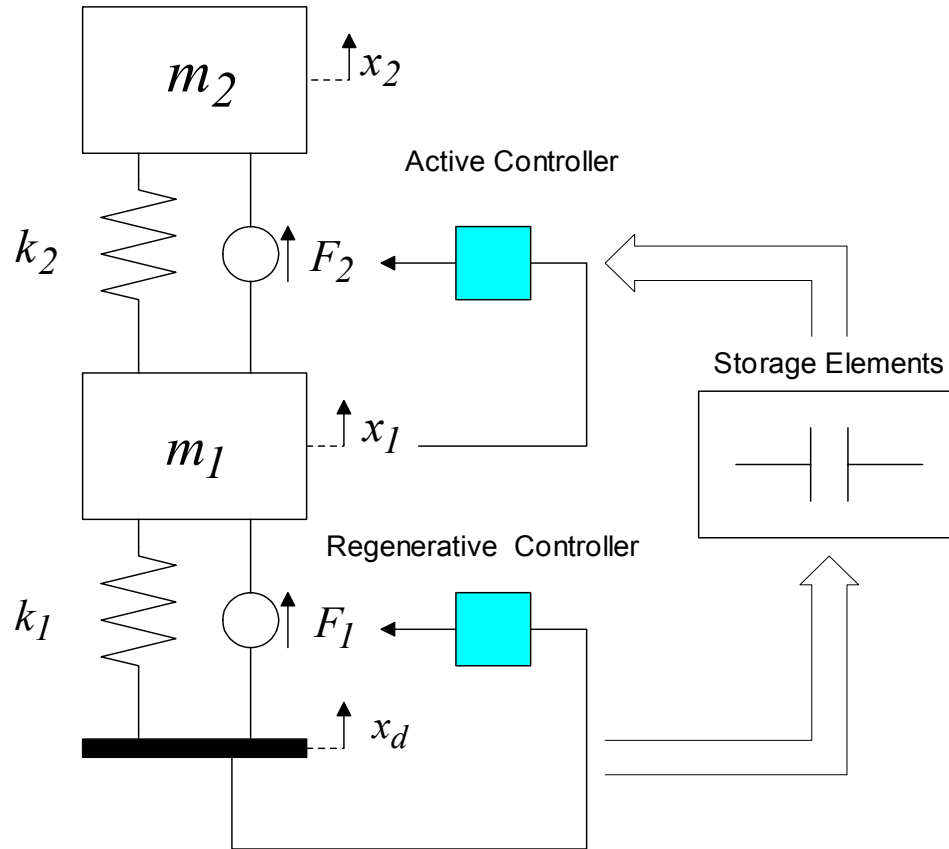


Figure 5.1: 2-DOF regenerative vibration isolation concept

- The developed concept of regenerative control can also be applied in the actual energy harvesting systems in order to optimize the energy regeneration. For example in a case of a self-powered PZT sensor for structural monitoring, where only a periodic sensing (once or twice a day) is required, all the other time of the day the sensor can be used in regenerative control mode for optimal electrical energy harvesting from parasitic vibrations.
- Finally it is necessary to continue this analytical analysis in the case of a random disturbance input. That may lead to a formulation of a cost function which accounts for energy regeneration and the level of vibration in closed loop. Once the cost function has been formulated an optimization problem can be solved for a maximizing the energy regeneration in case of a random disturbance.

Bibliography

Adinolfi, A., Lamedica, R., Modesto, C., Prudenzi, A., and Vimercati, S., *Experimental Assessment of Energy Saving due to Trains Regenerative Breaking in an Electrified Subway Line*, **Vehicle System Dynamics**, Vol. 13, No. 4, pp. 1536–1541, 1988.

Amirtharajah, R. and Chandrakasan, P., *Self-Powered Signal Processing Using Vibration-Based Power Generation*, **IEE Journal of Solid-State Circuits**, Vol. 33, No. 5, pp. 687–695, 1998.

Anderson, E., Evert, M., Gleese, R., Gooding, J., and Pendleton, S., *Stellite Ultraquite Technology Experiment (SUIT): Electromechanical Subsystems*, **SPIE Conference on Industrial and Commercial Applications of Smart Structures Technologies**, Vol. 3674, pp. 308–328, 1999.

ANSI/IEEE Standard 176, *IEEE Standard on Piezoelectricity*, **Standards Committee of the IEEE Ultrasonics, Ferroelectrics, and Frequency Control Society**, 1987.

Beranek, L. L., **Acoustics**, 2nd Ed., McGraw-Hill Book Company, 1954.

Carroll, C., 2001, “Piezoelectric Rotary Electrical Energy Generator,” U.S. Patent 6,194,815.

Chandrasekaran, S. and Lindner, D., *Power Flow Through Controlled Piezoelectric Actuators*, **Journal of Intelligent Material Systems and Structures**, Vol. 11, No. 6, pp. 496–481, 2000.

Chandrasekaran, S., Lindner, D., and Leo, D., *Effect of Feedback Control on the Power Consumption of Induced-Strain Actuators*, **Proceedings of the Adaptive Structures and Materials Symposium**, **ASME**, Vol. AD, No. 60, pp. 65–76, 2000.

- Chandrasekaran, S., Lindner, D., and Smith, R., *Optimized Design of Switching Amplifier for Piezoelectric Actuators*, **Journal of Intelligent Material Systems and Structures**, Vol. 35, pp. 887–901, 2001.
- Crawley, E. and de Louis, J., *Use of Piezoelectric Actuators as Elements of Intelligent Structures*, **AIAA Journal**, Vol. 25, No. 10, pp. 1373–1385, 1987.
- Culshaw, B., **Smart Structures and Materials**, Artech House, 1996.
- Duffy, J., 2001, “Clockwork warfare,” http://news.bbc.co.uk/hi/english/uk/newsid_1589000/1589318.stm.
- Elvin, N., Elvin, A., and Spector, M., *A self powered mechanical strain energy sensor*, **Smart Materials and Structures**, Vol. 10, pp. 293–299, 2001.
- Epstein, M. and Carroll, C., 1996, “Piezoelectric Electric Energy Generator,” U.S. Patent 5,512,795.
- Erickson, R. W. and Maksimovic, D., **Fundamentals of Power Electronics**, 2nd Ed., Kluwer Academic Publisher, 1999.
- Foshage, J., Davis, T., Sullivan, J., Hoffman, T., and Das, A., *Hybrid active/passive actuator for spacecraft vibration isolation and suppression*, **Proceedings of SPIE on Actuator Technology and Application Conference**, 1996.
- Freeplay, 2002, “Technology Background,” <http://www.freeplay.net/new/newsite/technology/hist.html>.
- Friedland, B., **Control System Design**, MacGraw-Hill, Boston, 1986.
- Hambley, A., **Electrical Engineering**, Prentice Hall, 1997.
- Hashimoto, Y., Takahashi, O., Miyazaki, H., Funasaka, T., and Furuhata, M., 1998, “Power Generation Method and Power Generation using a Piezoelectric Element, and Electronic Device using the Power,” U.S. Patent 5,835,996.
- Ikeda, T., **Fundamentals of Piezoelectricity**, Oxford Science Publications, Oxford, 1990.

Illinger, P., 2001, “The Pressure is on to Make Tires Talk,” http://w4.siemens.de/FuI/en/archiv/zeitschrift/heft2_99/artikel07/index.html.

Inman, D., **Engineering Vibration**, 2nd Ed., Prentice Hall, 2000.

Jaffe, B., Roth, R., and Marzullo, S., *Piezoelectric properties of lead zirconate-lead titanate solid-solution ceramics*, **J. Appl. Phys**, Vol. 6, No. 25, pp. 809–810, 1954.

Jolly, M., 1993, **Passive and Regenerative Solutions for Vibration Control**-Ph.D. Thesis, University of California Davis.

Jolly, M. and Margolis, D., *Assessing the Potential for Energy Regeneration in Dynamic Subsystems*, **Journal of Dynamic Systems, Measurements, and Control**, Vol. 119, pp. 265–270, 1997a.

Jolly, M. and Margolis, D., *Regenerative Systems for Vibration Control*, **Journal of Vibration and Acoustics**, Vol. 119, pp. 203–215, 1997b.

Karnopp, D. and Rosenberg, R., **Analysis and Simulation of Multiport System**, The M.I.T. Press, Cambridge, Massachusetts, 1968.

Karnopp, D. and Rosenberg, R., **System Dynamics: A Unified Approach**, John Wiley & Sons, New York, 1974.

Kishimoto, Y. and Bernstein, D., *Thermodynamic Modelling of Interconnected Systems, Part I: Conservative Coupling*, **Journal of Sound and Vibration**, Vol. 182, No. 1, pp. 23–58, 1995.

Leo, D., *Energy Analysis of Piezoelectric-Actuated Structure Driven by Linear Amplifiers*, **Journal of Intelligent Material Systems and Structure**, Vol. 10, No. 1, pp. 36–45, 1999.

Lindner, D., Vujic, N., Zhu, M., and Leo, D., *Comparison of Linear and Switching Drive Amplifiers for piezoelectric actuators*, **43rd AIAA/ASME/ASCE/AHS/ASC Structures, Structural Dynamics, and Materials Conference paper 2002-1352**, 2002.

Lyon, R. and Maidanik, G., *Power Flow Between Linearly Coupled Oscillators*, **Journal of Sound and Vibration**, Vol. 34, No. 5, pp. 623–639, 1962.

- Main, J., Newton, D., Garcia, E., and Massengill, L., *Efficient Power Amplifiers for Piezoelectric Applications*, **Smart Materials and Structures**, Vol. 5, pp. 776–775, 1996.
- Miller, D., Hall, S., and von Flotow, H., *Optimal Control of Power Flow at Structural Junctions*, **Journal of Sound and Vibration**, Vol. 140, No. 3, pp. 475–497, 1990.
- Mohan, N., Undeland, T., and Robbins, W., **Power Electronics**, 2nd Ed., John Wiley & Sons, 1989.
- Nakano, K., Suda, Y., and Nakadi, S., *Self-Powered Active Vibration Control Using Continuous Control Input*, **JSME International Journal**, Vol. Series, No. C, pp. 726–731, 2000.
- Nakano, K., Suda, Y., and Nakadi, S., *Anti-rolling System for Ships with Self-Powered Active Control*, **JSME International Journal**, Vol. Series, No. C, pp. 587–593, 2001.
- Nakano, K., Suda, Y., Nakadi, S., H., T., and T., W., *Self-powered active control applied to a track cab suspension*, **SAE of Japan**, Vol. 20, No. 511-516, pp. 511–516, 1999.
- Nasar, S. and Boldea, I., **Linear Electric Motors: Theory, Design, and Practical Application**, Prentice Hall, 1987.
- Nasser, K., 2000, **Development and Analysis of the Lumped Parameter Model of a Piezo-Hydraulic Actuator**, M.S. Thesis, Virginia Polytechnic Institute and State University.
- Nowak, R., 2002, “Energy Harvesting,” <http://www.darpa.mil/dso/thrust/md/energy/index.html>.
- Paine, J., Bennett, D., and Cuadros, C., *Compact Drive Electronics for Solid-State Actuators*, **Adaptive Structures and Materials Systems ASME**, Vol. AD, No. 60, pp. 77–84, 2000.
- Physik Instrumente, *PZT Fundamentals*, **Catalog: Products for Micropositioning**, 2002.
- Piezo Systems, *Introduction to Piezoelectricity*, **Catalog # 3**, 2000.
- Piezomechanik GmbH, *Piezoelectrical and Electrostrictive Stack Actuators and Ring Actuators*, **Catalog**, 2001.

Sciulli, D. and Griffin, S., *Hybrid Lurch Isolation System*, **SPIE Conference on Industrial and Commercial Applications of Smart Structures Technologies**, Vol. 3674, pp. 352–359, 1999.

Seiko, 2002, “How Seiko kinetic watches work,” http://seiko-kinetic-watches.watch-universe.com/seiko_kinetic_watches_wk.htm.

Serway, R., **Principles of Physics**, Harcourt Brace Publishers, Fort Worth, 1994.

Sharp, R. and Crolla, D., *Road Vehicle Suspension System Design - a review*, **Vehicle System Dynamics**, Vol. 16, pp. 167–192, 1987.

Starner, T., *Human-Powered wearable computing*, **IBM Systems Journal**, Vol. 35, No. 3, pp. 618–629, 1998.

Umeda, M., Nakamura, K., and Ueha, S., *Energy Storage Characteristics of a Piezo-Generator using Impact Induced Vibration*, **Japanese Journal of Applied Physics**, Vol. 36, pp. 3146–3151, 1997.

Vailon, L., Petitjean, B., Frapard, B., and Lebihan, D., *Active isolation in space truss structures: from concept to implementation*, **Smart Materials and Structures**, Vol. 8, No. 6, pp. 781–790, 1999.

Warkentin, D. and Crawley, E., *Power Amplification for Piezoelectric Actuator in Controlled Structures*, **MIT Space Engineering Research Center Report**, Vol. SERC, No. 4-95, 1995.

Zvonar, G. and Lindner, D., *Power flow analysis of electrostrictive actuators*, **Proceedings of the Adaptive Structures and Materials Symposium**, **ASME**, Vol. AD, No. 59, pp. 1–10, 1999.

Appendix A

Experimental and Simulated powers and efficiency plots in flow control topology with $g_1 = 4$

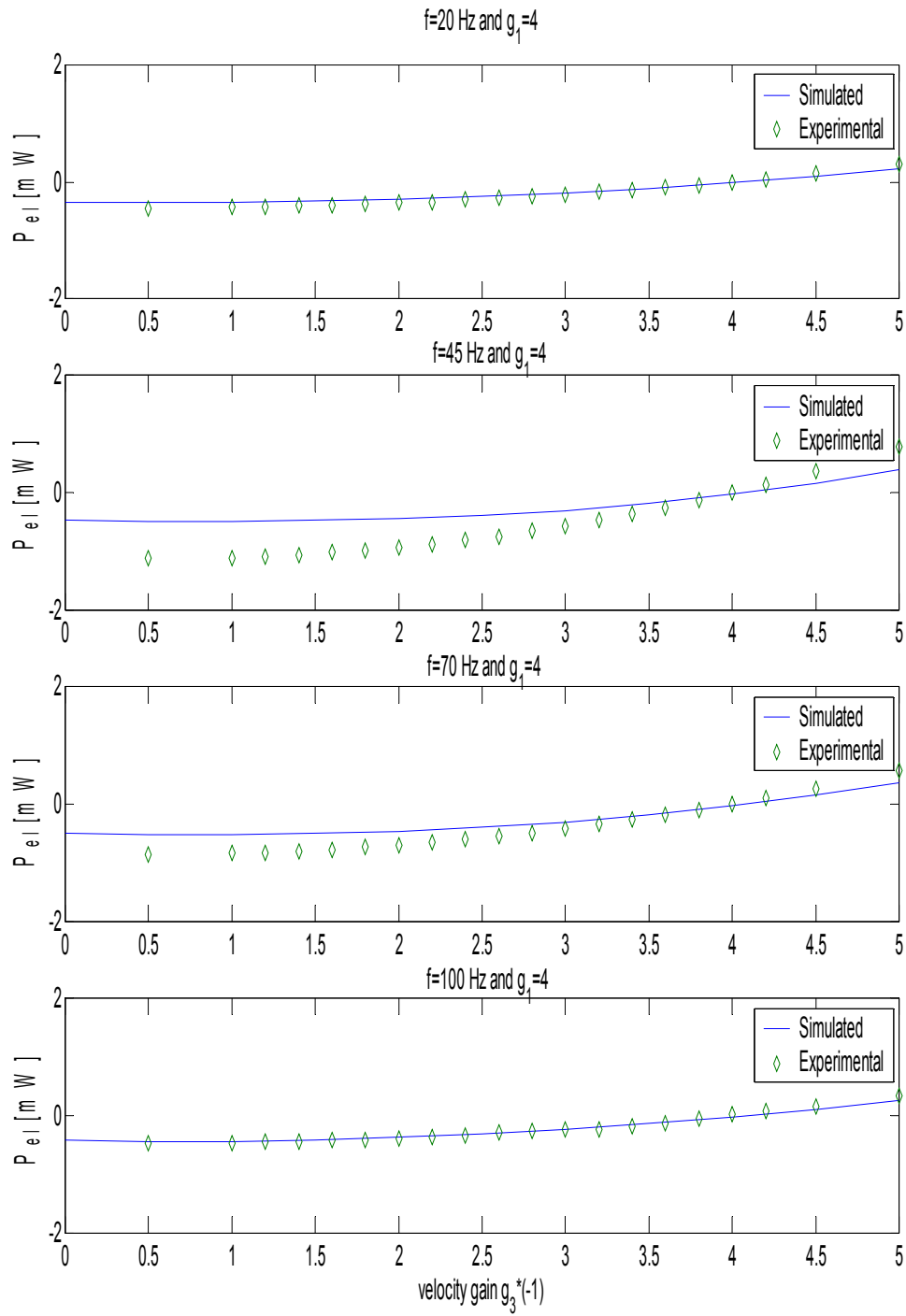


Figure A.1: Regenerated simulated and measured powers in flow control configuration

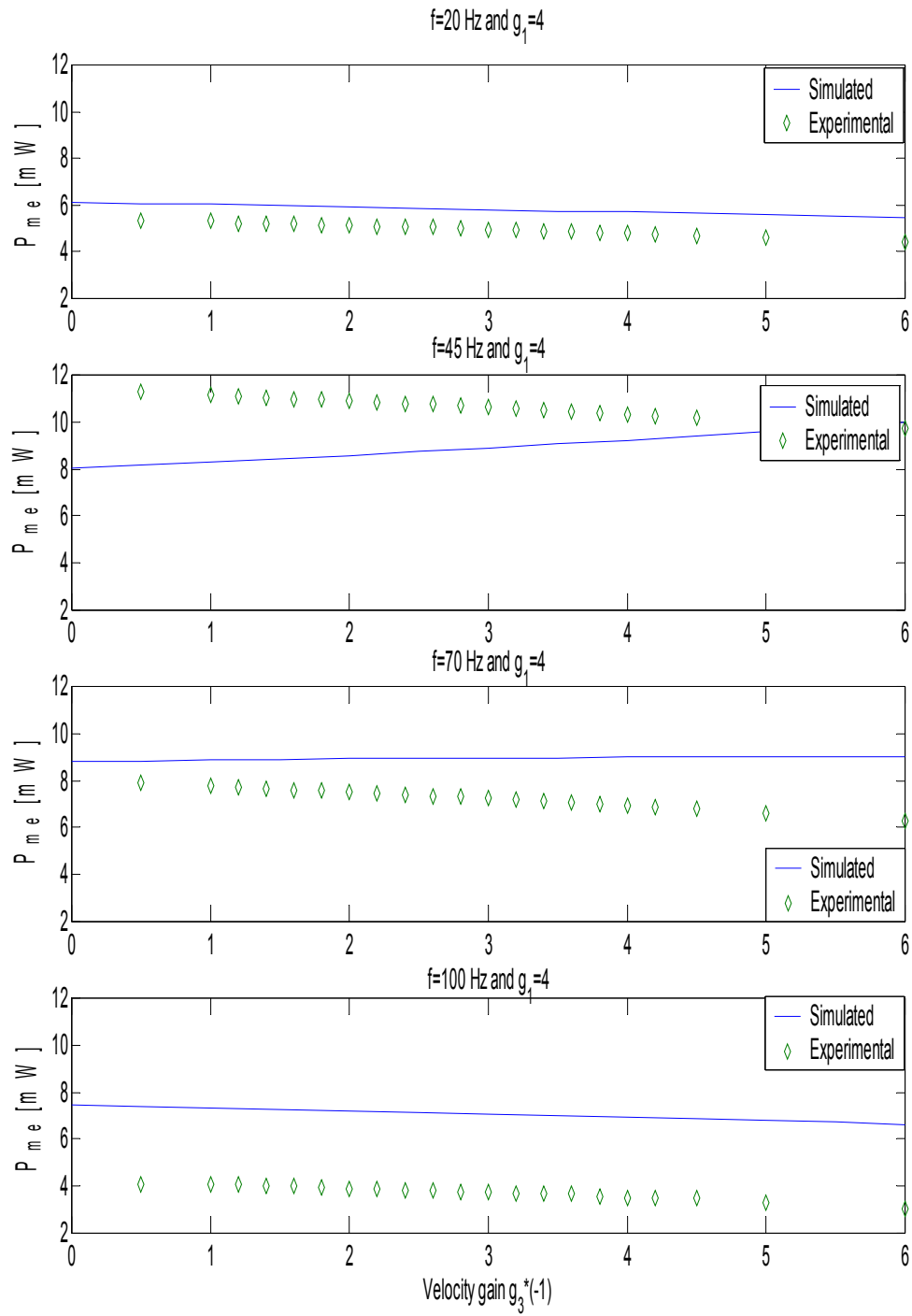


Figure A.2: Input Mechanical simulated and measured powers in flow control configuration

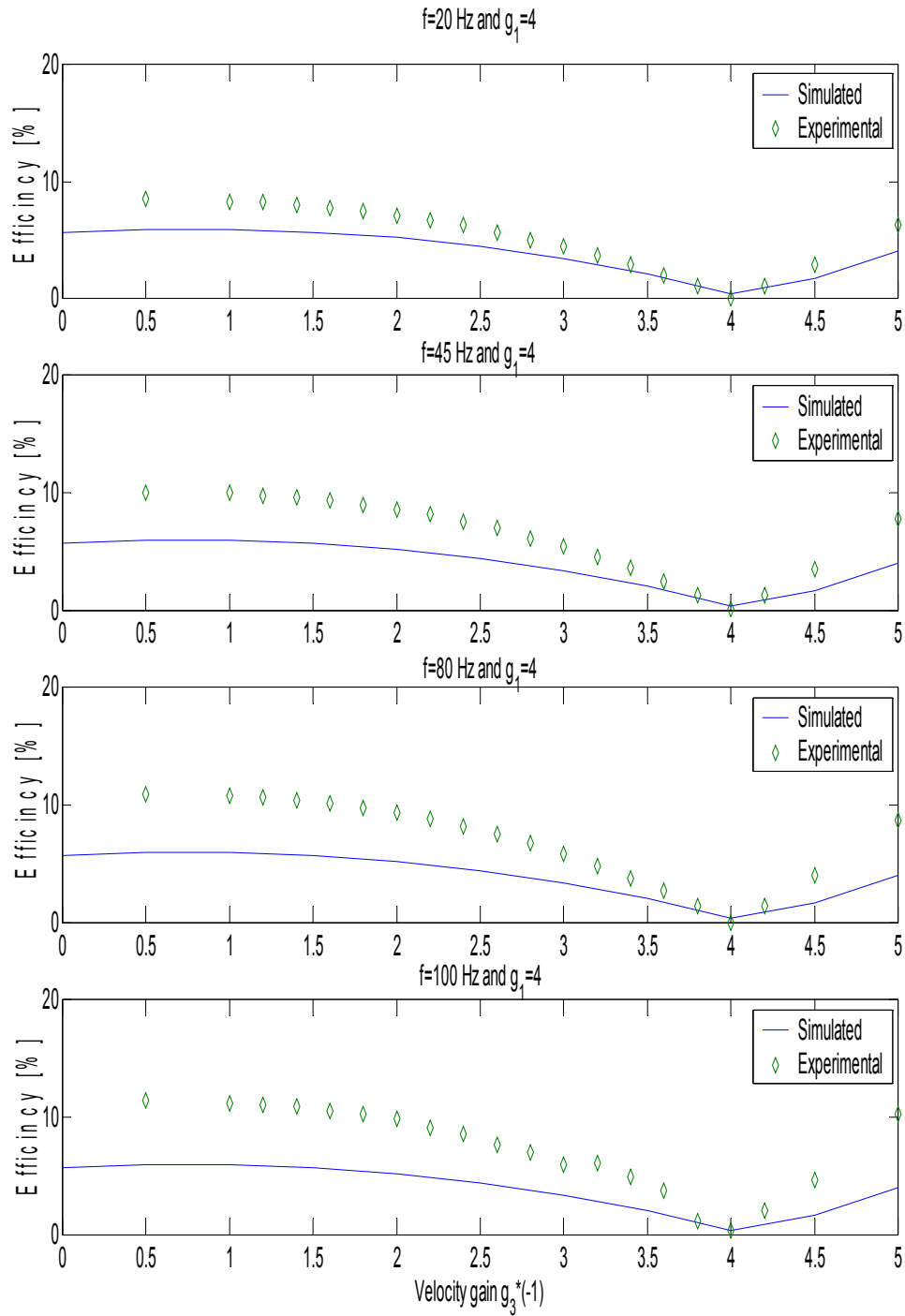


Figure A.3: Simulated and experimental efficiencies in flow control configuration

Appendix B

Electrical Power Expression in closed loop

The Electrical power expression in closed loop from Equation (3.36) is expressed in details in this Appendix.

$$\tilde{P}_{el} = \frac{\Omega^4}{|\Delta|^2} ((a_1 b_1 - a_0 b_2) \Omega^2 + a_0 b_0), \quad (\text{B.1})$$

with,

$$a_0 = -\tilde{g}_2 \quad (\text{B.2})$$

$$a_1 = -\tilde{g}_3 - \psi \quad (\text{B.3})$$

$$b_0 = \tilde{g}_1 \tilde{g}_2 - \tilde{g}_2(\beta + \tilde{g}_1) \quad (\text{B.4})$$

$$b_1 = -\tilde{g}_1(-\tilde{g}_3 - \psi) - \tilde{g}_2 - \tilde{g}_3(\beta + \tilde{g}_1) \quad (\text{B.5})$$

$$b_2 = -\tilde{g}_3 \quad (\text{B.6})$$

or,

$$(a_1 b_1 - a_0 b_2) \Omega^2 + a_0 b_0 = (-\tilde{g}_3 \tilde{g}_1 \psi - \tilde{g}_1 \psi^2 + \psi \tilde{g}_2^2 + \psi \tilde{g}_3^2 \beta + \tilde{g}_3^2 \beta) \Omega^2 + \tilde{g}_2^2 \beta \quad (\text{B.7})$$

and the denominator Δ is defined as:

$$|\Delta|^2 = \Omega^6 + d_5 \Omega^5 + d_4 \Omega^4 + d_3 \Omega^3 + d_2 \Omega^2 + d_1 \Omega + d_0, \quad (\text{B.8})$$

where,

$$d_0 = 2 \tilde{g}_1 \tilde{g}_2 + 2 \tilde{g}_2 \beta + \tilde{g}_1^2 + 2 \tilde{g}_1 \beta + \tilde{g}_2 + \beta^2 \quad (\text{B.9})$$

$$d_1 = 0 \quad (\text{B.10})$$

$$d_2 = 2 \psi - 2 \tilde{g}_1 \tilde{g}_2 - 4 \tilde{g}_1 \beta - 2 \tilde{g}_2 \beta + \psi^2 - 2 \tilde{g}_1^2 + 1 - 2 \beta^2 + 2 \tilde{g}_3 + \tilde{g}_3 + 2 \psi \tilde{g}_3 \quad (\text{B.11})$$

$$d_3 = 0 \quad (\text{B.12})$$

$$d_4 = -2 \tilde{g}_3^2 + 2 \tilde{g}_1 \beta - 2 \psi - 2 + \beta^2 + \tilde{g}_2^2 \quad (\text{B.13})$$

$$d_5 = 0. \quad (\text{B.14})$$

Vita

Nikola Vujic, son of Milan and Marie-Agnès Vujic, was born on February 1, 1976, in Sarajevo, Bosnia and Herzegovina (former Yugoslavia). He grew up in Sarajevo and moved to France in 1992. After obtaining his Baccalauréat in Mathematics and Physics in 1995 at the Lycée Etienne Oehmichen in Chalons en Champagne, France, Mr. Vujic was admitted in the Université de Technologie de Compiègne (UTC, France). After two years of general engineering, he entered the department of Mechanical Engineering and specialized in Electromechanical Engineering and Automation. He obtained the Diplôme d'Ingénieur in 2001 and choose to pursue graduate studies under Dr. Donald J. Leo at Virginia Polytechnic Institute and State University (VPI & SU). He joined the Center for Intelligent Material Systems and Structure (CIMSS) where he conducted his research on controls of electromechanical and hydraulic systems. Nikola intends to continue his work in the field of electromechanical engineering in industry.

Address: 5 Grande Rue
51600 Saint-Hilaire-le-Grand
France

This thesis was typeset with L^AT_EX 2_ε¹ by the author.

¹L^AT_EX 2_ε is an extension of L^AT_EX. L^AT_EX is a collection of macros for T_EX. T_EX is a trademark of the American Mathematical Society. The macros used in formatting this thesis were written by Greg Walker, Department of Mechanical Engineering, Virginia Tech.